11-14-2022

Studies of Roseau Cane Dieback in the Lower Mississippi River Delta Based on Remote Sensing Data Including Landsat, Worldview, and Drone

Nan Shang
Louisiana State University and Agricultural and Mechanical College

STUDIES OF ROSEAU CANE DIEBACK IN THE LOWER MISSISSIPPI RIVER DELTA BASED ON REMOTE SENSING DATA INCLUDING LANDSAT, WORLDVIEW, AND DRONE

A Dissertation

Submitted to the Graduate Faculty of the
Louisiana State University and
Agricultural and Mechanical College
in partial fulfillment of the
requirements for the degree of
Doctor of Philosophy

in

The Department of Geography and Anthropology

by
Nan Shang
B.E., Wuhan University, 2011
M.S., University of Chinese Academy of Sciences, 2014
December 2022

Acknowledgments

As Marx said, "At the entrance to science, however, the same requirement must be put as at the entrance to hell: those who are interested in marching into science must make up their mind, with fearless courage, and hard work, and be ready to devote themselves to science at any time". During the difficult years of studying abroad, I received the assistance of many good teachers and friends, which enriched my knowledge and emotions. Here, I would like to express my sincere thanks to all the following people.

I sincerely thank my advisor, Dr. Xuelian Meng. During many years of study at LSU, she has infected me with a rigorous academic attitude, profound professional knowledge, and a work style of excellence. She is strict with herself, has an approachable lifestyle, and has a superb personality. She provided me the continuous support throughout my Ph.D. study with her motivation, creativity, patience, and immense knowledge. I have benefited a lot from working with Dr. Meng these years.

Many thanks to my committee members, Dr. Lei Wang, Dr. Victor H, Rivera-Monroy, and Dr. Rebeca de Jesus Crespo. Dr. Lei Wang has been immersed in remote sensing research for many years and has extensive knowledge in the area. I get invaluable guidance from Dr. Lei Wang when I defended my proposal, and deeply inspired by his insight. I am also grateful to Dr. Victor H, Rivera-Monroy for his invaluable advice, especially in coastal study. I gratefully acknowledge Dr. Rebeca de Jesus Crespo for her invaluable services and time on this dissertation.

I would also like to thank Dr. Rodrigo Diaz and his great team. My work is funded by the Roseau project led by Dr. Rodrigo Diaz and sponsored by the USDA.

Thanks to my friends Jiang Anliu, Yuan Jianguo, Cao Wenjia, Liu Jiaxi, Li Ke, Peng

Zhongzhu, and Wang Zinan. I am lucky to be able to get along with them for many years, it enriched my life and let me not felt alone. I hope everything is well with them.

Finally, I would like to thank my parents and my sister. I missed them so much. I would not be able to finish this dissertation without their unconditional support and encouragement.

Table of Contents

List of Tables

List of Figures

Abstract

This research focused on the Roseau cane (*Phragmites australis*) dieback assessment in the lower MRD of Louisiana and introduced a comprehensive and systematic multi-source remote sensing method for assessing wetland and Roseau cane dieback and habitat dynamics analysis from three scale levels from large-scale to small scale.

Large-scale historical vegetation/land change analyses were conducted in the lower MRD based on Landsat in the past two decades (2001 - 2021). A strong increasing trend of vegetation was found since 2005. Around 51 km^2 of dieback area was detected which accounts for 11% of the overall vegetation coverage. This research showed that 65.8% of the dieback occurred in the Roseau cane area from 2010 to 2019 while the Roseau cane only accounted for 49.7% of overall vegetation coverage in 2010. The result proved that Roseau cane was more vulnerable to dieback in the lower MRD compared with other wetland vegetation.

A Roseau cane habitat classification scheme for two main passes in the lower MRD based on the mid-scale Worldview image is proposed. Through Support Vector Machine (SVM) classification method, the two variants of Roseau cane, the Delta Phragmites and European Phragmites can be separated in the study area. The results shared around 79% of agreement with the Landsat-derived classification result. In addition, the results indicated no significant differences between them in the detected areas where dieback occurred between 2019 and 2021.

Furthermore, this research monitored small-scale Roseau cane habitat dynamics in a selected drone mapping site in Pass-A-Loutre from the fall of 2020 to May 2022. This research developed a new sampling strategy based on drone which effectively solves the limited accessibility challenge in the coastal environment. The experimental results demonstrate that SVM could produce a reliable habitat mapping accuracy of over 85%. The massive death of vegetation

coverage indicated that the hurricane event had a severe impact on small-scale ecosystems, however, this research didn't observe a significant difference in damage level among the wetland vegetation species. The landscape indices used in this study can be used as a reference for the analysis of ecosystem landscape patterns in other small scales studies.

Chapter 1. Introduction

1.1. Background

The coastal wetland is one of the most productive ecosystems, accounting for 10 to 30 percent of the productivity of all marine life, known as the "Earth's kidneys" (Singh *et al*, 2017). The coastal wetland is a unique ecosystem formed by the dual role of sea and land. It provides many indispensable ecosystem services such as natural habitats for a variety of coastal organisms, plays a key role in storing blue carbon, slows coastal erosion, promotes sediment deposition, and accelerates tidal beach expansion (Barbier *et al*, 2011; Costanza *et al*, 2014; Duarte *et al*, 2013). However, biological invasion, human interference, natural disturbances, and other factors have caused significant wetlands loss in the past few decades worldwide (Temmerman *et al*, 2013). With the concern of the potential high wetland vanishing rate of coastal wetland ecosystems, coastal ecologists pay increasing attention to the monitoring and protection of the wetland (Zedler *et al*, 2005).

The Mississippi River Delta (MRD), with the main outlets entering the Gulf of Mexico from Louisiana state, is the seventh-largest river delta in the world (by watershed area), containing 12,000 km^2 of coastal wetlands and accounting for 40 percent of the salt marshes in the contiguous United States (Corbett *et al*, 2006). Considering the fragmented environment and diversified species habitat, this area is vital for ecological study. It has far-reaching significance in providing wildlife habitats, protecting biodiversity, and maintaining regional ecological balance. However, Louisiana suffered a football field-sized wetland loss per hour from 1932 to 2016 (Jaccard, 2018). In the MRD, Roseau cane (Phragmites australis) is a critical and rapidly changing landscape and plays a key role in the first line of defense against the loss of wetlands because of its flood-tolerant and salt-resistant adaptability.

Roseau cane is a typical perennial gramineous plant and often dominants many coastal wetland ecosystem plant communities (Chambers, *et al*, 1999; Antonelli *et al*, 2002). This is because the well-developed aerenchyma in the Roseau cane can transport the oxygen generated by photosynthesis of the aboveground part to the underground part, providing sufficient oxygen for the root zone microorganisms (Clevering, 1997). In addition, Roseau cane can adapt to the high-salinity environment by adjusting the level of solute permeability in leaves (Lissner, *et al*, 1997). Therefore, under different environmental conditions such as water depth, salinity, and extreme climate, Roseau cane can maintain high reproductive capacity through morphological and physiological characteristics changes. Studies have shown that when the width of Roseau cane habitat in coastal areas is more than 300 m, wind speed and wave height can be effectively reduced (Jiao, *et al*, 2015). Roseau cane also can effectively intercept silt and deposit it, gradually expanding the beach area, which provides a natural medium to deposit river sediment discharge to nearby wetlands instead of the deep ocean to prevent wetland loss (Hu, *et al*, 2021).

Roseau cane dieback has been observed in the past few decades, and the death of coastal marsh grass has been widespread in North America, Europe, and Asia (Knight, *et al*, 2018). Coastal officials and scientists start to pay intensive attention to studying and monitoring the Roseau cane dieback. The first cases of Roseau cane dieback in the MRD were reported around the fall of 2016 (Knight, *et al*, 2020). The dieback was presumed caused by a scale insect named *N. biwakoensis* (Suir, *et al*, 2018) or Roseau cane scale (RCS). Current observations suggest that Roseau cane diebacks are often followed by wetlands converted to open water, other wetland vegetation becoming dominant species, and in rare cases a return to healthier and robust stands of Roseau cane (Harris, 2020). Such different scenarios likely relate to differences in flooding stress, salinity stress, and/or the number of previous dieback events (Knight, *et al*, 2020).

Figure 1. Roseau cane dieback in the lower Mississippi river delta

Mapping the distribution of Roseau cane and assessing the impact of RCS on different host plant species is critical for managing this emerging crisis. Since 2016, scientists from institutes including Louisiana State University (LSU) and the United States Department of Agriculture (USDA) initiate the preliminary remote sensing-based method to monitor the health condition change in the MRD to detect the impact of scale invasion (Schneider, *et al*, 2019). The introduction of remote sensing technology including satellite and drone images effectively increased the speed of investigation in the MRD and serve the need for ecologists. While it is well-known that RCS have caused Roseau cane dieback in the MRD in recent years, how much of this dieback is the result of the macro-environmental changes and disturbances from other factors is still unknown and challenging to quantify. The application of large-scale satellite data analysis significantly benefited the investigation of the MRD. Analysis of satellite imagery by the US Army Corps of Engineers suggests diebacks may have begun earlier than 2016, and the analysis of NDVI change between years gives some indication of the severity of the Roseau cane dieback in the delta area (Suir, *et al*, 2018).

1.2. Research Questions

Mapping the Roseau cane habitat is critical to assess the spatial distribution of Roseau cane, its growth status, and its interactions with other wetland plants in response to wetland disturbances and environmental changes. Remote sensing monitoring of coastal wetland vegetation normally required long-term observations. Considering time traceability, data availability, and data spatial resolution, Landsat is the best data source for long-term large-scale research (Li, *et al*, 2021). In the wetland areas, there is also a phenomenon of mixed Roseau canes with other vegetation. The normally used Landsat series images often contained mixed pixels, making it difficult to obtain high-precision Roseau cane distribution information especially when there are multiple variants of Roseau cane coexist. Considering the limitation of hyperspectral imagery due to availability and high cost, storage, and data processing, developing methods for using high-resolution satellite and drone mapping of Roseau cane subspecies is highly desirable and valuable. Benefiting from the development of satellites, high-resolution satellite imagery, such as Worldview is more suitable for the classification of mixed vegetation. In the face of large-scale and high-frequency classification requirements of coastal salt marsh vegetation, spectral features of vegetation are difficult to distinguish from the coarse-resolution images. Furthermore, separating coastal wetland vegetation species is challenging with limited spectral bands and difficulty to get ground truth observation in wetlands. The remote sensing system of the drone or low-altitude unmanned aerial vehicle (UAV) has become increasingly popular and gradually applied in land mapping, which is a powerful supplement to satellite remote sensing and manned aerial remote sensing.

Current studies indicated limited awareness of the healthy status of Roseau cane and difficulty in mapping dieback areas in the MRD over a long period due to relatively high water dynamics, and most of the research is carried out at a single scale level, with various research methods and technologies, and a systematic multi-source observation method for Roseau cane has not yet been formed. This makes it difficult for geographers and ecologists or wetland managers with different scientific research and management purposes to choose remote sensing technologies and methods for Roseau cane monitoring. In addition, there are two major variants of Roseau cane in the MRD which showed significant differences in resistance with the scale infection (Cronin, *et al*, 2020). Fragmented coastal wetlands require studies based on high-resolution imagery while separating variants of Roseau cane with limited spectral bands is usually challenging for traditional methods. In general, this research will address these key research questions.

i. If the Roseau cane dieback distribution in the lower MRD can be assessed by large-scale remote sensing images such as Landsat? Is there any anomaly in Roseau cane in recent 20 years?

ii. Whether the distribution change of Roseau cane can be detected in the MRD through Landsat Archived imagery? Whether Roseau cane suffered more damage than other vegetation in the MRD?

iii. Given the condition of fragmented coastal wetlands, is it possible to map wetland habitat and Roseau cane distribution using high-resolution multispectral WorldView imagery? Is it possible to separate the variants of Delta and European Phragmites from this dataset?

iv. Can we develop a flexible and rapid mapping and monitoring solution for Roseau cane dieback and habitat mapping based on drone and multispectral cameras? What are the vegetation changes in the study site in the past year, especially after

Hurricane Ida damage happened in 2021?

1.3. Objectives

To solve these research questions, this research has set the following objectives:

i) Conduct a large-scale assessment of historical land/vegetation coverage change in the lower MRD based on Landsat Archived imagery to provide the macro wetland changes patterns in the past two decades in comparison to the changes in Roseau cane areas in selected years based on data availability and water level recording.

ii) Assess the overall trend of dieback in the lower MRD and identify areas with most dieback.

iii) Test the capability to map Roseau cane distribution at a large scale through Landsat imagery and ancillary data and conduct large-scale Roseau cane change analysis.

iv) Experiment to map Roseau cane habitat distribution in a mid-scale moderate extent of major river outlets based on the first high-resolution multispectral WorldView satellite imagery and test its capability to separate Roseau cane variants.

v) Develop a rapid, multi-seasonal, and small-scale drone mapping solution to monitor Roseau cane habitat dynamics and test the capability to map Roseau cane variants through drone sensors.

1.4. Contributions and Significance

Considering the limitation of hyperspectral imagery due to availability and high cost, developing methods for using high-resolution satellite and drone mapping of different Roseau cane variants and habitat dynamics is highly desirable and valuable. Also, it is worthwhile to examine the linkage between the dieback area and the response from different vegetation classes.

To conduct a comprehensive investigation of the spatial and temporal heterogeneity of Roseau cane in the MRD, this research proposed a comprehensive multi-source remote sensing study in this research. The major contributions of this research include:

i. Besides assessing the overall wetland dieback, this study also successfully extracted the spatial distribution of Roseau cane and compared Roseau cane dieback with the overall wetland dieback. The final analysis result revealed that Roseau cane has undergone much more severe damage than other non-Roseau cane vegetation in the MRD in recent years.

ii. Classification based on high-resolution multispectral imagery successfully generated vegetation habitat mapping and differentiated Roseau cane variants. The result also cross-validated the Landsat-derived Roseau cane distribution.

iii. This research developed a drone mapping solution by combining field sampling with a drone sampling approach to overcome the significant challenges of limited accessibility in coastal wetlands and lack of sufficient samples. This method not only makes reliable wetland habitat mapping possible but also provides a solution to rescue data from past field trips that lack sufficient samples for classification.

As a result, the application of multi-source remote sensing data analysis will greatly increase the wetland manager's awareness of the spatial distribution and overall health status of Roseau cane. It could help them identify the severe dieback areas and increase their capabilities in response to further dieback events.

Chapter 2. Literature Review

In recent years, the acceleration of the development of human society has led to the deterioration of the ecological environment, especially in coastal areas. The coastal wetland vegetations mostly grow near water. With complex and diverse structure types, they are one of the most fragile and economically valuable ecosystems (Kaplan *et al*, 2017). Considering that coastal wetland vegetation plays a vital role in ecosystem and is indispensable to the protection of the coastal areas, acquiring accurate and timely dynamic change of vegetation coverage is necessary for wetland management (Gedan *et al*, 2011). With increasing attention paid to ecological issues, many studies focusing on monitoring the coastal wetlands vegetation have emerged (Berni *et al*, 2009; Watts *et al*, 2012). The research purpose of these studies includes guiding wetland protection/restoration decisions.

2.1. Roseau cane dieback

The term "dieback" refers to biotic (such as disease) or abiotic (such as temperature) factors leading to the gradual death of the above-ground parts of plants from the top down (Mueller-Dombois, 2008). Taking the Roseau cane dieback in wetland ecosystem in North America as an example, its typical characteristics are the above-ground part of the Roseau cane turns chlorosis from the top down, withered, and died rapidly in a short period (Alber *et al*, 2008; Elmer *et al*, 2013).

Although Roseau cane dieback is widely spread in a variety of ecosystems around the world, the related mechanism of its outbreak is still unclear (Beaudette, 2020). Among many abiotic factors, the weather conditions have a profound impact on ecosystem structure and processes, and many processes related to climate factors may result in dieback. For example, an increase in global temperature may cause some regions to become unusually drought, and plants respond to drought by adjusting their physiological behavior, which will eventually lead to the death of plants (DaMatta *et al*, 2006). In addition, salinity, soil physicochemical properties, nutrient availability, and toxic substance content also could affect plant growth (Knight, *et al*, 2020). Under these unfavorable conditions, the plants could become more sensitive, fragile, and prone to death.

In addition to the abiotic factors, more studies have found that biotic factors, such as invasive species, play a more important role in the occurrence of Roseau cane dieback. The invasion of a scale insect named *N. biwakoensis* might cause the major Roseau cane dieback in the MRD region (Suir, *et al*, 2018). This scale could cause similar dieback symptoms under 2 years round controlled experiment (Knight, *et al*, 2020). In addition, the plant's conditions, such as genetic diversity and adaptability to the environment, also affect the occurrence of dieback. A team of researchers in Europe, the Netherlands, and Germany found that Roseau cane populations with lower genetic diversity were more prone to dieback (Brix, 1999). Furthermore, the research team from LSU found that the dominant variant of Roseau cane in the MRD, the Delta Phragmites variant is more vulnerable to dieback when facing scale infection compared with the European Phragmites variant, which might have a profound impact on the wetland vegetation cover change in the future (Knight, *et al*, 2020).

Most previous research produces the result from field and aerial surveys (Li *et al,* 2020). Due to the unique location and complexity of the coastal wetland vegetation, the investigation of these regions is costly and challenging. The fragmented nature of the coastal wetland also restricted the relatively large-scale study of the landscape functional characteristics and spatial pattern changes (Carle *et al*, 2014), which also limited our ability to detect the Roseau cane dieback. To solve this problem, this research introduced multi-source remote sensing technology for wetland vegetation monitoring and dieback identification.

2.2. Wetland Vegetation Monitoring and dieback identification Based on Remote Sensing

Historically, aerial photography was the first remote sensing method used to assist the wetland vegetation investigation (Sharitz, 1986). However, it is costly and time-consuming to map and monitor wetland vegetation on a regional scale by aerial photography. In the mid-1970s, the appearance of satellite remote sensing greatly improved the method of collecting spatial-temporal data (Xie *et al*, 2018). Since then, remote sensing technology had entered an era of rapid development, including the advance of sensors with various spectral and spatial resolutions and the use of multiple remote sensing satellites with various orbits and revisit periods. The precision of remote sensing data was also greatly improved due to the synchronous development of algorithms and computer technology, and the hardware cost of data processing is correspondingly reduced. Therefore, multi-spectral and multi-temporal remote sensing data became available in various fields of coastal environmental research. Up to now, remote sensing technology has become the main source of coastal surface cover information extraction, landscape type change detection, and biological invasion monitoring, and has been successfully applied to vegetation classification and mapping (Kumar *et al*, 2015).

2.2.1. Large-scale optical Remote sensing for dieback detection

Optical remote sensing image data is the most widely used remote sensing data for large-scale coastal wetland vegetation study due to its large historical archived dataset, relatively mature and diversified classification methods, and rapid data acquisition period. Previous scholars have used optical images to study the distribution of salt marshes in the coastal zones and achieved a relatively high classification accuracy of the coastal wetland vegetation species. Remote sensing technology is also the main method for ecologists to obtain large-scale and multi-scale geographic and ecological data (Hu *et al*, 2015). The most widely used dataset is Landsat. The spatial resolution of Landsat is 30m, but the temporal resolution is relatively low (1 scene in 16 days), and the images are greatly affected by the atmosphere. Case studies like Liu used Landsat images to extract the distribution of Spartina alterniflora in China's coastal zones in 1990, 2000, 2013, and 2018 (Liu *et al*, 2022). Xu detected the boundary of the salt marshes in Jiangsu coastal zones based on the Landsat images and calculated their ecosystem service values (ESV) of them (Xu, 2016).

For the dieback detection, O'Donnell successfully extracted the biomass decline of S. alterniflora caused by dieback events based on 25 years Landsat Archived dataset in the Georgia coast region (O'Donnell *et al*, 2016). Li combined 20 years of Landsat-derived NDVI with a stacked autoencoder neural network to identify the dieback in the North Inlet-Winyah Bay, South Carolina. (Li *et al*, 2020). The NDVI-based dieback detection proved effective in large-scale coastal wetland vegetation coverage change research.

2.2.2. High-Resolution Remote sensing for Wetland Vegetation Research

Wetland vegetation classification is an important direction of wetland vegetation remote sensing research, which can be used to accurately grasp the dynamic changes of wetland vegetation spatial distribution and identify the dieback area through classified dead vegetation coverage. However, the research is normally limited by the spatial resolution and spectral resolution of remote sensing images, and there will be issues that "same object with different spectrum" and "different object with the same spectrum" (Ren *et al*, 2019). Belluco used ROSIS, CASI, MIVIS, IKONOS, and QuickBird remote sensing data to obtain vegetation maps through unsupervised K-means and supervised algorithms. His result proved that spatial resolution affected classification accuracy more significantly than spectral resolution (Belluco *et al*, 2006).

At present, the data used for remote sensing monitoring of coastal wetland vegetation has gradually changed from moderate-resolution satellite data such as Landsat and SPOT to high-resolution satellite imagery, such as Worldview serials data and QuickBird. Sebastien Rapinel (Rapinel *et al*, 2015), Wang (Wang *et al*, 2021), and Liu (Liu *et al,* 2016) used moderate-resolution data for their studies, while other scholars using high-resolution data, such as Thomas Richard Allen (Richard *et al*, 2013) and Zhou (Zhou *et al*, 2016), concluded that the high-resolution data were more suitable for the classification of mixed vegetation. Although the resolution of moderate-resolution remote sensing images is not as good as that of high-resolution data, it is still suitable for large-scale research due to the free-of-cost-to-purchase datasets. In addition, scholars also started to explore the applicability of the fusion of high-resolution remote sensing data with other remote sensing data in wetland vegetation research. Amani et al. conducted wetland vegetation classification based on multi-source and multitemporal satellite data methods (Amani *et al*, 2017). Besides, hyperspectral, LiDAR, and aerial imaging techniques have been gradually applied to the extraction of wetland vegetation in small-area investigations (Pande-Chhetri *et al*, 2017).

2.2.3. Wetland Vegetation Classification Methods

In terms of the application of remote sensing classification methods in wetland research and dieback detection, Maximum Likelihood Classification (MLC), Support Vector Machine (SVM), Decision Tree model (DT), K-Nearest Neighbor (KNN), and Neural Network (NN) are the most used method. Wang extracted the Normalized Difference Vegetation Index (NDVI) and Vegetation Water Index (VWI) derived from Beijing-1 data and implemented the vegetation classification of the Poyang Lake wetland by using SVM (Wang *et al*, 2012). Jing used a visible light vegetation index to establish decision tree rules to extract aquatic vegetation in the study area (Jing *et al*, 2016). Besides, some scholars used multi-temporal remote sensing images to classify wetland vegetation based on the seasonal growth cycle of wetland vegetation. Dechka used IKONOS-2 images in spring and summer to analyze NDVI and extract texture features to differentiate the wetland vegetation species (Dechka *et al*, 2002). Davranche used a binary classification tree algorithm to estimate the area of the Roseau cane and submerged plants in the Ganges and Indus River basins based on multi-temporal SPOT5 images (Davranche *et al*, 2010). Laba used QuickBird data to extract invasive vegetation and Roseau cane in 4 wetlands located in the Hudson River using the MLC (Laba *et al*, 2008). Zhang used an object-oriented method to analyze Hyperion data and identified 14 plantation communities in the Kissimmee River Valley wetland in South Florida through machine learning classification (Zhang *et al*, 2013).

Some vegetation in coastal wetlands is annual herbaceous plants, which undergo a complete phenological cycle including the germination, growth, and wilt in a year. The plant morphology and chlorophyll content change constantly. Many studies have shown that the different characteristics of salt marsh vegetation at different seasons can be reflected in the difference in its spectral characteristics (Hladik *et al*, 2013). Based on this characteristic, Fernandes successfully separated the Roseau cane from other wetland vegetation species (Fernandes *et al*, 2013).

2.3. Drone-related study in wetland vegetation monitoring

Optical images in coastal zones are greatly affected by cloud cover and tidal inundation, and the availability of optical remote sensing data is often sparse and uneven, so it is difficult to obtain appropriate seasonal phase images throughout the year. For long-term monitoring, the frequency of marsh data updates in some areas is more than three years. For the rapidly changing coastal area, there are still gaps and challenges in obtaining salt marsh information (Sun *et al*, 2018). In recent decades, the drone-based remote sensing system has become a powerful research tool for wetland vegetation investigation. This kind of low-altitude remote sensing system with high flexibility, high efficiency, high resolution, and low-cost features could meet the requirements of geographical spatial information acquisition in the fragmented coastal zone area. As an effective supplement to satellite remote sensing and conventional aerial photogrammetry, drone remote sensing system has the advantages of high mobility, high timeliness, high resolution, and low cost in the application research of drone remote sensing in island coastal zone monitoring (Colomina *et al*, 2014).

Compared with satellites, the drone can observe a smaller research area at any time with fewer restrictions and obtain hyperspectral images quickly (Cao *et al*, 2020). In addition, compared with satellite platforms, the flight observation height of drones on low-altitude remote sensing platforms greatly reduces the distance between sensors and ground objects, and the spatial resolution of acquired image data can reach centimeter-level. Due to the advantages of low cost, high operational flexibility, high spatial resolution, and high spectral resolution in the data acquisition work of the UAV platform, the platform makes many manual remote sensing data acquisition tasks faster and more time-efficient (Li *et al*, 2019), however, the application of a drone to obtain spatial information of the wetland is not perfect. There is also still a limitation in the field work procedure, such as the limitation of flight time and the fragmented ground environment with restricted access to the land targets. Thus, the study of drone mapping with insufficient ground samples has great value for fieldwork.

In general, with the increasing diversification of remote sensing data, the efficiency of vegetation status detection and classification accuracy is constantly improving. The combination of multi-source remote sensing data and classification method is beneficial for coastal wetland vegetation monitoring and dieback detection.

2.4. Methodology Overview

This research involves the usage of Landsat satellite imagery, high-resolution Worldview satellite imagery, and modern multi-spectral drone technology, combined with auxiliary data including aerial photos accessed from the National Agriculture Imagery Program (NAIP) and hourly water level recording from the Coastwide Reference Monitoring System (CRMS).

For large-scale Roseau cane monitoring, this research collected 20 years historical Landsat imagery. Comparing multiple thresholds of land/water and vegetation boundaries based on various vegetation indices, the most accurate one was applied to generate historical vegetation coverage change in the lower MRD. Then dieback area was detected based on vegetation index change. The vegetated area will also be classified as Roseau cane versus non-Roseau cane based on corresponding aerial photos for further analysis.

For mid-scale wetland vegetation habitat mapping based on high-resolution satellite imagery, this research selected and experimented with multiple pixel-based classification methods to classify Roseau cane habitats and other wetland vegetation using Worldview image, especially the two major variants in the region. The SVM method have the highest accuracy in the classified results. In addition, the classified distribution of the Roseau cane area is used for further validating the corresponding Landsat classification result and checking whether there is a significant difference in the distribution of these two variants of Roseau cane in the dieback area.

For the small-scale drone mapping with rapid surveys, this research conducted multi-season field data collection and developed a new sampling strategy to map wetland habitats based on high resolution drone image. Using a second drone to get drone sampling points with fewer spectral bands and higher resolution could greatly improve the classification method, especially in a situation with restrained field access to sufficient sampling points.

Chapter 3. Study Area and Data Collection

3.1. Lower Mississippi River Delta

The study site is located at the lower Mississippi River Delta as showed in Figure 2. The Mississippi River has a total length of about 6,260 km and is the longest river flowing in North America. It is the fourth-longest river (in length) and the fifteenth-largest river (in volume) in the world (Mehlhorn *et al*, 2019). The Mississippi River basin (including the Atchafalaya River basin) covers an area of 3.34×10^6 km^2, accounting for more than 40% of the continental area of the United States (Piazza, 2014). The total amount of freshwater flowing into the Gulf of Mexico is around 450 km^3 per year (Tweel *et al*, 2012). The Mississippi River forms a subtropical landscape consisting of rivers, wetlands, and small islands on the lower coast, flowing south into the Gulf of Mexico. At the edge of the delta, the Chandeleur Islands provide protection against ocean storms in the densely populated coastal areas of Louisiana, including New Orleans. In the Mississippi River estuary, several strands composite the bays of the river branch and enter the sea, the sediment accumulation in each branch exceeds the erosion rate of the waves, then the sediment deposition extends along the branches, forming large sediment bars that branch out into the sea and forming the lower Mississippi River delta which is like birds' feet from the view of the satellite (Blum and Harry, 2012). The delta region is relatively low and flat, with an elevation of -3 ~ 2 m relative to sea level. Over the past century, at least 37 major floods have occurred in the Mississippi River, leading to the distribution of wetlands and depressions on both sides of the riverbank (Coleman *et al*, 1998).

The waterbodies within the Mississippi River Delta are a natural wildlife breeding ground. The river carries a large amount of organic matter into the bay, creating a nutritious environment for fish, shrimp, shellfish, and other wildlife to breed and grow. The Mississippi Delta provides a range of natural habitats and resources that are beneficial not only to Louisiana and the coastal areas but to the entire United States. The coastal area has a variety of wetland landscapes, connecting the land and the sea. Louisiana wetlands are one of the most productive and important natural resources in the United States (Costanza *et al*, 1989; Elsey-Quirk *et al*, 2021). Natural embankments, barrier islands, forests, salt marshes, and other areas constitute a complex ecosystem and habitat.

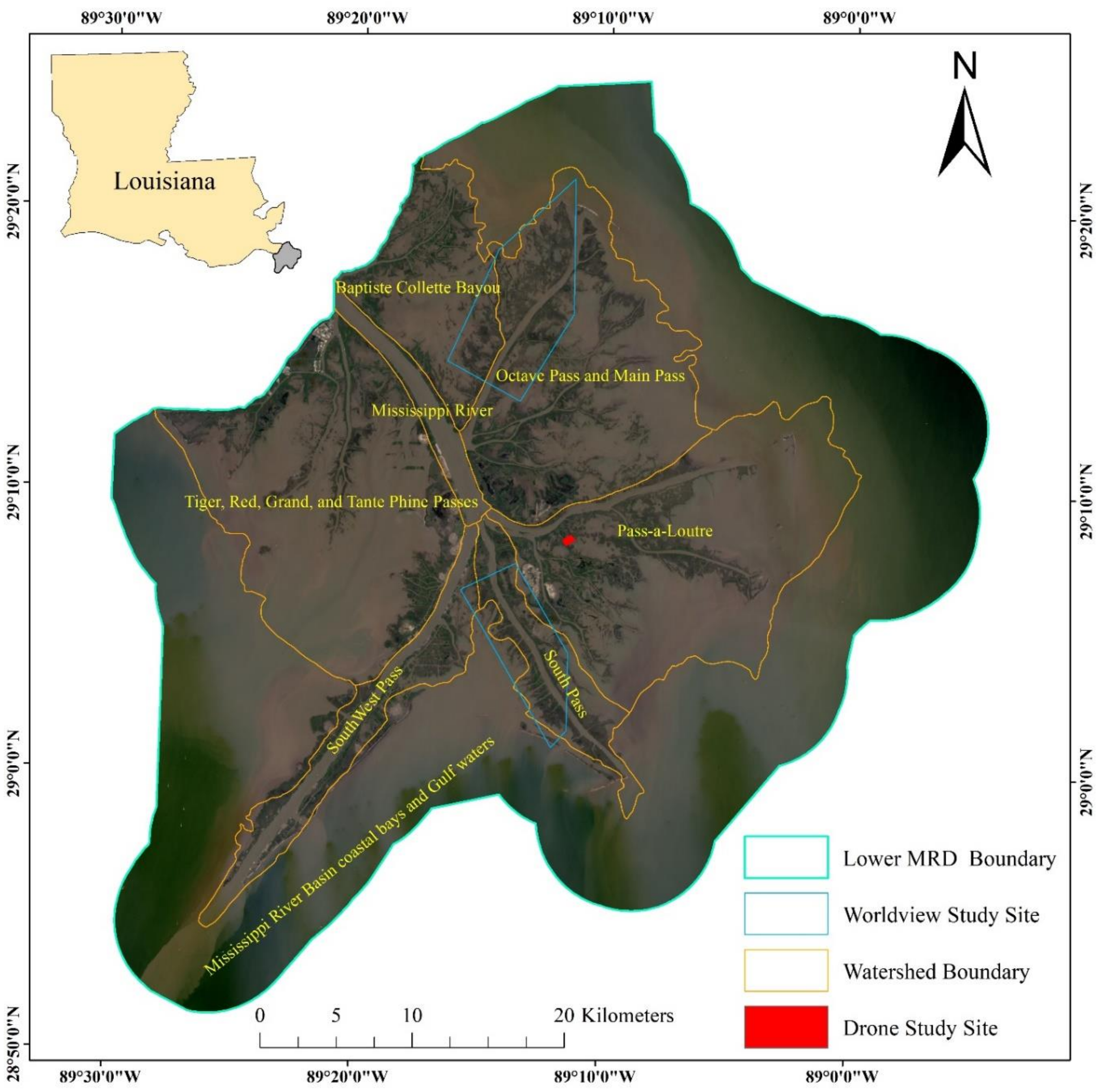

Figure 2. The study area of the MRD

In the MRD, wetland vegetation is a critical and rapidly changing landscape. Roseau cane is a perennial plant, with a stem height of around 1-3 m. The leaves are lanceolate and linear, normally around 30 cm long, and 2 cm wide. The Roseau cane flowers are highly recognizable and normally produced around late August, 15 - 40 cm long and 10 cm wide (Elias and Peter, 1990). Other typical vegetation species in the MRD include bull tongue, cutgrass, and cattail. From our plant survey conducted at our drone site starting in September 2020, the typical wetland vegetation species are listed in Figure 3.

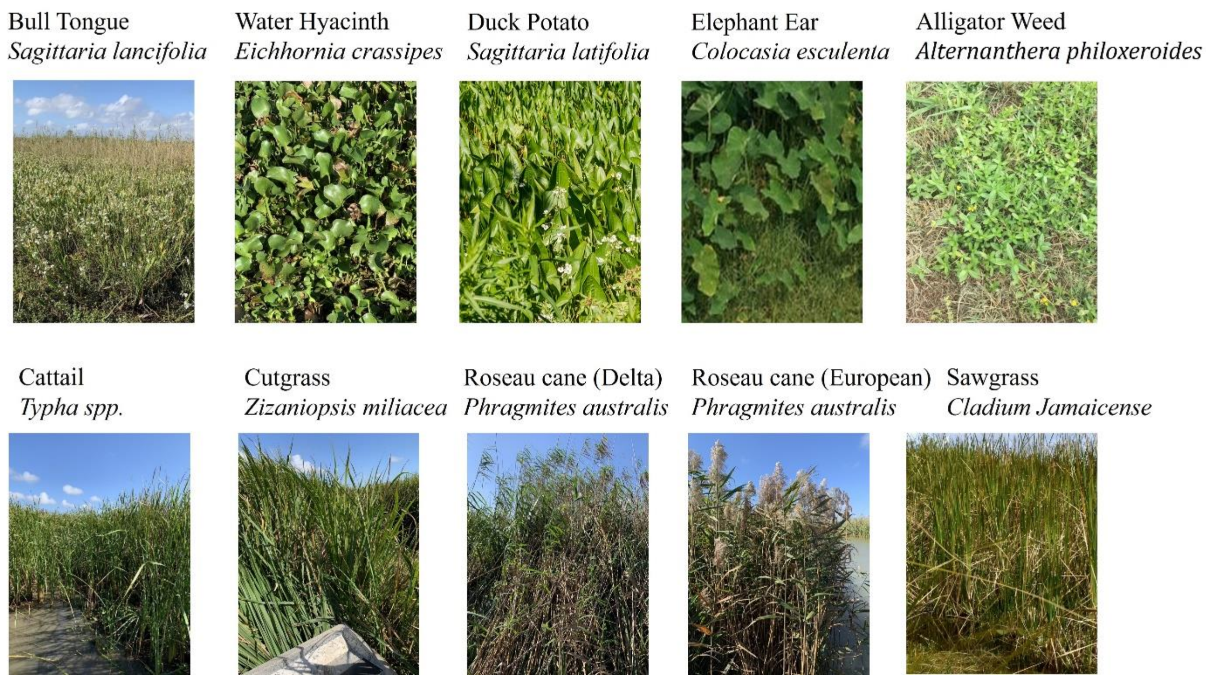

Figure 3. Typical wetland vegetation species in MRD

3.2. The datasets

To monitor the wetland in the region, this research proposes to conduct multi-source remote sensing-based integrated research. The primary data used for MRD-wide Roseau cane dieback monitoring is the Landsat dataset. This research collected 20 years (2001-2021) historical archived cloud-free multispectral Landsat collection 2 level 2 dataset product from the United States Geological Survey (USGS), the sensor including 30 m resolution Landsat 5 Thematic

Mapper (TM) images (2001-2012) and 30 m resolution Landsat 8 Operational Land Imager (OLI) images (2013-2021). The auxiliary datasets for the Landsat study include corresponding hourly CRMS water level recording and meter/sub-meter resolution NAIP aerial photos.

The dataset used for differentiating variants of Roseau cane is the Worldview-2 dataset. As the first high-resolution satellite sensor with multispectral bands, the Worldview series of imagery has gained wide attention for various research. The Worldview-2 satellite was first launched on October 6, 2009, and operates in a 770 km high sun-synchronous orbit, capable of providing 0.46 m resolution panchromatic images and 1.8 m resolution multi-spectral images. Worldview space-borne multi-spectral remote sensor not only has four standard spectral segments (Red, Green, Blue, and Near-infrared) but also includes four additional diverse spectral segments (Coast, Yellow, Red-edge, and Near-infrared), which will provide the ability to conduct accurate change detection and mapping (Upadhyay *et al*, 2012). For this study, this research purchased 0.5 m resolution pan-sharpened 8-bands multispectral Worldview images from Apollo Mapping company.

The drone datasets in this research mainly include multi-spectral datasets collected from the 10 bands Micasense Rededge-M/MX dual camera. The drone Platform used in the study is DJI 600 Pro which capable to fly for around 20 minutes with 1 set batteries. The flight height is 120 m with 75% overlap, the orthophotos generated could archive 8 cm resolution. A Phantom 4 RGB camera was also applied in the field survey, these datasets are collected at 40 m flight height which is available to produce 2 cm resolution orthophotos for drone sampling tests. In addition, multiple field surveys were conducted using cm-level RTK GPS to retrieve ground truth sample location for the research.

Chapter 4. Large-scale Assessment of Wetland and Roseau Cane Dieback Based on Landsat imagery

4.1. Introduction

Since 2016, there is a break of dieback events reported in lower MRD associated with scale infection, and its impact may be traceable to longer history (Suir, *et al*, 2018). There is a strong need to conduct a long-term MRD-wide survey of vegetation to assess the macro-environmental change for the Roseau cane habitat through historical vegetation/land change detection, however, traditional methods face the challenge of lack of sufficient data archive. Landsat is a continuous Earth Observation satellite program developed under a joint program of the USGS and NASA. The Landsat program has an extremely long duration and provides abundant data through multi-spectral sensors. Its data are relatively stable, have global coverage, and are easy to obtain. This research proposed using Landsat as the primary dataset for long-term large-scale wetland monitoring in lower MRD.

For historical vegetation/land dynamic change, it is important to detect the accurate vegetation/land boundary. Theoretically, the segmentation thresholds of the vegetation/water body indices are all 0. However, some studies have shown that in practice, it is still necessary to adjust the threshold according to the specific scene to achieve optimal segmentation results (Ji *et al*, 2009). This study will test the adjusted threshold method in lower MRD and check whether it is still capable of achieving higher accuracy than the normal threshold.

The distribution and dieback of wetland vegetation have vital value for the wetland manager to oversee the entire region and is beneficial for designing better protection and restoration plan in the MRD. To deal with the challenge of intense water level dynamics and its impact on vegetation and land appearance in coastal regions, this study first examined water levels for all Landsat images in the past two decades and found the images from 2010 and 2019 are the most suitable dataset for dieback assessment. The images will extract the vegetation coverage based on the adjusted threshold values of vegetation indices. Then, NDVI-derived statistical thresholds were applied for dieback assessment on these vegetation coverage areas.

Due to the challenge to identify vegetation species from coarse resolution images, separating Roseau cane from other wetland vegetation species typically requires large-scale field sampling of vegetation types, which is challenging for coastal wetlands due to its fragmentation characteristics, limited accessibility, and high costs. One objective of this chapter is to test the hypothesis of whether this study can extract large-scale Roseau cane distribution through Landsat imagery with the support of high-resolution aerial photos. If the hypothesis is true, it will allow this research to compare the overall wetland dieback with mixed vegetation to those diebacks from Roseau cane.

4.2. Method

The overall objective of this section is to introduce a research method to monitor the wetland vegetation coverage change throughout the lower MRD based on moderate-resolution remote sensing data (Landsat). This chapter introduce the method and results of a large-scale assessment of wetland and Roseau cane dieback based on Landsat images. The workflow consists of three main stages shown in Figure 4. After collecting and preprocessing all the historical archived datasets, stage 1 of this section compared multiple water/vegetation boundary extraction thresholds based on the vegetation/water index combination. These thresholds will be validated through the randomly generated points from corresponding NAIP aerial photos and selected as the best-fitting one to generate 20 years of land/vegetation coverage products in lower MRD. Stage 2 will introduce the NDVI-derived dieback detection method to identify the anomaly region of the study area based on the vegetation coverage extracted from the last step. In this stage, image pairs (2010, 2019) were selected referencing CRMS water level recording and available NAIP aerial photos. Stage 3 will conduct SVM classification of Landsat images with the training samples from the interpretation of auxiliary NAIP aerial photos to distinguish Roseau cane and non-Roseau cane vegetation types. After the generation of all the datasets, a statistical assessment was conducted on the vegetation coverage changes and dieback conditions in the lower MRD.

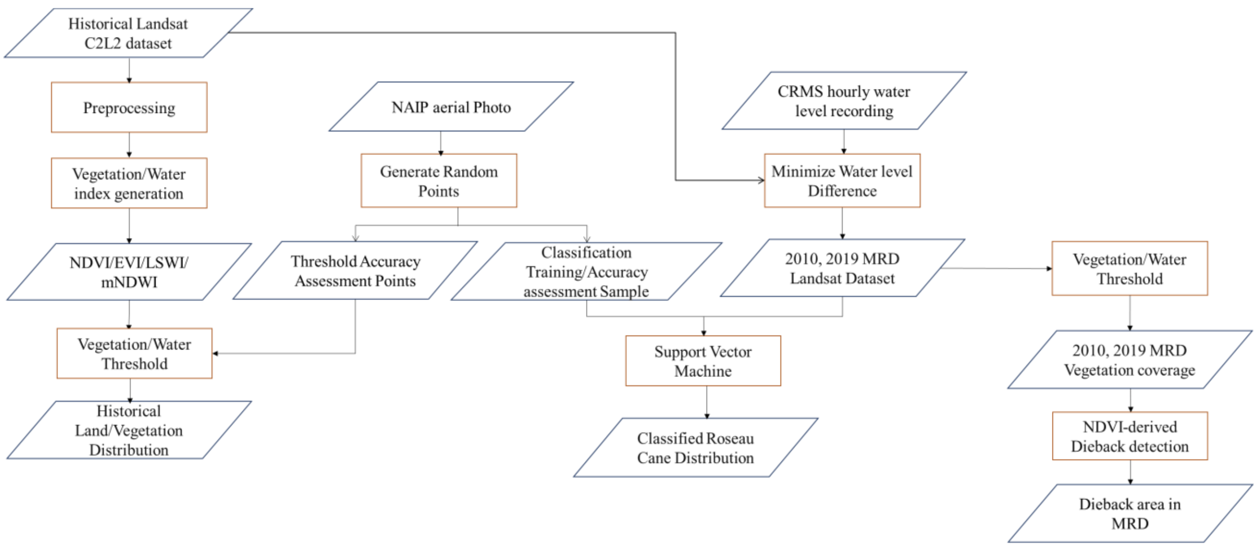

Figure 4. Workflow for Landsat-based wetland historical vegetation coverage change and dieback assessment

4.3. Dataset and pre-processing

The primary data we used for large-scale wetland and Roseau cane dieback monitoring is the Landsat dataset. We also collected corresponding NAIP images for the accuracy assessment of the newly adjusted threshold values and used them to generate training/accuracy assessment samples for the classification of Roseau cane. In addition, we collected water level data from CRMS for the selection of images with minimal water level differences.

Launched on March 1, 1984, Landsat 5 was designed and built at the same time as Landsat 4 and carried the same sensor: Thematic Mapper (TM) and Multispectral Scanner System (MSS).

In November 2011, the TM sensor ceased operation due to aging electronics, and a few months later engineers turned the MSS sensor back on (Wulder *et al*, 2016).

Launched on February 11, 2013, Landsat 8 carries two sensors, OLI (operational land imager, land imager) and TIRS (thermal infrared sensor, thermal infrared sensor). The images acquired by the OLI land imager were used in this study. The Landsat 8 OLI image includes 9 bands, one panchromatic band with a resolution of 15 m and eight multispectral bands with a resolution of 30 m, with an imaging width of 185 km×185 km. The spatial resolution of the images acquired by the TIRS thermal infrared sensor is 100 m, this dataset was not used in our study. Compared with the previous Landsat series satellites, the red, near-infrared, and short-wave infrared bands on Landsat 8 are narrowed, the radiation resolution (radiation resolution) is increased to 16 bits, and the signal-to-noise ratio (signal-to-noise ratio) is improved. These improvements increased the vegetation discrimination capability of the Landsat 8 satellite.

Table 1. Bands information on Landsat satellite dataset

	Landsat-5	**Landsat-8**
Sensor	TM	OLI
Lunch date	March 1984	February 2013
Spatial Resolution (m)	30	30
Band name	**Bandwidth (μm)**	
Coastal aerosol	N/A	0.43-0.45
Blue	0.45-0.52	0.45-0.51
Green	0.52-0.60	0.53-0.59
Red	0.63-0.69	0.63-0.67
Near Infrared (NIR)	0.77-0.90	0.85-0.87
Short-wave infrared 1 (SWIR 1)	1.55-1.75	1.56-1.65
Short-wave infrared 2 (SWIR 2)	2.08-2.35	2.10-2.29
Repeat-Cycle	16 days	16 days

The USGS published Landsat Collection 2 dataset in 2020. Collection 2 datasets include Level 1 and Level 2 data, no subscription is required, and can be downloaded directly at query time. Collection 2 Level 1 data has improved the accuracy of geometric correction and radiometric calibration comparing to Collection 1 Level 1 data. In particular, the accuracy of geometric corrections has been greatly improved with the introduction of a new version of ground control points (GCPs Phase 4). GCPs Phase 4 combines the control points of Landsat 8 and ESA's Sentinel-2, which greatly improves the accuracy of image ensemble correction. Unlike the ordered Collection 1 Level 2 data (except for the US), the Collection 2 Level 2 data includes both surface reflectance in the multispectral band and surface temperature in the thermal infrared band. The algorithm used for atmospheric correction has also been improved. The algorithm for processing Landsat 8 images is the Land Surface Reflectance Code (LaSRC) algorithm (version 1.5.0), and the algorithm for processing Landsat 4-7 images are the Landsat Ecosystem Disturbance Adaptive Processing System (LEDAPS) algorithm (version 3.4.0). The DN value of the Collection 2 level 2 dataset image needs to be multiplied by 0.0000275 (scale factor) and then subtracted by 0.2 to convert to the value of surface reflectance. For example, if the DN value of the image multispectral band of Collection 2 Level 2 is 32000, then the reflectance value of this pixel is 0.68. This research collected 38 scenes of cloud-free Landsat C2L2 images from USGS spanning from 2001 to 2021. The Landsat images are listed in Table 2.

Table 2. Cloud-free Landsat images in lower MRD from 2001 to 2021

Sensors	Year	Month	Day	Start Time (GMT)	End Time (GMT)
Landsat 8 OLI	2021	4	21	16:25	16:26
	2021	4	5	16:25	16:26
	2021	3	4	16:26	16:26
	2021	1	15	16:26	16:26
	2020	4	2	16:25	16:26
	2019	10	9	16:26	16:26
	2019	9	7	16:26	16:26
	2019	4	16	16:25	16:26
	2019	1	10	16:25	16:26
	2018	4	29	16:25	16:25
	2018	4	13	16:25	16:25
	2016	4	23	16:25	16:26
	2016	4	7	16:25	16:26
	2016	3	22	16:25	16:26
	2016	1	18	16:26	16:26
	2015	10	14	16:26	16:26
	2014	12	14	16:26	16:26
	2014	11	28	16:26	16:26
	2014	1	12	16:27	16:27
	2013	10	24	16:27	16:28
Landsat 5 TM	2011	10	3	16:14	16:14
	2010	10	16	16:16	16:16
	2010	9	30	16:16	16:16
	2009	1	30	16:11	16:12
	2008	10	26	16:09	16:10
	2008	3	16	16:16	16:16
	2007	1	25	16:21	16:21
	2006	11	22	16:20	16:21
	2005	10	18	16:14	16:14
	2005	9	16	16:14	16:14
	2004	10	15	16:10	16:11
	2004	3	21	16:05	16:05
	2004	2	18	16:05	16:05
	2003	11	14	16:04	16:04
	2003	3	19	15:59	16:00
	2003	1	14	15:58	15:58
	2002	12	29	15:58	15:58
	2001	12	26	16:05	16:05

The orthophoto aerial images mainly used in this research are provided by the National Agricultural Imagery Program (NAIP). The NAIP began in 2003 with the primary goal of making digital orthophotos available to government agencies and the public within a year. NAIP imagery is administered by the U.S. Department of Agriculture (USDA). The dataset can be used for crop hazard measurement, change detection, land classification, forestry management, and environmental investigation. The NAIP image data are high-resolution aerial images (1 meter GSD), including 4 spectral bands: blue band: 400 ~ 580 nm; green band: 500 ~ 650 nm; red band: 590 ~ 675 nm; and near-infrared band: 675 ~ 850 nm. The NAIP image is mostly collected from the crop growing season, generally from May to October in a 5-year cycle (after 2009, it changed into a 3-year cycle), the cloud cover is less than 10%, and the solar elevation angle is the horizontal direction of the collection is greater than 30°. NAIP imagery is orthorectified and data quality is checked before the supplier delivers it to the user. To meet the experimental requirements of this paper, preprocessing operations include image mosaic and projection.

Coastwide Reference Monitoring System (CRMS) is a long-term wetland monitoring program funded by Coastal Wetlands Planning, Protection, and Restoring Act (CWPPRA) since 1990. This program has set up approximately 390 sites in the coastal area of Louisiana. The CRMS website provides hourly recorded water level data from 2008, which helps our research to select the Landsat dataset to minimize the difference of water level in the Landsat images for NDVI-derived dieback detection. ArcGIS is the major software platform used for conducting the processing procedure and further analyzing the result of these datasets in this research.

4.4. Task 1: Historical land and vegetated area dynamics in lower MRD

The purpose in this section is to assess the historical vegetation dynamics in the region to reflect the macro-environmental change for the Roseau cane habitat. In open ocean waters and estuarine wetlands, due to the lack of sufficient ground data, limited accessibility in wetlands, and high cost of field investigation, the application of remote sensing estimation is particularly important. Compared with the traditional field sampling methods, Landsat is a suitable image for that large-scale assessment which can provide vital information for monitoring the wetland species.

There are many methods for vegetation coverage and water body extraction, which can be roughly divided as the single-band method (Lu *et al*, 2011), the multi-band spectral relationship method (Gao *et al*, 2016), the vegetation/ water body index method (Xiong *et al*, 2010), and image classification method (Nghi *et al*, 2008). For example, based on Landsat MSS data, Shih used the density segmentation method and the unsupervised classification method to extract water bodies, and the difference in the accuracy of the results obtained by the two methods was about 3% (Shih *et al*, 2016). Barton used the AVHRR image to extract the water body and monitored the flood by using the ratio operation of the near-infrared and red bands (Barton *et al*, 2016). Lu Jiaju used the threshold method, the chromaticity discrimination method, and the ratio measurement method to extract the water body from the TM data, which could identify small water bodies (Lu *et al*, 1992). McFeeters found that the ratio operation between the green band and the near-infrared band can largely suppress the vegetation and highlight the information about the water body. Therefore, Normalized Difference Water Index (NDWI) was created based on these two bands and used for water extraction (McFeeters *et al*, 1996). Xu found that the short-wave infrared band can reflect more water features than the near-infrared band. Therefore, the short-wave infrared band was used to replace the near-infrared band to construct a modified Normalized Difference Water Index (mNDWI), which could achieve a better water body extraction result (Xu *et al*, 2005). In general, the vegetation/ water body index method, especially the several key vegetation/ water body indices listed below, is currently the most widely used algorithm in vegetation coverage extraction and water body extraction due to its simplicity and effectiveness. This research implemented this vegetation/water index method and selected the best-fitting index threshold in the study.

4.4.1 Vegetation and water indices for land and vegetated area extraction

1. Normalized Difference Vegetation Index (NDVI): NDVI calculates vegetation index within a value range between -1 to 1 based on a simple equation as below and is the most widely used vegetation index tested in various studies.

$$NDVI = \frac{R_{nir} - R_{red}}{R_{nir} + R_{red}}$$

Where R_{nir} and R_{red} represent the reflectance values of the red and near-infrared bands respectively.

2. Enhanced Vegetation Index (EVI): EVI is often used in areas covered by dense vegetation. The formula showed below:

$$EVI = 2.5 \times \frac{R_{nir} - R_{red}}{R_{nir} + 6 \times R_{red} - 7.5 \times R_{blue} + 1}$$

Where R_{nir}, R_{red}, and R_{blue} represent the reflectance values of the near-infrared, red, and blue bands. The range of the value is -1~1, and the range of normal green vegetation area is 0.2-0.8. The EVI is one of the main indexes used in the biophysical parameter products, which can reduce the influence of atmospheric and soil noise at the same time, and stably reflect the vegetation conditions in the measured area. The EVI can detect detailed surface vegetation characteristics. The range of the red band and the near-infrared band is narrower, which not only improves the ability to detect sparse vegetation but also reduces the influence of water vapor. At the same time, the application of the blue band corrects the scattering of atmospheric

3. Land Surface Moisture Index (LSWI): LSWI is the normalized value of the reflectance in the near-infrared and short-wave infrared bands. LSWI representation refers to the moisture content in the vegetation canopy, which has a wide range of applications in the extraction of wetland feature information. Its calculation formula is as follows:

$$LSWI = \frac{R_{nir} - R_{swir}}{R_{nir} + R_{swir}}$$

In this equation, R_{nir} is the near-infrared band; R_{swir} is the shortwave infrared band.

4. modified Normalized Difference Water Index (mNDWI): McFeeters proposed NDWI in 1996, namely:

$$NDWI = \frac{R_{green} - R_{nir}}{R_{green} + R_{nir}}$$

where: R_{green} is the green band; R_{nir} is the near-infrared band (McFeeters *et al*, 1996). NDWI mainly utilizes the characteristics of strong water absorption and almost no reflection in the near-infrared band, while vegetation reflectivity is very strong. However, since NDWI only considers vegetation factors, ignoring the two important features of buildings and soil, when extracting water body information through NDWI, the reflectivity of the green band is much higher than that of the near-infrared band, so the extraction results inevitably contain many mixtures pixel, especially soil and building object, the accuracy will decrease. Based on the analysis of NDWI, Xu modified the band combination that constituted the index, replaced the near-infrared band in NDWI with the short-wave infrared band (SWIR), and proposed mNDWI, which showed below:

$$mNDWI = \frac{R_{green} - R_{swir}}{R_{green} + R_{swir}}$$

The spectral characteristics of shadows such as buildings in the green band and near-infrared bands are similar to water bodies (Xu *et al*, 2005). When the short-wave infrared band replaced the near-infrared band, the contrast between the calculated indices of water and buildings can be significantly enhanced, and the difference between these two objects can be greatly increased. Xu conducted experiments with this index on remote sensing images containing different types of water bodies, and most of them obtained better results than NDWI (Xu *et al*, 2005). The experiment also found that mNDWI can reveal the small-scale features of water bodies, such as the distribution of suspended sediments, and changes in water quality compared with the NDWI.

4.4.2. Determine thresholds for land and vegetated area mapping

The vegetation/water body index can highlight the spectral difference between the vegetation coverage and water body with other land objects, but to extract the exact vegetation/water boundary, the index image needs to be segmented by threshold. To better determine the optimal threshold of our research area, auxiliary data such as remote sensing images and terrain data with higher spatial resolution in the same area can be combined, and through adjustment of the threshold, most water bodies can be extracted while reducing the erroneous extraction of other ground objects categories (Liu *et al*, 2012).

Considering the fragmented nature of wetland vegetation and the existence of floating vegetation in the MRD, the NDVI threshold value of vegetation is normally slightly higher, normally above 0.2 (Couvillion *et al*, 2013). Wang conducted a comprehensive wetland vegetation coverage/water boundary experiment along the coastal area of China and found that the mNDWI/VIs method which combined mNDWI, and EVI could achieve 98% accuracy in water body extraction. In addition, the combination of EVI, NDVI, and LSWI also archived 96.2% accuracy of vegetation boundary extraction (Wang *et al*, 2020), this adjusted threshold showed in

Table 3. This research will test whether this threshold could produce more accurate vegetation/water bodies in lower MRD.

Table 3. Adjusted Threshold for Vegetation/Water Boundary extraction in the MRD

	Threshold
Water Boundary	mNDWI > EVI and EVI < 0.1
Vegetation Boundary	EVI ≥ 0.1, NDVI ≥ 0.2 and LSWI > 0

4.4.3. Accuracy Assessment

Accuracy assessment is an important step in remote sensing research, and it is also an important test to check whether the extraction method of vegetation coverage/water body is reliable. Water body extraction means that the objects in the study area are divided into two categories: water body and land area, so the method of image classification accuracy is used to evaluate the extraction results.

In remote sensing, normally the ground-truth observation data were used and calculate the percentage of correctly identified objects to determine the overall accuracy. This study used NAIP images as the ground reference for accuracy assessment. This research generated 120 random points in the research area and generated the classified accuracy assessment dataset based on visual interpretation. The accuracy assessment points have been classified as water/non-water or vegetation/no-vegetation based on their location and surrounding texture. There are 50 points located in the water area while 70 points are in the non-water region, for vegetation coverage, 47 points are in the vegetated area while 73 points are in the non-vegetation area. The distribution of these points showed in Figure 5.

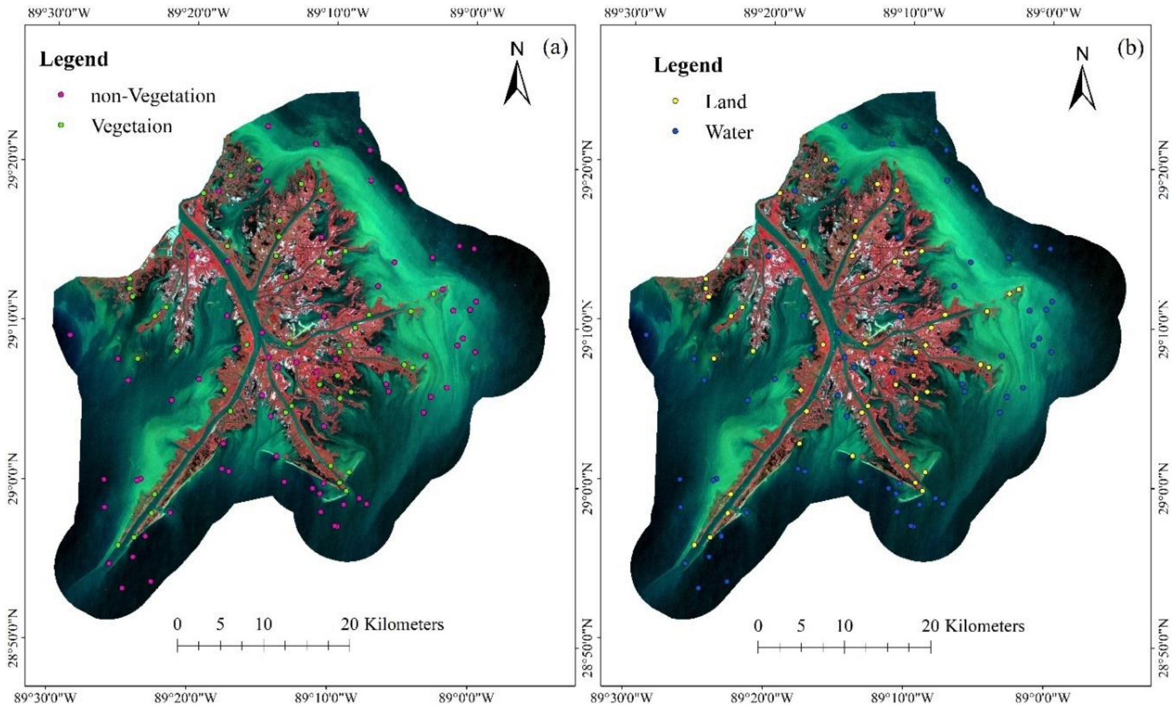

Figure 5. Distribution of the randomly generated accuracy assessment points: (a) Vegetation Coverage; (b) Water Boundary Extraction

4.4.4. Vegetation/Land Boundary Extraction

This study used September 30, 2010, Landsat 5 TM image for the vegetation/land boundary extraction test since it has a relatively low water level recording and abundant NAIP images which benefit accuracy assessment. 46 scenes of NAIP aerial photos taken from May 10, 2010, were also collected to evaluate the accuracy of the threshold selected.

Based on the vegetation/water body index image, NDVI = 0.2 is used as the initial threshold for vegetation coverage detection, and mNDWI = 0 is also used as the initial threshold for water body extraction. Then the segmented vegetation/water body index image is generated based on the initiating threshold, while the vegetation coverage/water body distribution of Landsat images based on the adjusted threshold is also obtained and compared with the result. The extraction results showed in Figure 6 and Figure 7.

It can be seen from Table 4 that the overall accuracy of the adjusted threshold extraction results is generally better than the initiating threshold. Compared with the Landsat images, it can be found that the adjusted threshold method is better than the initiating threshold in the shallower waters. Considering the wetland environment, the initiating threshold is more likely to be affected by some other factors, such as planktonic algae on the water surface, which will cause misclassified of the water body boundary. Therefore, for the region of the shallow or vegetated water on the MRD, the appropriate vegetation coverage/water body extraction should use the adjusted threshold. The adjusted threshold this research applied could extract more detailed information about water and vegetation, the extraction of shallow water is more accurate, and the overall accuracy is better than the single index initiate threshold.

Table 4. Classification Accuracy of the Threshold Applied for Vegetation/Water Boundary extraction in the MRD

	Initiate Threshold	**Adjusted Threshold**
Vegetation Boundary	95.8 %	98.3 %
Water Boundary	97.5 %	99.2 %

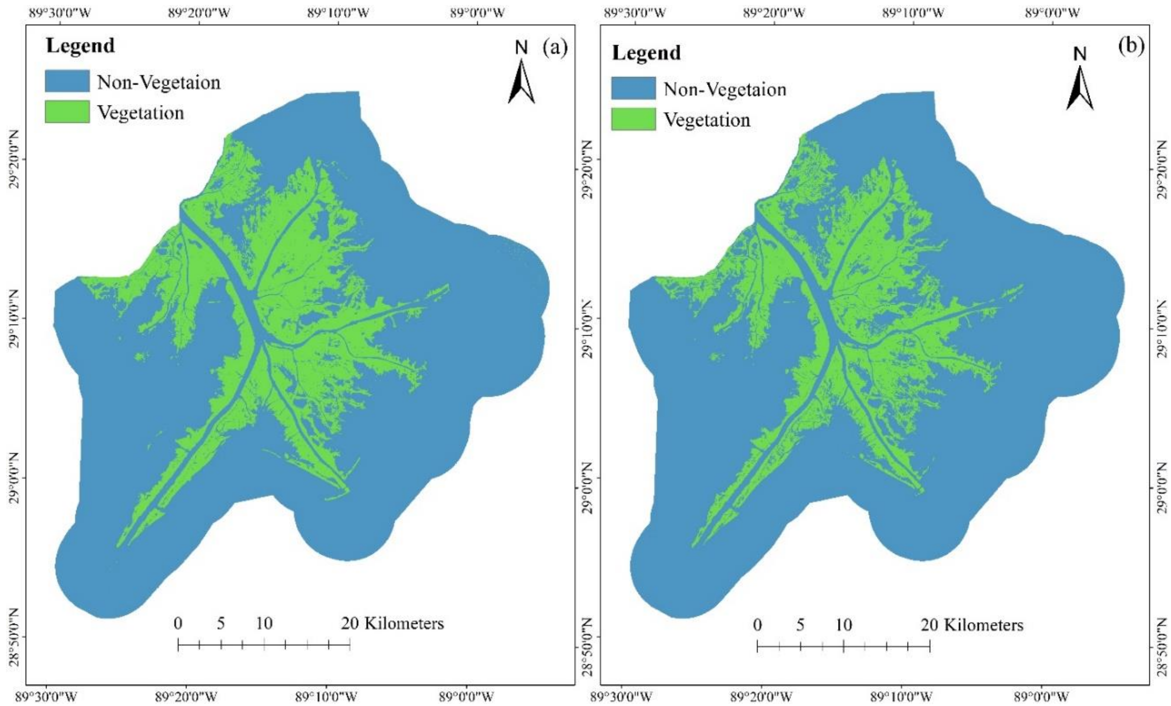

Figure 6. Vegetation boundary extracted in the lower MRD: (a) Initiate threshold; (b) Adjusted Threshold

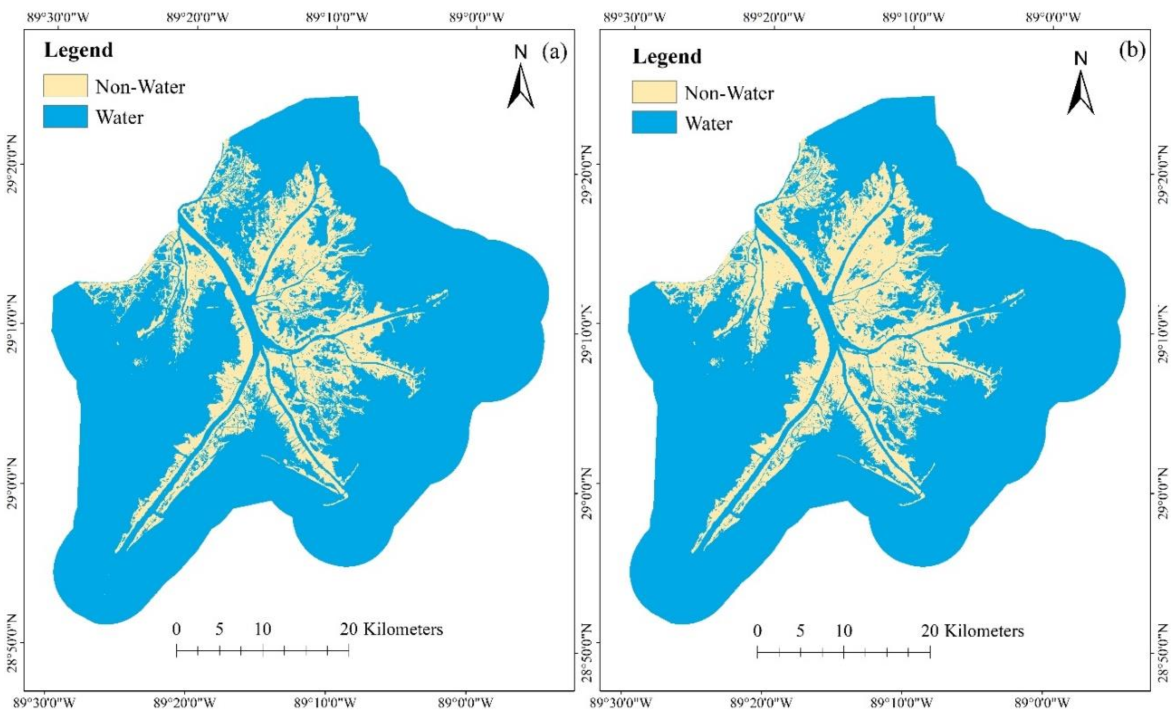

Figure 7. Water boundary extracted in the lower MRD: (a) Initiate threshold; (b) Adjusted Threshold

4.4.5. Historical vegetation coverage/Water boundary dynamics in lower MRD

In the last section, this research proved that the adjusted threshold values could extract more accurate vegetation/land boundaries in the lower MRD. This research then further applied this method in the lower MRD through the long-time series Landsat archived dataset and quantitatively analyzed the produced result.

From the historical change shown in Figure 8, despite the significant season variations, the results indicated the overall vegetation coverage in the region is slightly increasing while the land area is decreasing in the past two decades. This region experienced a relatively significant decrease of land and vegetation coverage since the beginning of 2016 which corresponded with the first reported case of scale infection of the Roseau cane in the MRD. This research also observed a strong decrease of land and vegetation area since 2020, which might relate to cold weather event at that following time which might lead to the massive death of wetland vegetation. If concentered on the growing season data (August-October), then a strong increasing trend existed in the MRD region since 2005 shown in Figure 9. This might indicate the vegetation's continuous expansion during the growing season in the lower MRD.

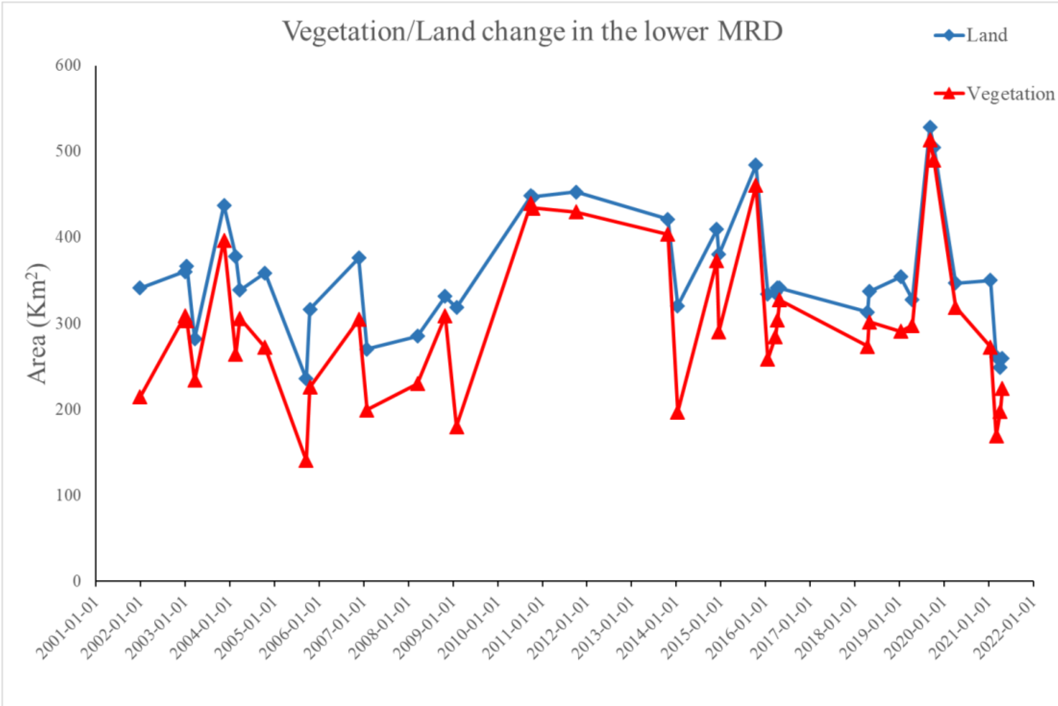

Figure 8. Land and vegetated area Change in the lower MRD

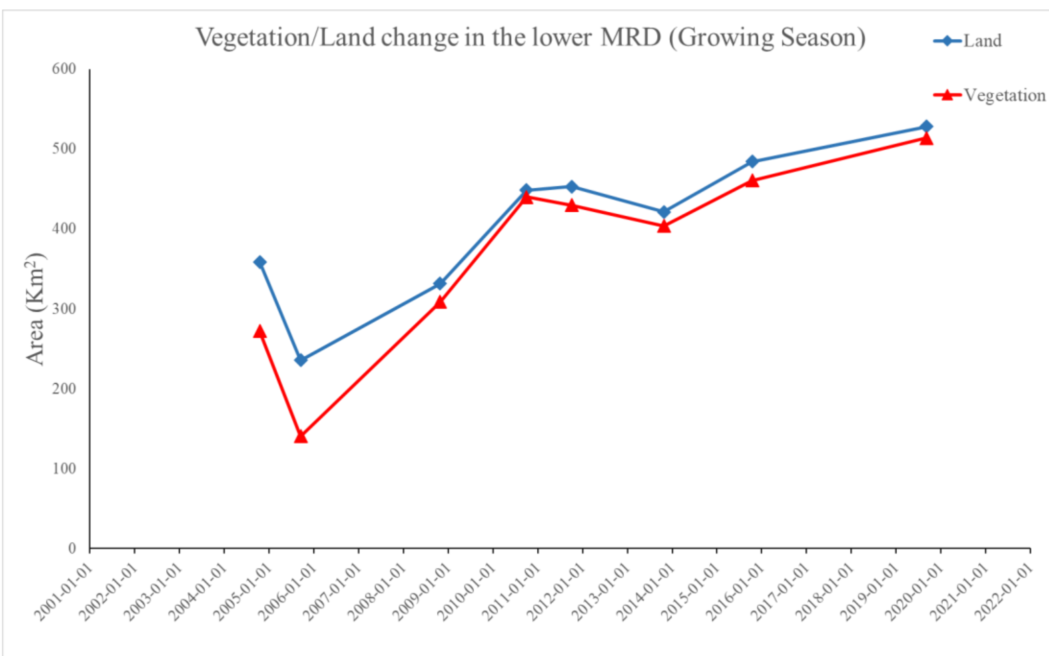

Figure 9. Land and vegetated area change in the lower MRD based on images in Growing Season (August - October).

Considering the geographic location characteristics, the changing pattern may vary in the different subregions of watersheds. For example, watersheds close to inland may be more sheltered from storm surges and erosions and grow more land through the sediment from the Mississippi river. However, watersheds face directly open gulf water and waves may have a higher chance of losing more land and vegetation, which offset the changes in the entire study site. Therefore, this research examined the land and vegetated area change dynamics in these subregions of watersheds as shown in Figure 10 and Figure 11. Much severe variation of vegetation and land area change can be observed in the Octave Pass and Main Pass watershed area while relatively stable in the Southern part of the MRD including the Pass-a-Loutre, Southwest, and South Pass region. This might cause by relatively more Roseau cane distributed in this southern part of the MRD.

In summary, the historical vegetation/land change analysis provided an overall assessment of the wetland vegetation status from 2001 to 2021 across the lower MRD, it still missing the detailed information of the dieback distribution. In the next section, NDVI-derived dieback detection will be introduced to get an overview of this phenomenon in the lower MRD region.

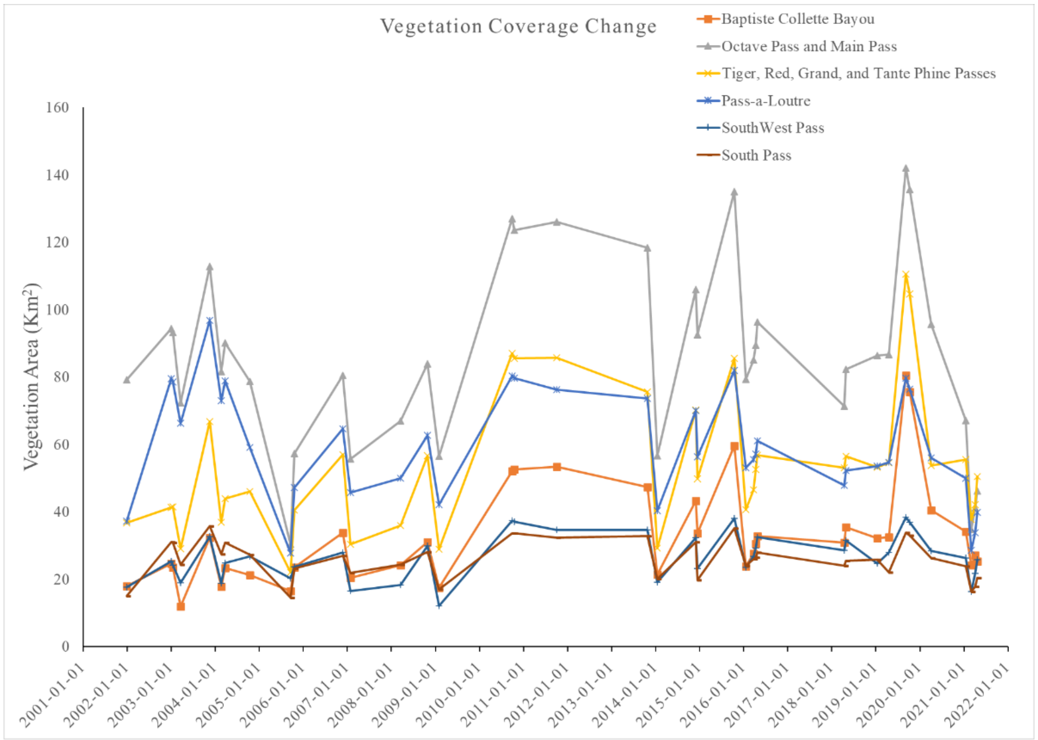

Figure 10. Vegetation Coverage Change in lower MRD watersheds

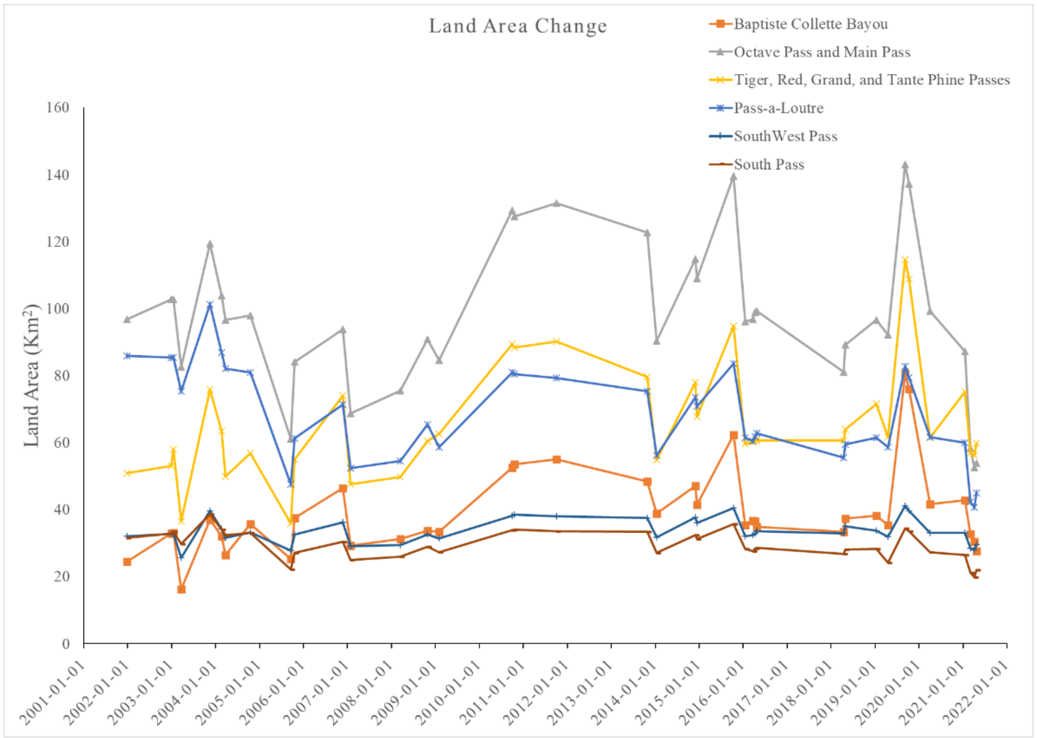

Figure 11. Land Area Change in MRD watersheds

4.5. Task 2: Wetland and Roseau cane dieback assessment

The detection of dieback regions in lower MRD is one of the main objectives of this research. In this section, the distribution and dieback of wetland vegetation are detected and quantitatively analyzed based on the selected Landsat images.

Normally, the NDVI value can reflect a reduction in vegetation growth conditions due to wetland vegetation diebacks which could result in thinning or death of vegetation. Considering the thresholding methods are often applied in change detection analysis (Wang *et al*, 2007), Miller has successfully used statistics characteristic of NDVI difference value to identify the dieback region in South Carolina (Miller *et al*, 2018). However, their result is based on the threshold values derived from the entire study area NDVI difference, while this research will apply the method to the vegetated area extracted from the adjusted threshold values from the last section for vegetation dieback in the lower MRD.

First, this research collected the Landsat-derived vegetation coverage map for NDVI change analysis. Then calculate the difference in NDVI value between these two images. Following the statistic threshold principle, this research divided the pixel of the NDVI-difference map into three categories:

1) Dieback area where the value difference of NDVI is less than -1 standard deviation, which means this vegetated area suffered from significant vegetation decline.
2) No significant change area where the absolute value difference of NDVI is less than 1 standard deviation which means the NDVI value change is not significant from a statistical perspective and considering this research tested this threshold only on the vegetated environment, this area is classified as no change.
3) Increased Vegetation area where the NDVI difference is bigger than 1 standard deviation,

indicating that the vegetated area has denser vegetation or grows better than in previous years.

4.5.1. Dataset Selection

Dieback assessment based on vegetation index change in the coastal areas needs to deal with the challenging issue of constantly changing water levels and its impact on land and area appearance on satellite images. Therefore, this research aimed to select images with desired time frame, similar seasonality, and minimal water level difference. As a result, this research selected the Landsat C2L2 products retrieved on October 9, 2019, and September 30, 2010, around 4 pm GMT, from the two decades of cloud-free images, which has the lowest mean water level difference of around 2cm, shown in Table 5. This research collected the hourly recorded water level data from the CRMS website. Among all the stations located in coastal Louisiana, three CRMS stations were selected located in the MRD region. Both images were collected during the growing season of Roseau cane (August - October).

Table 5. Selected CRMS water level hourly recording in the MRD in the growing season Landsat images from 2010 to 2019

Adjusted Water Elevation to Datum (m)				**Average Water Elevation (m)**
Date	**CRMS0162**	**CRMS0159**	**CRMS2634**	
10/9/2019	**0.652272**	**0.551688**	**0.691896**	**0.631952**
9/7/2019	0.286512	0.21336	0.374904	0.291592
10/14/2015	N/A	0.109728	0.158496	0.134112
10/24/2013	-0.070104	-0.036576	0.079248	-0.009144
10/16/2010	N/A	0.41148	0.615696	0.513588
9/30/2010	**N/A**	**0.51816**	**0.795528**	**0.656844**

4.5.2. Result

The purpose of this section is to assess vegetation dieback in the entire site through NDVI change analysis. In Figure 12, this research classified the NDVI difference map between 2010 with 2019 to vegetation dieback level assessment in the lower MRD.

The results indicated around 51.09 km^2 of dieback area in the MRD from 2010 to 2019, which accounted for around 11.61% of the overall wetland vegetation in the MRD as shown in Table 6. Besides, around 9.67% of the vegetated area experienced a total loss of vegetation in 2019. It clearly showed most of the dieback and vegetation loss areas located in the outskirt of the east and south regions of the lower MRD. This result indicted the wetland manager should put more focus on the protection of wetland vegetation in these dieback and vegetation loss regions. While the relatively stable vegetation areas accounted for 65.68% and may cause less concern for wetland conservation.

Table 6. Statistics of vegetation change area (km^2) in the MRD

Class type	Area	Percentage of overall vegetation coverage
Vegetation to non-Vegetation	42.54	9.67 %
Dieback	51.09	11.61%
non-Vegetation to Vegetation	92.27	20.98%
Vegetation (No change)	288.9	65.68%
Increased Vegetation	57.26	13.02%
Overall Vegetation Coverage (2010)	439.88	

In addition, this research also identified 20.98% of areas that changed from non-vegetation areas to vegetated areas and 13.02% increased vegetation areas which are mostly located in the side area of each channel, and largely happened in the northern part of the MRD. These changes should be the results of sediment deposits from the Mississippi river, marsh protection projects to conserve wetlands, and vegetation expansion.

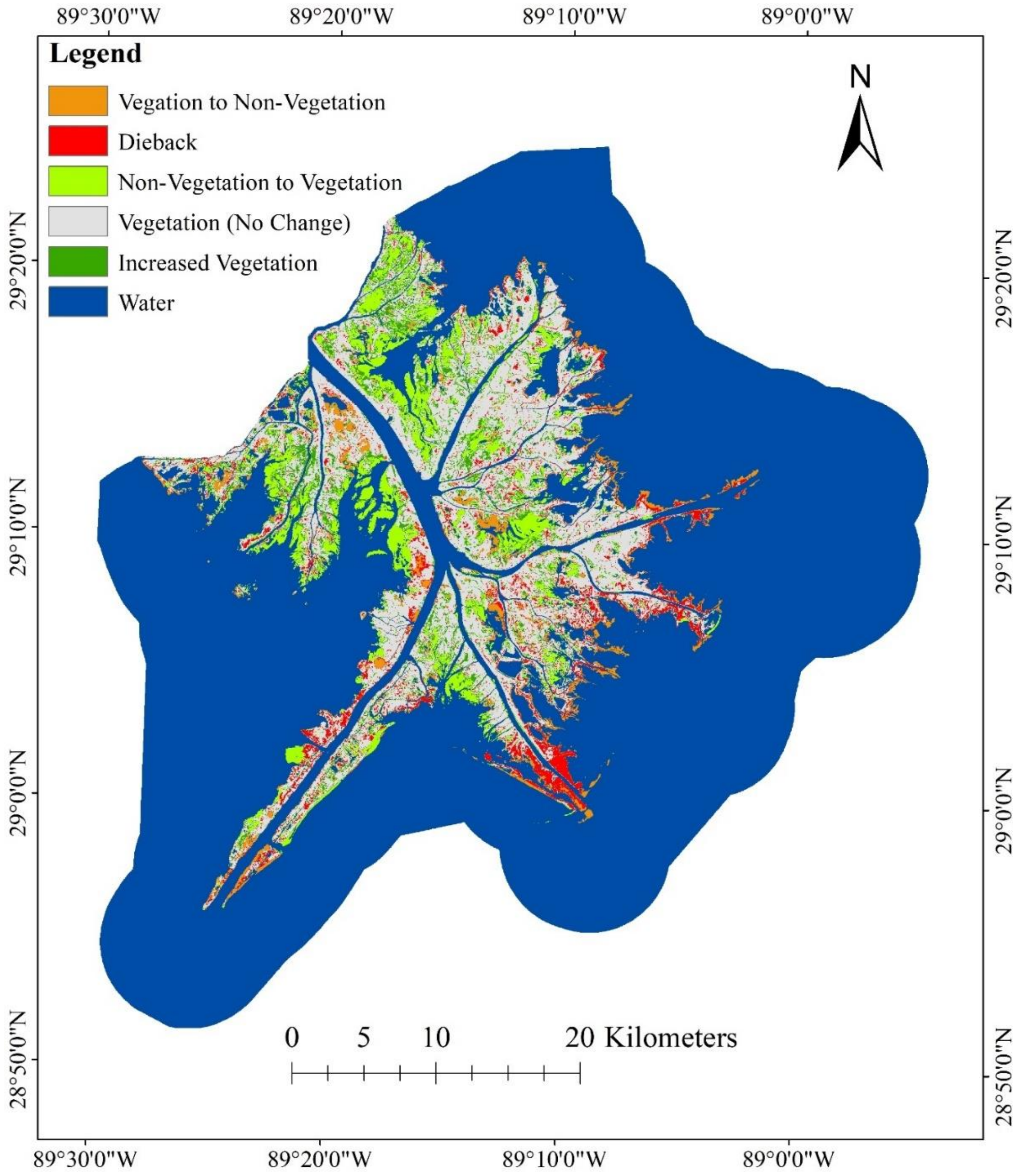

Figure 12. Vegetation dieback assessment map based on NDVI change in the lower MRD from 2010 to 2019.

4.6. Task 3: Roseau cane distribution mapping

The purpose of this section is to test the capability to separate Roseau cane from other vegetation classes using Landsat images. Considering the difficulty to get sufficient ground samples and the difficulty of visual interpreting the distribution of Roseau cane due to the coarse resolution of Landsat images, it is necessary to use a high-resolution auxiliary dataset for the task. Samiappan applied a two-class classification of Roseau cane and non-Roseau cane to identify its distribution based on UAV images (Samiappan *et al*, 2017). This research conducted a similar experiment to classify these two classes based on Landsat and meter-level resolution aerial photos. Specifically, this research applied pixel-based SVM classification on the Landsat images based on the training and accuracy assessment samples identified from the high-resolution NAIP aerial photos.

4.6.1. SVM

A fast and high-precision classification algorithm of remote sensing images is the key to implementing dynamic monitoring, evaluation, and forecasting of the wetland environment. The SVM algorithm is designed on the VC dimension theory of statistical learning theory and the principle of minimum structural risk. This algorithm seeks to obtain the best generalization ability and the best compromise between the complexity of the model and the learning ability from limited sample information (Bao *et al*, 2009). SVM has become a simple, robust, and reliable classification method and is widely applied in many remote sensing studies (Zhang and Xie, 2013). Therefore, this research adopted SVM for classification.

4.6.2. Impact of texture analysis on Roseau cane classification

Remote sensing images contain abundant spectral information as well as valuable texture information. In traditional vegetation classification research, the spectral information of remote sensing images acts as the main source for the classifier, and the texture information is often ignored (Lu *et al*, 2007). Adding texture features may result in improving the classification accuracy. Especially, Roseau cane has unique structural characteristics could seem from high solution images. It is usually much taller than other marsh species, occupied larger areas, and may have a coarse texture. Yet, in higher resolution images such as those from drones, gaps, and understory vegetation may be visible. This research would like to test the hypothesis of whether adding texture images in the classification can improve the accuracy of Roseau cane classification. The results may be scale-dependent due to the above reasons. Therefore, this research will test this hypothesis both in Landsat, WorldView, and drone images.

Landsat-8 texture images were extracted to supplement the spectral information for the classification of the wetland vegetation in the MRD region. Relevant studies have proved that for texture images, the extraction window size is a key parameter (Chen *et al*, 2004). How the window size affects the accuracy of texture improvement in wetland classification is still unknown. A larger window size increases the chance of finding bigger texture patterns, thereby reducing errors in classification. However, considering the fragmented nature of the wetland vegetation environment, especially the Roseau cane habitat patch size is relatively small compared to the 30 m resolution of Landsat images, this research set the maximum tested window size as 7 × 7 pixels size (210 × 210 meters). The window size was initially set to 3×3 pixels size and was later increased to 5×5 and 7×7 pixels size. The texture features were selected using the standard deviation value of the window size.

4.6.3. Accuracy Assessment

To assess the overall classification accuracy and the effectiveness of texture information, high-resolution NAIP images were used to support the training of the classifier and accuracy assessment. For each Landsat image, we generated 100 random points in the extracted vegetation area and visually identified each point whether it is in the Roseau cane habitat or not in the NAIP images. Among them, 80 points were selected as the training dataset to extract the spectral and texture information from the Landsat images, the number of each class is shown in Table 7. The other 20 points served as the accuracy points to assess the final product generated after SVM classification, each class contains 10 points.

Table 7. Training sample numbers for Landsat classification in the MRD

Image Date	Roseau cane	non-Roseau cane
2010	42	38
2019	39	41

4.6.4. Roseau cane classification results

The SVM classification produced a high overall accuracy at 75% result, this result proved the method is capable of separating Roseau cane and non-Roseau cane vegetation classes. After successfully classifying the Landsat images using the SVM method, this research found that the texture feature introduced method could archive a classification accuracy of around 80% to 90%, which is higher than the spectral-only classification accuracy with a 75% accuracy as shown in Table 8. This result indicates that the texture feature is beneficial to improve Roseau cane classification for the large scale with Landsat imagery. Through the extraction of texture features, the texture information between different objects is strengthened, making it easier to distinguish between different vegetation covers.

Table 8. Overall Classification Accuracy (%) for Landsat in the MRD

Image Date	SVM	SVM+Texture (3×3)	SVM+Texture (5×5)	SVM+Texture (7×7)
2019	75	80	80	75
2010	75	70	90	80

For texture images with different window sizes, the impact on vegetation classification is also different. In this study, the vegetation classification accuracy of the 5 × 5 window size is slightly higher than other window sizes. When the window size is too large, it oversimplified the ground feature texture, and a smaller window size ensures the homogeneity of pixels within the window but also reduces the texture difference between different objects. For this study area, a window size of 5 × 5 is more suitable for the classification of vegetation than other window sizes.

From the classified MRD vegetation statistic, this study found the overall vegetation coverage in the lower MRD increased by around 11% from 2010 to 2019 during the growing season while the Roseau cane coverage decreased by around 5% at the same time shown in Table 9. In addition, this study also found that Roseau cane occupied around two thirds of the dieback area distribution in the region listed in Table 10. These results indicate the Roseau cane experienced much more damage than other non-Roseau cane wetland vegetation species which might relate to the scale infection since 2016.

Table 9. Classified Roseau cane and non-Roseau cane area (km2) in the MRD

Image Date	Roseau cane	Non-Roseau cane	Overall	Roseau cane Percentage
2010	218.53	221.34	439.88	49.7%
2019	204.73	284.89	489.62	41.8%

The final product of the classified Roseau cane distribution in the MRD showed in Figure 13. From the distribution map, the main Roseau cane decreased areas were in the southern part of the MRD, especially the river estuary area.

Table 10. Statistic of Roseau cane and non-Roseau cane in the dieback area

Vegetation type	Area	Percentage of overall dieback area
Roseau cane	33.65	65.86%
non-Roseau cane	17.44	34.14%
Overall Dieback	51.09	

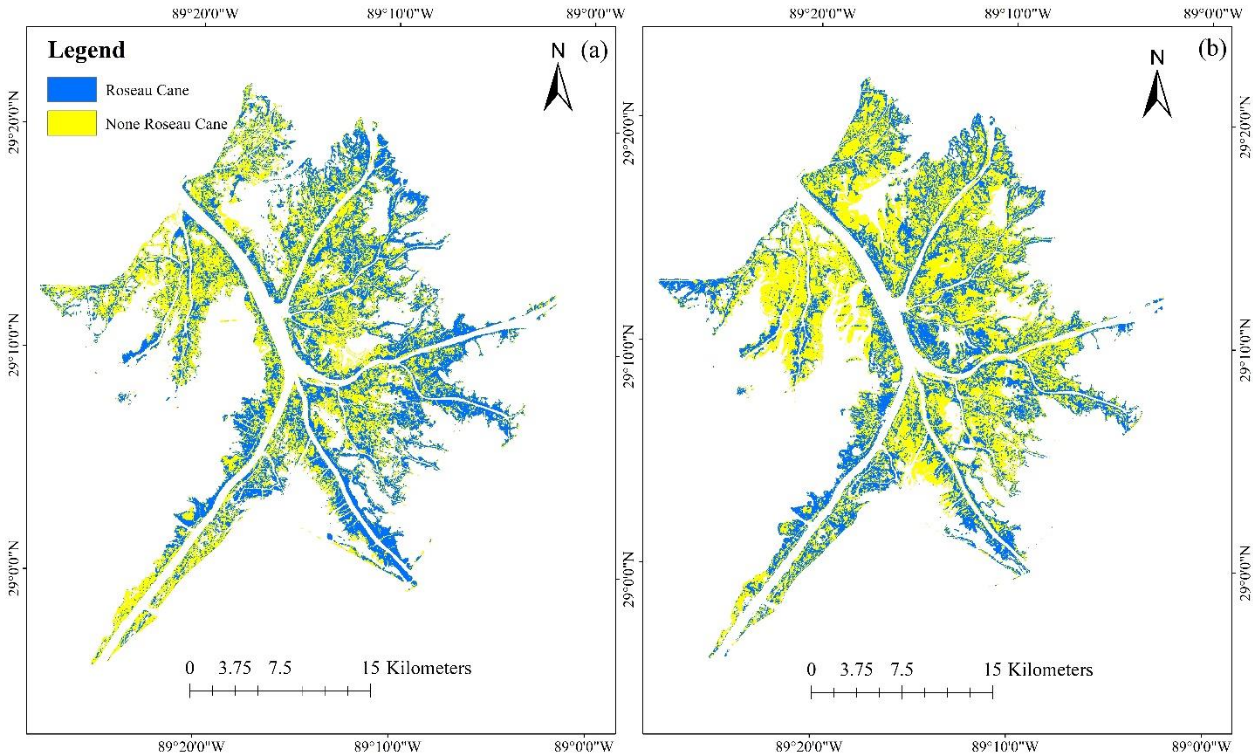

Figure 13. Roseau cane distribution in MRD for (a) 2010 and (b) 2019 based on Landsat images.

4.7. Summary

This chapter introduced a comprehensive, systematic large-scale remote sensing method for assessing wetland and Roseau cane dieback in lower MRD. The proposed methodology in this section creates a series of vegetation/land change maps in lower MRD from 2001 – 2021 as well as large-scale Roseau cane distribution maps.

This research tested the adjusted threshold values for vegetation/water body boundary extraction based on the combination of NDVI, EVI, LSWI, and mNDWI. The result proved it could archive higher accuracy comparing initiate threshold methods. Then we applied this method to extract 20 years of vegetation/water change in the lower MRD. The results indicated the overall vegetation coverage in the region is slightly increasing while the land area is decreasing in the past two decades. While other subregions showed slightly increased vegetation coverage, the vegetation coverage in Pass-a-Loutre subregion decreased. Further effort should assess whether

Pass-a-Loutre is subjected to more severe scale infection as well. In future research, these macro wetland changes will be combined with the delta-wide scale samples in the Roseau cane areas to analyze their relationship.

One major objective of this study is to assess the dieback conditions in lower MRD. Through the vegetation NDVI change, the dieback region was successfully extracted in the lower MRD and found around 51 km^2 of the wetland experienced vegetation dieback in the lower MRD which accounted for 11% of the overall wetland vegetation coverage and around 9% of vegetation coverage losses in the MRD from 2010 to 2019.

Our classification test produced high-accuracy results to separate Roseau cane from non-Roseau cane. This research further tested whether the addition of texture information could improve the accuracy of supervised SVM classification in the lower MRD. The results proved the texture information could increase the overall classification accuracy by around 5-15% and the 5×5 window size generated the best result.

Through the final classified result, this research found the Roseau cane decreasing while other marsh land cover increased in the lower MRD from 2010 to 2019. The result concluded that the major dieback events happened on Roseau cane in the MRD, which indicated that Roseau cane is especially vulnerable to dieback in the lower MRD, and extra attention should be paid to further investigate their impact on wetland recovery.

Chapter 5. Mid-scale Roseau Cane Habitat Mapping Through High-resolution Multispectral WorldView Imagery

5.1 Introduction

There is a study showing the two variants of Roseau cane - Delta Phragmites and European Phragmites have significant differences facing RCS infection (Cronin *et al*, 2010), the biomass of European Phragmites is less impacted by scale infection compared to Delta Phragmites under small-scale controlled experiment. How this difference of resistance will affect their distribution on a larger scale is still unknown. It is imperative for wetland management to know the distribution characteristics of the two variants of Roseau cane on a relatively larger scale and its habitat environment.

Considering the variants of Roseau cane share similar spectral characteristics, the Landsat dataset is not suitable for this task because the resolution was too coarse and limited bands. This research selected Worldview images for mid-scale analysis considering it is capable to provide high-resolution multispectral information of the study site. Whether Worldview images can effectively separate Delta Phragmites and European Phragmites based on mainstream classification algorithms and technical tools is still a challenge.

Based on the usage of each classifier algorithm in the current research of classification problems, this paper compares four classification methods of K Nearest Neighbor (KNN), Maximum Likelihood Classifier (MLC), Support Vector Machine (SVM), and Random Forests (RF) to test their capability for separating Roseau cane variants and habitat classification The study area includes two main river outlets: the main pass and south pass of the lower MRD. Typical wetland vegetation species are identified and investigated in the field survey. Ancillary data such as aerial photographs, Landsat images, and expert opinions from wetland ecologists have cooperated in the field survey. The final classified Worldview result was used to cross-validate the Roseau cane distribution results from Landsat Classification established in Chapter 4.

5.2 Method

This chapter introduced the method and results of Worldview-based wetland vegetation classification research. Mid-scale wetland Roseau cane habitat classification is used to obtain the spatial distribution of the Roseau cane in the main pass located in the Delta National Wildlife Refuge and the South Pass of the MRD. The south pass is the southmost river outlet extended from the main Mississippi river flow direction and subjects to gulf wave impact, while the main pass is located in the east-north of the bird-foot delta that may be sheltered more by the Pass-a-Loutre region. This research selected these two outlets based on their geographical representative locations as well as data coverage in the 2021 WorldView imagery. The two major variants of the Roseau cane may be difficult to identify on moderate-resolution optical remote sensing images such as Landsat 8. This research selected high-resolution 8-band WorldView-2 (WV-2) images with 0.5m spatial resolution to classify Reseau cane habitat, and especially to differentiate the two major variants of Roseau cane in the lower MRD. The main research steps in this section are as follows.

(i) First, WV-2 images and field survey GPS sampling points were collected and preprocessed.

(ii) To solve the registration issue, this research further checked each sample point and slightly adjusted the location to ensure correct matching of the field samples and the image locations Then, this research performed visual interpretation on the WV-2 images to generate extra training samples and accuracy assessment samples for each class designed in this research.

(iii) This research compared MLC, SVM, KNN, and RF classification using ArcGIS software to identify the optimal classification method for Roseau cane habitat classification. This research then further adds texture to this optimal classification method to assess whether texture can help improve Roseau cane habitat classification accuracy.

(iv) Finally, the best Roseau cane habitat classification result based on SVM was selected to detect different wetland vegetation classes. This research further used the classified Roseau cane distribution in these two outlets to cross-validate the Roseau cane distribution extracted from the corresponding Landsat image to assess the reliability of its distribution in a large area and assess the difference of distribution of Delta Phragmites with European Phragmites in the detected dieback area.

5.3 Dataset and field data collection

5.3.1. Worldview 2 image

The WorldView-2 satellite was launched on October 6, 2009, with an orbital altitude of 770 km and a revisit period of 1.1 days. It is the first commercial high-resolution imagery with multispectral bands that preferable for vegetation habitat classification (Shridhar *et al*, 2015). The WV-2 image used in this study has eight multispectral bands with 1.85 m spatial resolution in the wavelength range of 400-1040 nm as shown in Table 11 but pan-sharpened to 0.5 m resolution by the vendor.

Table 11. Satellite parameters of WorldView-2

Launch Date	October 6, 2009	
Revisit time	1.1 day	
Orbit	Altitude	770 km (Sun-synchronous)
	Period	93.4 min
	Equator Crossing Time	10:30 am descending node
Bands	Panchromatic band (0.46m)	450-1040 nm
	Multispectral bands (1.85m)	Coastal Blue: 400-450 nm
		Blue: 450-510 nm
		Green: 510-580 nm
		Yellow: 585-625 nm
		Red: 630-690 nm
		Rededge: 705-745 nm
		Near-infrared 1: 770-895 nm
		Near-infrared 2: 860-1040 nm

In addition to the traditional blue, green, red, and near-infrared bands, WV-2 also has four distinctive bands: Coastal Blue (400-450nm), Yellow (585-625 nm), Red Edge (705-745 nm), and Near Infrared 2 (NIR2, 860-1040 nm). The Coastal band is proved effective in plant identification and analysis and is sensitive to chlorophyll absorption of healthy vegetation (Heenkenda *et al*, 2014). In addition, this band is very useful for water depth research and supports oceanography research based on the specification parameter of chlorophyll. Because the band is often affected by atmospheric scattering, atmospheric correction techniques have been applied. The Yellow band is a very important band to test the characteristic index of "yellowness", both on land and in water. At the same time, the panchromatic band can be used as an auxiliary correction for the true color band combination, which improves the effectiveness of visual interpretation of vegetation habitat.

The red-edge band is a newly added band, in which some vegetation types strongly respond to the highly reflective bands, which can assist the analysis of plant growth, directly reflect the relevant information about plant health status, and assist the classification of vegetation types. The NIR2 band partially overlaps the NIR 1 band but is less affected by the atmosphere. This band supports plant analysis and the quantitative study of wetland vegetation (Li *et al*, 2019). Larger spectrum range and targeted eight-band design capable of detecting the corresponding natural ecosystems such as land, sea, forest, grassland, and wetland. This capability makes the application of WV-2 images could improve the classification characteristics and serves better for the wetland vegetation information extraction and analysis of these regions.

The WV-2 optical images used in this study were acquired on September 11, 2021, to detect the growing season spectral characteristics of the Roseau cane. The study area at lower MRD was at low tide with no cloud cover. The 1+8-band bundle of WV-2 is currently priced around $24-44/km^2$, which is still relatively expensive. Considering the Roseau cane distribution in MRD is extremely fragmented, the images that covered the main pass and south pass of MRD were purchased for this study due to funding limitations and research needs.

The WV-2 images were captured at a 36.2 off-nadir. It is orthorectified and pan-sharpened by the company. The images were also geometrically corrected according to the GPS coordinates of landmark features collected in the field and corresponding NAIP images, and the Root-mean-square deviation (RMSE) was controlled to 0.6 m.

5.3.2. Field data collection

The Roseau cane field surveys were conducted in the study area on November 9, 2021. This research first generated 150 accessible randomly distributed points along each pass as the initiate survey locations for the field data collection. The vegetation class information was collected based on the field survey of those accessible location with the assistance of wetland experts from the AgCenter, LSU.

Considering the vast area of our study, the base station of our Trimble R10 RTK-GPS (Real-Time Kinematics Global Positioning System) is not sufficient to cover the whole study site. This research used handheld GPS Trimble GEO7X in field survey to measure the location of wetland vegetation sampling points. The horizontal positioning accuracy of this device could archive 0.22 m according to our field test experiment with Trimble R10 RTK GPS.

Since the interior of the study area is mainly swamp with limited accessibility for walking in combination with the low tide season sampling that limits boat accessibility, this research ended up with collected 132 points in the main pass and 154 points in the south pass. To enrich the training sample set and validation sample set, the survey team performed multiple collections on each vegetation class found at a location to ensure sufficient training and accuracy assessment samples for each class.

5.3.3. Classification Scheme

According to the field survey, the main wetland vegetation type in the study area was Roseau cane, and it has two major variants in the study area including widely spread Delta Phragmites and relatively less distributed invasive European Phragmites. The Delta Phragmites is confirmed as the dominant wetland vegetation species in the area through field survey. Other wetland vegetation includes Alligator Weed, Saw Grass, Cutgrass, Cattail, Bull tongue, etc. This research used spectrometer to measure the spectral difference of Delta Phragmites with European Phragmites, showed in Figure 14. They shared similar spectral curve, however the field data still showed Delta Phragmites have relatively higher reflectance compared to European Phragmites in all wavelengths especially in red band and red edge band. This spectral difference indicate it is possible to separate them based on multi spectral bands images.

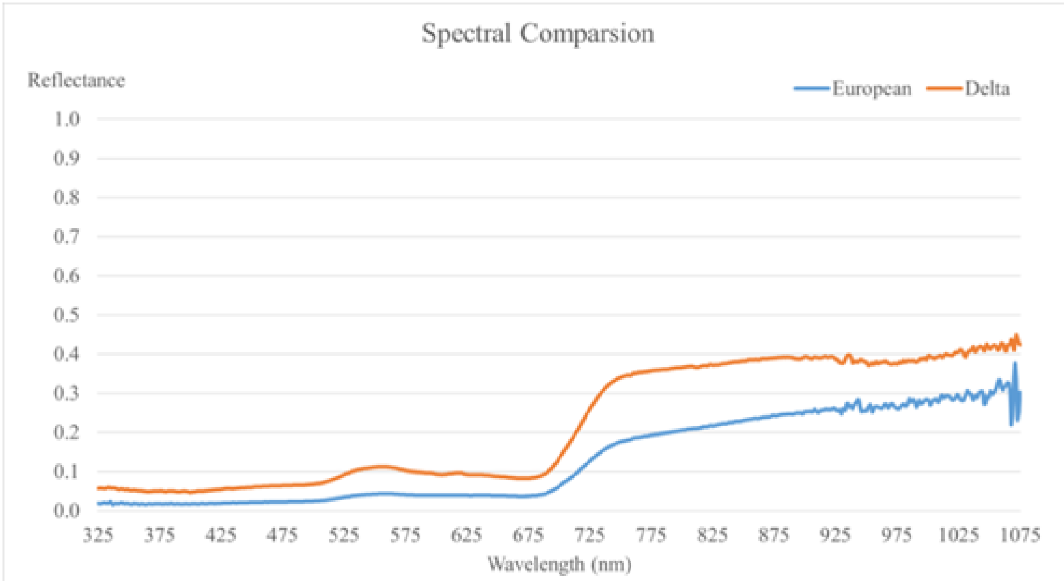

Figure 14. Spectral comparison of Delta Phragmites with European Phragmites

According to the research need and sample numbers for each vegetation, this research composed nine categories for classification including water, marsh grass, Delta Phragmites, European Phragmites, shrub/woody vegetation, dead vegetation, mud, bare soil, and man-made. A total of 240 sample points were GPS surveyed in the research area and randomly divided into training samples and validation samples according to the ratio of 8:2. However, the available samples covering all category classes in the study area are still not sufficient for some minority classes. Therefore, this research added a few samples in those classes based on visual interpretation.

The visual interpretation of remote sensing images refers to the manual interpretation and extraction of remote sensing images by professionals with solid professional knowledge (Sabins, 2007). In wetland vegetation classification at the mid-scale, researchers can interpret some vegetation classes from the high-resolution images based on empirical knowledge of field mapping and correlation between image features, especially on 0.5 m WV-2 images. For wetland vegetation identification, visual interpretation may not replace field survey as the main vegetation typing method but is useful to add more samples in those identifiable areas to solve the challenging issue of limited samples in those classes with insufficient training samples. A total of 131 extra sampling points were visually identified and divided as training and accuracy assessment samples, the overall training sample and accuracy assessment sample number for each class are shown in Table 12, and the spatial distribution of these sample points is shown in Figure 15. The patch of some wetland vegetation species is relatively small and fragmented and might be in the inaccessible area in the field, limiting our ability to retrieve sufficient GPS samples for classification. Considering the difficulty for field survey, the total training and accuracy assessment dataset is relatively small, while there is study showed this small number dataset could still achieve reasonable classification results (Lou *et al*, 2020).

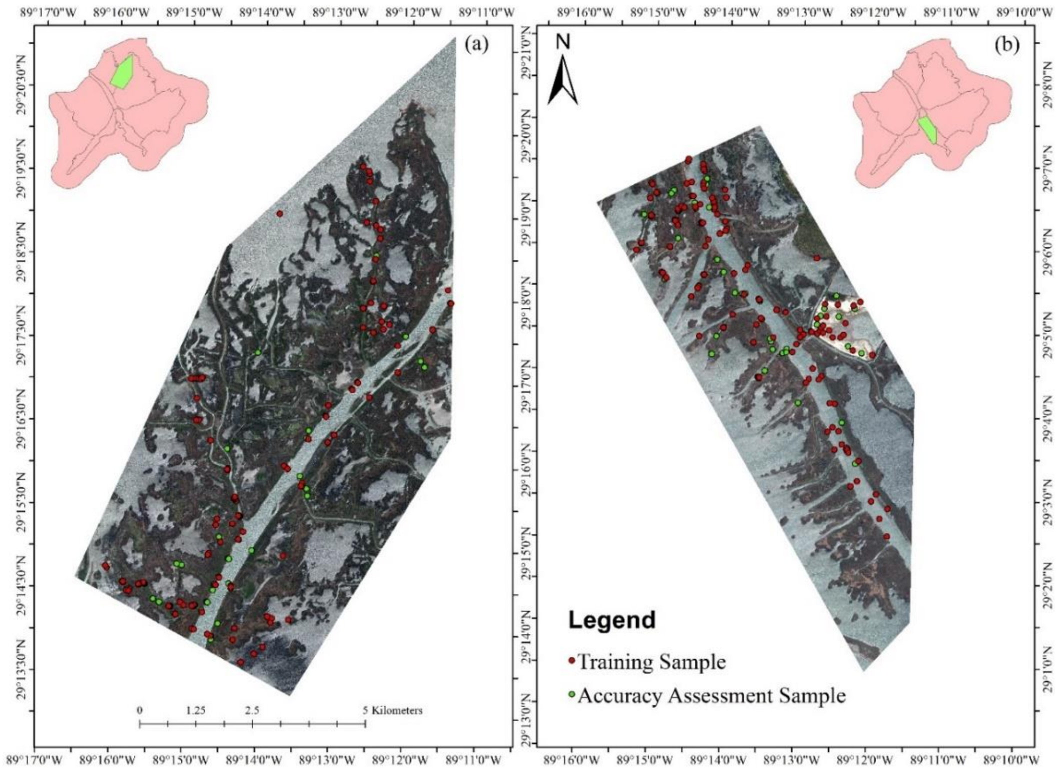

Figure 15. Distribution of the Training and Accuracy Assessment Samples for WV-2 images: (a) the Main Pass; (b) the South Pass

Table 12. Training and accuracy assessment sample numbers for WV-2 classification

Classes	Individual Species	Training sample	Acracy Assessment
Water	Water	59	12
Marsh Grass	Alligator Weed Saw Grass Cutgrass Bull Tongue Cattail	43	10
Delta Phragmites	Delta Phragmites	71	13
European Phragmites	European Phragmites	21	10
Shrub/Woody Vegetation	Black Widow	21	10
Dead Vegetation	All dead plant types	20	10
Mud	Mud	24	11
Barren Soil	Soil	15	7
Man-made	Boat, Concreate Platform, Tank	10	5
Overall		284	87

5.4 WV-2 Classification

The classification of remote sensing images is the most critical part of remote sensing work. The advantages and disadvantages of different classifiers and classification methods largely determine the accuracy of classification results. Therefore, it is crucial to select a classifier that is suitable for wetland vegetation classification in the MRD.

There are many studies on the classification of wetland vegetation using optical remote sensing images, and the accuracy of classification has been improving with the improvement of spatial resolution and the development of the classification of methods. In recent years, many representative classification methods have emerged in the research of remote sensing data classification (Yang, *et al*, 2003). Each of these classification methods has its characteristics, and early studies mostly used simple classifiers (Du, *et al*, 2012), and later, with the continuous development of machine learning theory, various new classifier algorithms emerged (Mountrakis *et al*, 2011), and were successfully applied in remote sensing data classification tasks. This section focuses on a comparative study of several commonly used classification methods including KNN, MLC, SVM, and RF for Roseau cane variants and habitat classification.

5.4.1. Classification methods

1. KNN

The KNN classification method stands for K-nearest neighbors and is the simplest method among all selected classification algorithms. The basic idea of this classification method (Wang and Zhang, 2013) is to find the K nearest samples in the feature space and assign classes based on majority voting or distance-weighted voting. In the KNN algorithm, the neighboring samples selected are training samples that have been correctly identified. The method determines the class based on the majority category of the N nearest ones or weighted voting. Therefore, the KNN method is only relevant to a very small number of neighboring samples when making category decisions.

2. MLC

MLC classifies images into two or more categories by statistically establishing a set of nonlinear discriminant functions based on the maximum likelihood ratio Bayesian criterion method. MLC assumes that the distribution functions of each category are normally distributed and automatically selected training areas and calculates the attribution probabilities of each sample area for classification.

3. SVM

SVM is a machine learning algorithm based on the statistical learning theory proposed by Vapnik et al. in 1999 (Vapnik, 1999). For multi-classification problems, one-to-one methods (OAO), one-to-many methods (OAA), etc. are usually used in SVM (Hsu and Lin, 2002). For two-class SVMs, the basic principle of classification is that the two classes of sample points in the training sample can be separated by finding a classification hyperplane and as far as possible from that plane. Since SVM is based on the structural risk minimization criterion, its generalization ability is significantly better than some traditional learning methods. It can show good generalization ability in classification problems and obtain relatively high classification accuracy.

4. RF

The principle of RF (Random Forest) was based on the Bootstrapping method, in a given M sample data set, after M times of random sampling, a sample set containing M training samples can be obtained and then based on each sample set for training to construct a decision tree, and at the node of the decision tree, a subset containing K attributes is first randomly selected from the set of attributes of that node, and then an optimal attribute is selected from this subset for division (Breiman, 2001).

When the random forest is constructed, the test samples are inputted into each decision tree for class output or regression output; in the case of classification problems, the final category is output based on voting, and in the case of regression problems, the mean value of each decision tree output is used as the result. This study used RF embedded in ArcGIS, which used Leo Breiman's Random Forest Algorithm (O'Neil *et al*, 2018).

5.4.2. Does add texture improve Roseau cane habitat classification accuracy?

Once the optimal classification method is selected in the above section, this research take experiment on the hypothesis of whether adding texture information can improve Roseau cane habitat classification accuracy in the scale of WV-2 images. Texture features are calculatable properties of ground objects from high-resolution imagery and are widely used for classification. The basic units of texture are called texture elements, and texture is usually a composite of either a regular or random arrangement of texture elements. In the field of image vision, the texture is considered as a two dimensions function of the variation and repetition of grayscale or color of the pixel (Peters, 2007). Remote sensing images are processed to reflect the spectral characteristics of features by reflectance values, and texture structure can be characterized by inter-image pixel values, which can detect the macroscopic and microscopic structures of images comprehensively. In this study, the difference in texture features between different wetland species might be used for classification. This study considers the unique tall stem of Roseau cane as the most outstanding difference from other wetland vegetation, which may generate a rougher texture. Therefore, this research selected standard deviation for the texture experiment, the different window sizes of Texture images include 3×3, 5×5, and 7×7.

5.5. Result

The accuracy verification of WV-2 image classification aims to determine the accuracy of the classification process, and this study uses multiple criteria to verify the accuracy of Roseau cane habitat classification. The specific criteria include: Overall Accuracy (OA), which is a probabilistic statistic that indicates the probability that a random sample matches the actual type of the area in the classification result for any random sample; Producer Accuracy (PA) indicates the conditional probability that a random sample selected arbitrarily from the reference data has a feature type that matches the feature type at the same location on the classification result image; User Accuracy (UA), which is the conditional probability that the feature type of a random sample selected from the classification result is consistent with the actual type of the ground; Kappa coefficient is a method to quantitatively evaluate the consistency between the classification map and the reference data which is more objectivity. The results are shown in Table 13.

Table 13. Classification Accuracy (%) comparison of WV-2 classification in the MRD.

	KNN		**MLC**		**SVM**		**RF**	
Class	UA	PA	UA	PA	UA	PA	UA	PA
Barren Soil	100.00	100.00	100.00	100.00	100.00	100.00	77.78	100.00
Dead Vegetation	100.00	70.00	100.00	90.00	100.00	80.00	100.00	70.00
Delta Phragmites	52.94	69.23	72.73	61.54	73.33	84.62	52.94	69.23
European Phragmites	66.67	80.00	61.54	80.00	90.91	100.00	80.00	40.00
Man Made	66.67	80.00	100.00	60.00	100.00	100.00	100.00	60.00
Marsh Grass	50.00	66.67	53.85	77.78	87.50	77.78	41.18	77.78
Mud	80.00	72.73	84.62	100.00	84.62	100.00	71.43	90.91
Open Water	92.31	100.00	92.31	100.00	100.00	100.00	100.00	91.67
Shrub/Woody Vegetation	100.00	30.00	100.00	50.00	100.00	80.00	100.00	40.00
Overall Accuracy	73.56		80.50		90.80		71.26	
Kappa	0.70		0.78		0.90		0.67	

The results show that the OA of the KNN algorithm is 73.56%, the kappa is 0.70, the OA of the MLC algorithm is 80.5%, the kappa is 0.78, while the OA of the SVM algorithm is the highest one which is 90.8%, kappa is 0.9, and the OA of RF algorithm is lowest at 71.26%, kappa is 0.67. The classified distribution of each class showed in Figure 16 and Figure 17. The KNN classified result have a relative overestimation of the European Phragmites and contained many misclassified water pixels to man-made. The other two methods showed an underestimation of European Phragmites and an overestimation of the marsh grass class. These two methods couldn't distinguish Delta Phragmites from European Phragmites in the research region compared with SVM. The result proved that the SVM was more suitable for classification than the other 3 methods and was selected for further analysis.

For the SVM result, most of the classes could be well distinguished and the producer and user accuracies were mostly above 80%, with the highest precision in the Bare soil, Man-made, and Water, followed by European Phragmites and Dead vegetation. The classification accuracies of the two Roseau cane variants, European Phragmites and Delta Phragmites, are good in general, and the producer and user accuracies of these two variants range from 73.33% to 100.00%. It is seen in Table 14, there is around 45.1% vegetation coverage in the study area. The Delta Phragmites are the dominant species in the region, accounting for 80.8% of the overall vegetation coverage in the research area; While European Phragmites account for 2.7% of the overall vegetation coverage. In addition to the two variants of the Roseau cane, Dead Vegetation consists of 3.46% of the overall vegetation coverage.

Table 14. The percentage of the total area for each class

Class type	Area (km^2)	% Of Total area	% Of Total Vegetation area
Bare Soil	0.75	0.70	
Dead Vegetation	1.66	1.56	3.46
Delta Phragmites	38.75	36.43	80.80
European Phragmites	1.29	1.22	2.70
Man Made	0.11	0.11	
Marsh Grass	4.26	4.01	8.89
Mud	3.72	3.50	
Open Water	53.82	50.60	
Shrub/Woody Vegetation	1.99	1.87	4.14
Total Vegetation Area	47.96	45.1	
Total Area	106.36		

The addition of texture information, on the other hand, only slightly improved the overall classification accuracy, showed in Table 15. Besides, the classified result presented more salt and pepper noise, which might be caused by the fragmented appearance of Roseau cane stands in the high-resolution WV imagery.

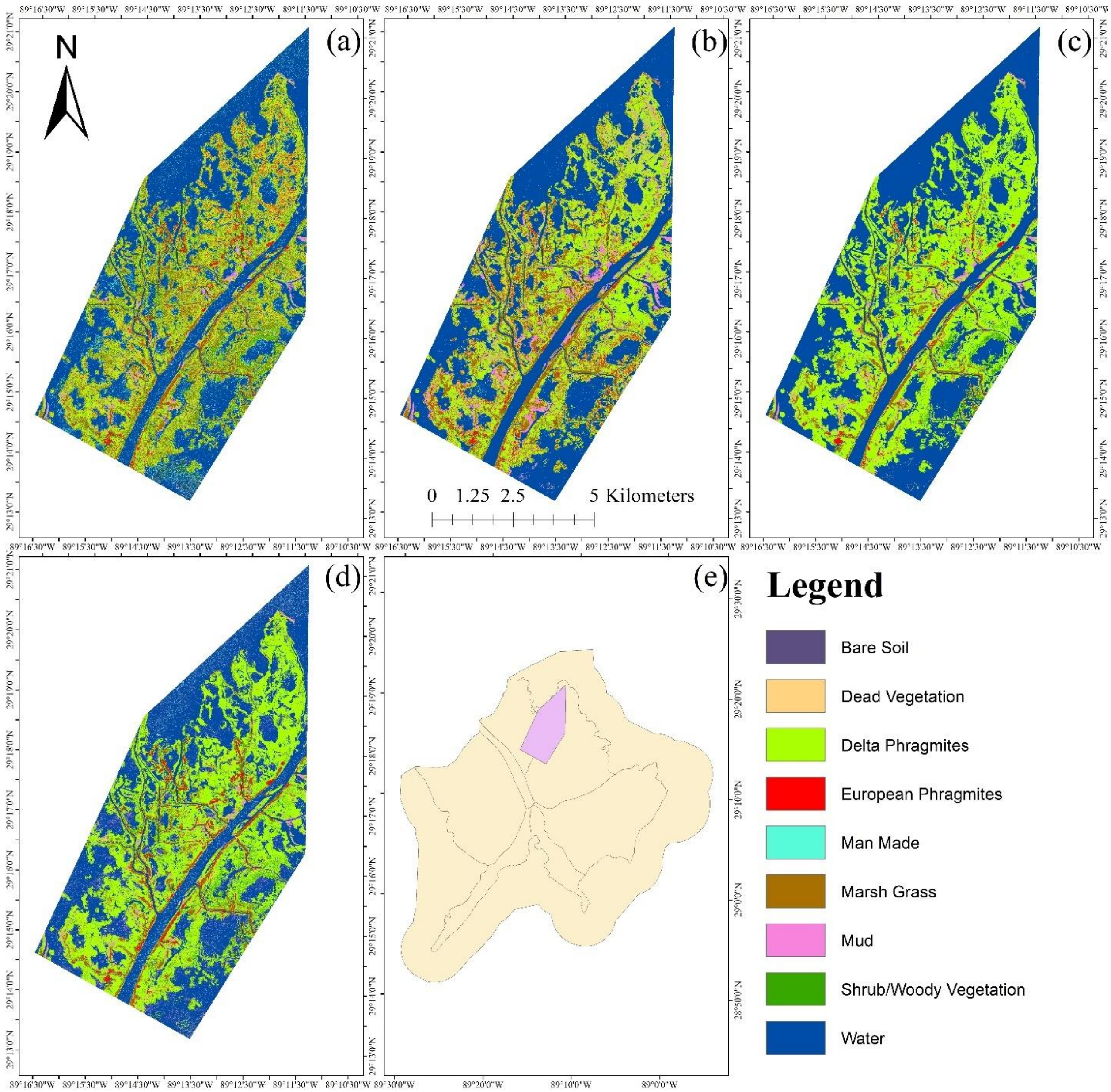

Figure 16. Classification Results for Worldview 2 in Main Pass: (a) KNN; (b) MLC; (c) SVM; (d) RF; (e) Study area in Main Pass.

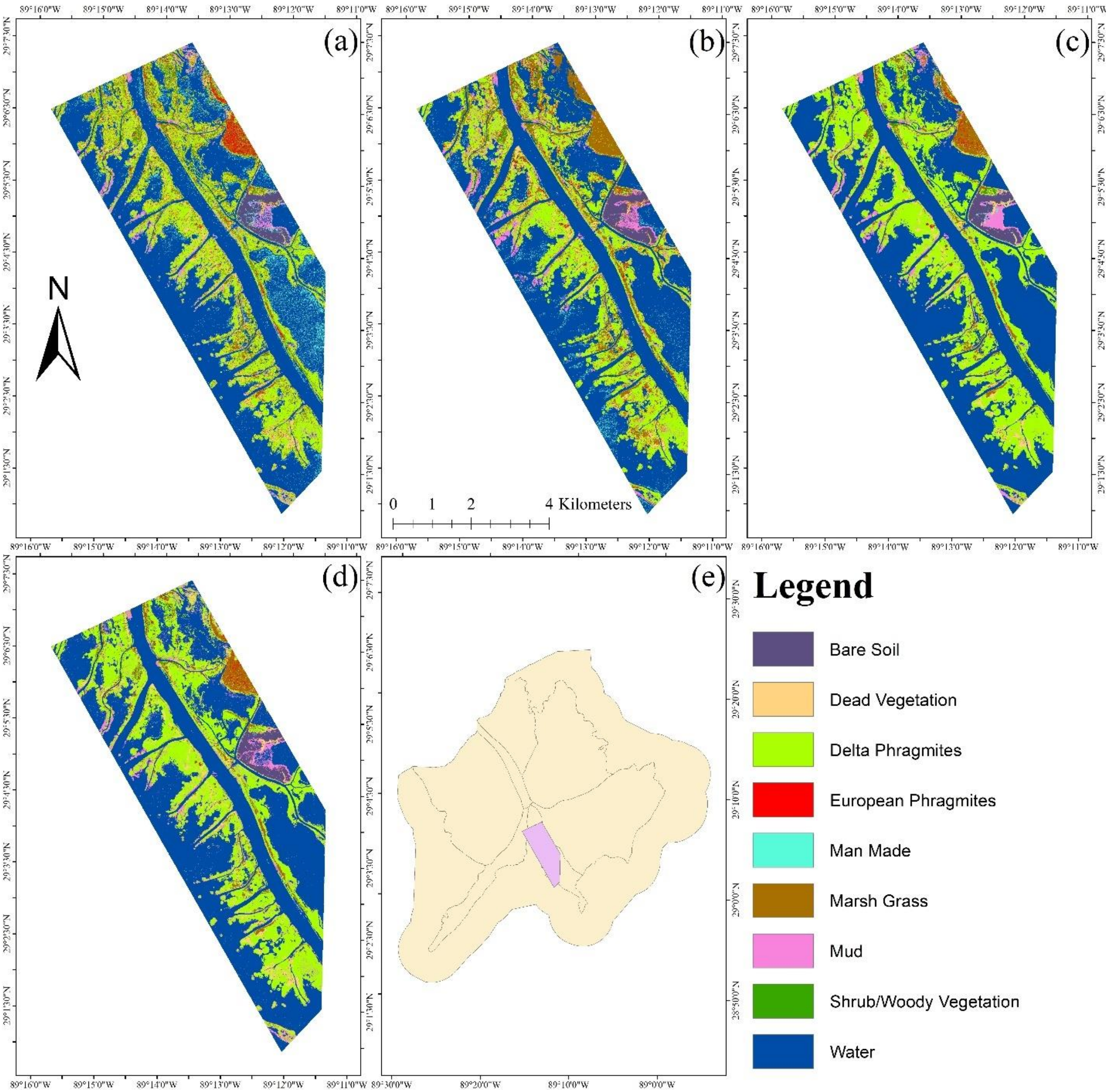

Figure 17. Classification Results for WV-2 in South Pass: (a) KNN; (b) MLC; (c) SVM; (d) RF; (e) Study area in Main Pass.

Table 15. Classification Accuracy of Texture Image added to the SVM classification (%)

	SVM		SVM+Texture (3×3)		SVM+Texture (5×5)		SVM+Texture (7×7)	
Class	**UA**	**PA**	**UA**	**PA**	**UA**	**PA**	**UA**	**PA**
Barren Soil	100.00	100.00	100.00	100.00	100.00	100.00	100.00	100.00
Dead Vegetation	100.00	80.00	100.00	80.00	100.00	80.00	100.00	80.00
Delta Phragmites	73.33	84.62	64.71	84.62	78.57	84.62	76.47	100.00
European Phragmites	90.91	100.00	100.00	100.00	100.00	100.00	100.00	100.00
Man Made	100.00	100.00	100.00	100.00	83.33	100.00	100.00	100.00
Marsh Grass	87.50	77.78	87.50	77.78	88.89	88.89	100.00	88.89
Mud	84.62	100.00	90.91	90.91	83.33	90.91	78.57	100.00
Open Water	100.00	100.00	100.00	100.00	100.00	91.67	100.00	91.67
Shrub/Woody Vegetation	100.00	80.00	88.89	80.00	90.00	90.00	100.00	70.00
Overall Accuracy	90.80		89.66		90.80		91.95	
Kappa	0.90		0.88		0.90		0.91	

5.6 Cross-validation with Landsat Classification

This research selected the Landsat image obtained on November 15, 2021, which is the closest cloud-free image to the WV image, for cross-validation the classification results. NAIP images obtained between November 30 and December 2 of 2021 were also collected for visual interpretation of one hundred randomly distributed Roseau cane and non-Roseau cane samples following the procedure described in Chapter 4. These points are then further divided into training and accuracy assessments. SVM classification was applied to the Landsat images, the final classified product reached an 85% overall accuracy. The classified Landsat images were then further cropped and resampled according to the WV-2 image extent.

The classified results comparison showed in Figure 18 and Figure 19. The results based on Roseau cane percentages showed around 79% agreement between the two classified results, seen in Table 16. This result validated the effectiveness of the Landsat classified result. From the change detection analysis, the Landsat classified result showed a slight underestimation of the Roseau cane distribution, most of the misclassified Roseau cane is along the banks of water channels.

Table 16. Agreement of Worldview Classified Result (W) with Landsat Classified Result (L)

Class type	**Area (km^2)**	**Percentage**
Roseau cane (W & L)	27.11	69.94
Roseau cane (W), non-Roseau cane (L)	5.08	13.10
non-Roseau cane (W & L)	3.56	9.18
non-Roseau cane (W), Roseau cane (L)	3.02	7.78

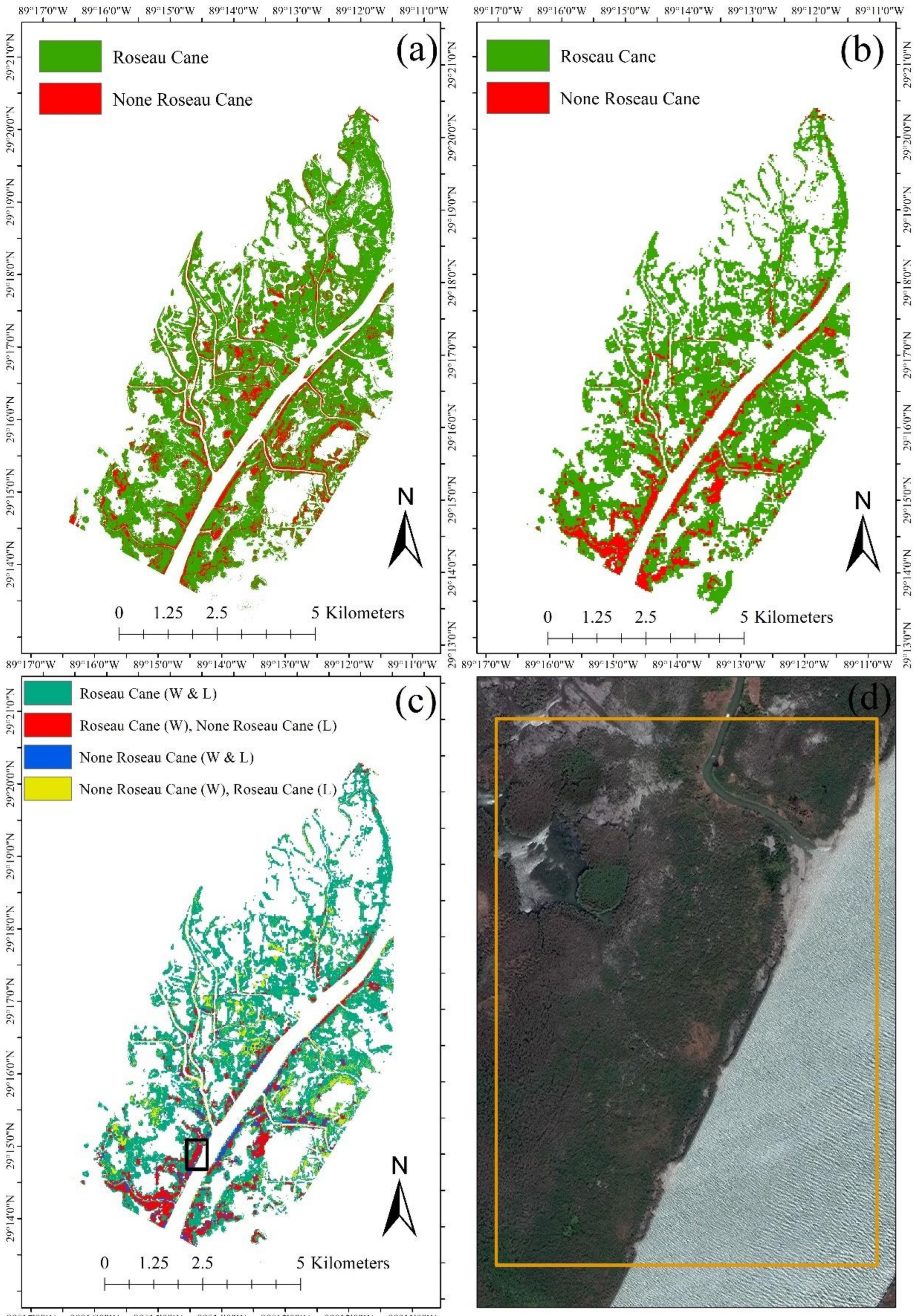

Figure 18. Comparison of Classification Results of Worldview 2 (W) (a) with Landsat 8 (L) (b) in the Main Pass and agreement classification (c).

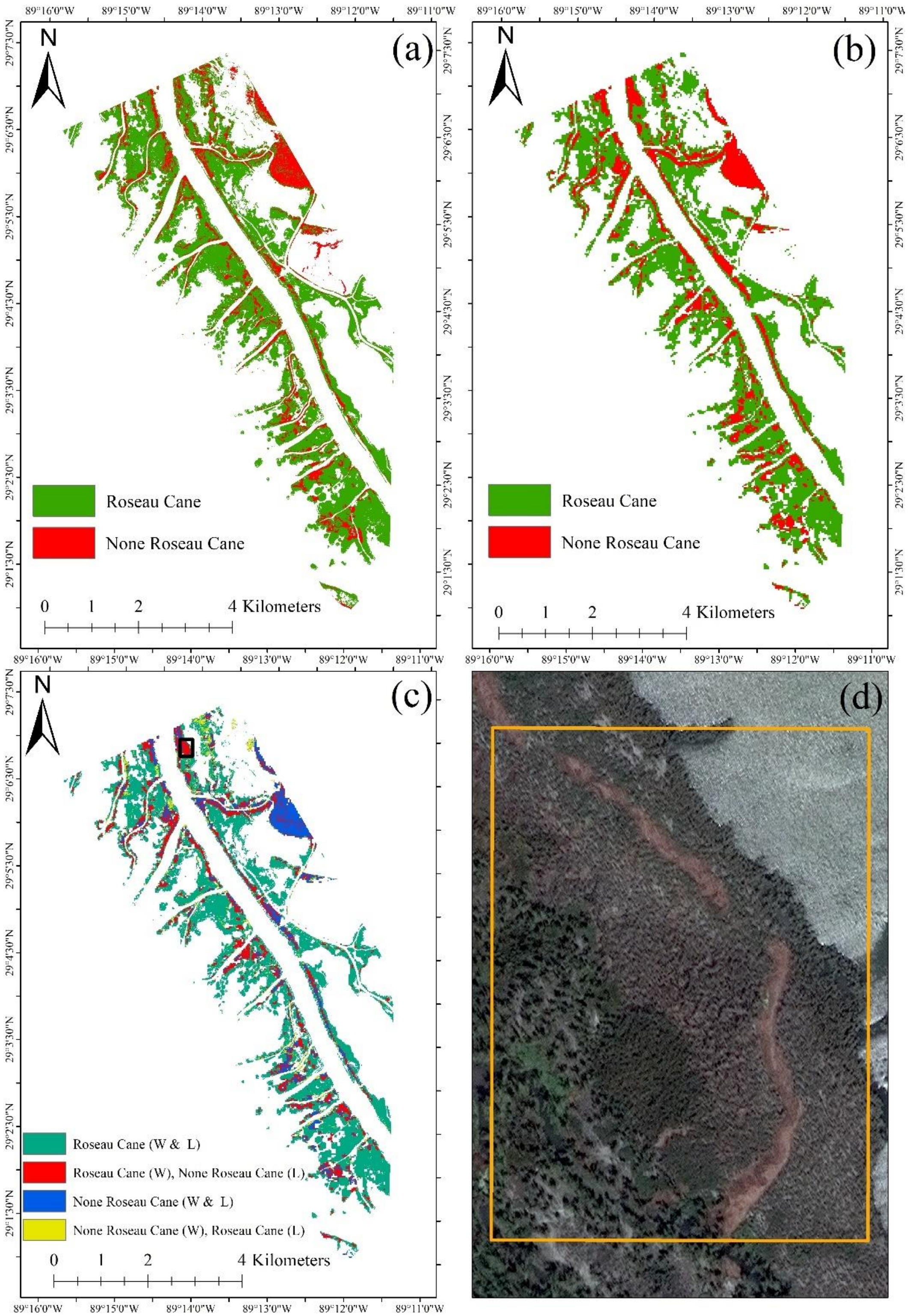

Figure 19. Comparison of Classification Results of Worldview 2 (W) (a) with Landsat 8 (L) (b) in the South Pass and their agreement classification (c).

5.7 Difference of Roseau cane Variants Distribution in the Dieback Area

Landsat images obtained on November 15 of 2021 were selected for dieback analysis. Landsat images of September 30, 2019, were selected as the baseline of dieback detection, considering this research region has continuously recorded scale infection starting from 2019. The next step is to apply the adjusted threshold in both images to generate vegetation coverage and then calculate the NDVI difference of the vegetated area between them. Based on the statistics calculation of the NDVI difference value, the dieback region was successfully extracted. The extracted dieback area was then further cropped to the same area as the Worldview images and resampled to the same pixel size.

The next step of this research was to extract the classified vegetation area of Worldview results, overlapping with the detected dieback area from Landsat. The percentage of each vegetation type in the dieback is shown in Table 17. Comparing each vegetation type percentage of the overall vegetation coverage in the research region, no significant differences between them were observed in this research, especially Delta Phragmites (79.5% vs 80.8%) and European Phragmites (3.65% vs 2.7%), which indicates that no evidence in our experiment showing Delta Phragmites significantly more than European Phragmites distributed in dieback. Considering Delta Phragmites are much more vulnerable than European Phragmites facing scale infection, this might indicate that other stressors besides the scale infection also play important roles in the Roseau cane dieback in this area especially the damage of Hurricane Ida happened in September 2021.

Table 17. The percentage of each vegetation type in the dieback area and the total vegetated area.

Class type	Area (km^2)	% Of Total Vegetation Dieback Area	% Of The Class type to Total Vegetation Coverage
Dead Vegetation	0.49	2.72	3.46
Delta Phragmites	14.31	79.53	80.8
European Phragmites	0.66	3.65	2.7
Marsh Grass	1.58	8.79	8.89
Shrub/Woody Vegetation	0.96	5.31	4.14

5.8 Summary

This chapter conducted a comparative analysis of several remote sensing classification methods based on WV-2 including KNN, RF, CNN, and SVM. Among all these four classification methods, SVM proved to be the most accurate one with highest OA and kappa. The addition of texture information in SVM provided no significant improvement in the classification accuracy but generated wide-speared salt and pepper noise, which indicated a problem with texture-aided classification at the mid-scale due to the fragmented appearance of Roseau cane stands.

The SVM result was used to identify and map the Roseau cane habitat. It could effectively distinguish the Delta Phragmites from the European Phragmites. The classified result showed the Delta Phragmites occupied around 80% of the overall vegetation coverage in the study area while only 2.7 % of the vegetation area belong to the European Phragmites.

Finally, the classified Worldview result was cross-validated with the Landsat classification method established in Chapter 4. The result showed an agreement of around 79%, indicating a reliable Roseau cane extraction from the large-scale Landsat images for the entire study site. Most of the difference was detected in the banks of the water channel area. Furthermore, although Delta

Phragmite consisted of nearly 80% of the dieback area, the dieback rates for most categories were comparable to their percentage.

Chapter 6. Roseau Cane Habitat Mapping and Monitoring through Rapid and Multi-Seasonal Drone Sensors

6.1 Introduction

Wetland ecosystems are vulnerable to natural and human disturbances. Current methods of monitoring estuarine wetlands are often based on field surveys in small plots, difficult to monitor in a large area. In addition, the highly heterogeneous landscape pattern of estuarine wetlands greatly increased the difficulty of wetland vegetation species investigation and identification. There is a growing need for more rapid and responsive remote sensing data acquisition in wetland vegetation research. Satellite-based multispectral remote sensing images can take advantage of their large observation range, fixed revisit period, and extensive historical data in long-term and wide-range remote sensing applications and monitoring (Slagter *et al*, 2020). However, in small-scale wetland remote sensing monitoring, multispectral satellite images are easily constrained by factors such as spatial resolution and image availability, which need to be supplemented by other data resources.

With the development of drone technology and small multispectral sensor technology in recent decades, drone-based low-altitude remote sensing has become another important methods for remote sensing image acquisition. Capable of carrying multispectral cameras and flying at lower altitudes, drone technology is not only easy to acquire remote sensing images with high spatial resolution but also convenient for drone takeoff and landing to acquire remote sensing images with a high temporal resolution, which is critical for studying unexpected disturbances such as a hurricane, storm surges, and freeze events (Goodbody *et al*, 2017).

This study designed comparative experiments to determine whether the newly introduced 10 bands drone remote sensing images can achieve high accuracy of wetland species classification especially the two variants of the Roseau Cane. Various landscape types of estuarine wetlands in

MRD, including various vegetation plants, were extracted by using the drone remote sensing image based on supervised classification methods. Wetland vegetation information extraction aslo designed for seasonal change analysis. Given the difficult accessibility of wetland field sampling, this study developed a drone sampling strategy for classification, which might help conduct small-scale ecosystem landscape research. In addition, the research will also test the capability to detect the damaged area of Roseau cane and assess the seasonal change pattern of the wetland vegetation coverage.

6.2 Method

This section proposes multi-temporal drone remote sensing image change analysis, which is specifically divided into five steps.

In the first step, the multispectral drone is used to acquire seasonal remote sensing images for pre-processing. This research analyzed the errors generated in the process of wetland vegetation classification and found many challenges. To avoid noise and image quality degradation due to insufficient light for the camera and the time limit spent for traveling to sites, the flight time is generally from 11:00 am to 4:00 pm in the wetland sites.

Step 2 is to take field investigation, construct the classification scheme of the estuary wetland landscape, divide the RTK-GPS surveyed samples as training samples, and verify samples. However, limited wetland accessibility may lead to not evenly distributed sampling points in the study area and a lack of sufficient samples for a certain type of wetland species. To solve this issue, a phantom 4 nature color drone is used to gather drone sampling images with lower flight height and higher spatial resolution.

In the third step, this research generates randomly distributed sample points in the study area following the drone sampling procedure and identifies extra training samples and accuracy assessment samples to supplement the GPS-surveyed samples for classification. However, due to the angle of sunlight and tall vegetation types, some areas of the images are covered with shadows, which increases the heterogeneity of similar species and the similarity of different species, thus making the classification process more difficult. To deal with this problem, shadow was added as a separate class in the classification test.

The fourth step uses the overall training samples to generate multiple classifiers and compare the classification result. The confusion matrix is used to evaluate the accuracy of the classified results, then choose the most accurate one for wetland habit mapping.

In the last step, the seasonal change pattern of the wetland vegetation coverage change is explored through Landscape indices.

6.3 Dataset and Preprocessing

6.3.1. Study Area

A 0.2 km^2 study site located in Pass-a-Loutre of lower MRD was selected for the drone mapping study. The major vegetation type in the study area includes Delta Phragmites, European Phragmites, Cutgrass, and Cattail. The vegetation growth condition in this study area is a mixed growth pattern of Roseau cane and Marsh Grass, and the area is a typical wetland vegetation type of the MRD. The south part of the study site has relatively shallow water and is difficult to access in person during the fall season of 2021 due to extremely low water levels. This research area experienced extremely cold weather during February 2021 and heavy damage from Hurricane Ida in September 2021, many dead vegetation areas were observed in the study site. By referring to the actual ground vegetation growth area, this research designed the drone flight path to carry out the drone multispectral image acquisition on March 22, September 24, November 7, 2021, and April 28, 2022. The location of the drone field data collection area in this experiment is shown in Figure 20.

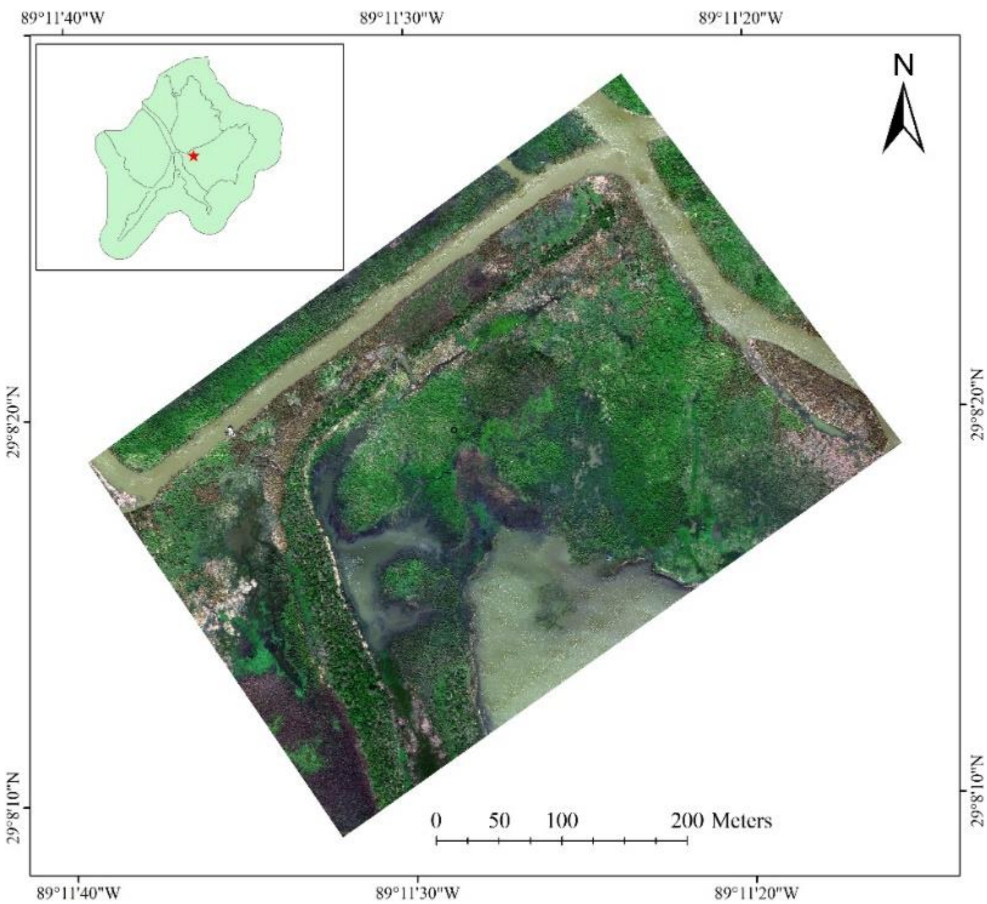

Figure 20. The drone monitoring site in Pass-A-Loutre of lower MRD (March 22, 2021).

6.3.2. RedEdge-MX Dual Camera System

Micasense Multispectral Camera Company, USA, has recently developed and designed a RedEdge-MX Blue multispectral camera based on RedEdge-MX. This new RedEdge-MX Blue together with the previous RedEdge M forms the RedEdge-MX Dual Camera 10-band imaging system. The system corresponds to the multiple bands of imaging sensors carried by Landsat8 and Sentinel-2A satellites and acquires more spectral information in one flight, which can be used in many fields such as agriculture, forestry, urban planning, and water quality monitoring. The

MicaSense Dual camera which capable of simultaneously collect 10 discrete spectral bands contains two cameras with a focal length of 5.5 mm, a field of view of 47.2°, and the image resolution of 1280×960 for each camera. The camera system was calibrated with the 0.3 m×0.3 m gray plate reflectance before and after a flight. The band parameters of the MicaSense RedEdgeM multispectral imager are shown in Table 18.

Table 18. Band information of Micasense RedEdge-MX Dual Camera system

RedEdge M			**RedEdge MX - Blue**		
Band	**Center Wavelength (nm)**	**Bandwidth (nm)**	**Band**	**Center Wavelength (nm)**	**Bandwidth (nm)**
Blue	475	32	Coastal Blue	444	28
Green	560	27	Green	531	14
Red	668	14	Red	650	16
Red Edge	717	12	Red Edge	705	10
Near IR	842	57	Red Edge	740	18

6.3.3. Orthophoto Generation

Drone images are significantly different from satellite images in terms of navigation, positioning, and payload (Colomina *et al*, 2014). Because of these differences, drone images need to be preprocessed before image analysis, which includes air-triple encryption, orthorectification, and image stitching. Nowadays, with the continuous development of science and technology, the cost of software for processing drone aerial survey images is decreasing and the processing capacity is increasing. It has become a reality to use low-altitude drones to quickly acquire and generate orthophoto images for analysis.

Agisoft Metashape (previously Agisoft Photoscan) is a 3D scanning software system from the Russian company Agisoft LLC. The software uses computer vision methods to process small-size, large numbers, and high-overlap images acquired by low-altitude drones. It is capable of automatically reconstructing 3D point clouds and generating digital surface models (DSM) from the point clouds, and then generates Digital Orthophoto Map (DOM). Agisoft Metashape can obtain the flight attitude parameters and GPS information directly from the image without a camera check and can centralize any photo according to the latest multi-view 3D reconstruction technology with high efficiency and accuracy. In addition, the software can generate 3D models with ground coordinates by adding multiple control points. The entire workflow, both the orientation of the image and the reconstruction of the 3D model is fully automated. Since Agisoft Metashape can generate high-resolution orthophotos and DEM models with fine color textures after the above steps, it has been widely used in many related studies (Sona *et al*, 2014).

Agisoft Metashape mainly uses Structure from Motion SfM (SfM) algorithm to preprocess drone images by using multiple drone images Position Orientation System (POS) data to align all images spatially. In the term of SfM, the structure refers to the 3D point cloud of the scene, the motion refers to the position and direction of the camera, and the SfM is capable of generating the position of the point cloud through the moving camera to the interconnection between points (Ma *et al*, 2015). The motion information is used to computationally recover the projection matrix of the drone camera and the three-dimensional structure of the scene, thereby obtaining a three-dimensional scene with coordinate information, and finally generating a three-dimensional point cloud (Turner *et al*, 2012). The SfM technique mainly uses the Scale-Invariant Feature Transform (SIFT) algorithm, which extracts the feature points and performs centralized vectorization on the extracted feature points. The SIFT algorithm extracts the feature points, matches the feature points with the vector description in the rated pattern, eliminates the mismatched points after the software self-tested matching results, and finally uses the corrected matching feature points to do image stitching (Komárek *et al*, 2018).

Agisoft Metashape was used to generate the orthophotos of the study area, and the process was as follows.

(1) Data input. Input all the filtered 10 bands images and the POS data corresponding to each image into the software. Input the reflectance calibration parameters from the reflectance calibration board to transfer the initiated DN value of the image to the reflectance value.

(2) Image alignment. It is automatically processed by Agisoft Metashape at this stage, is used to build a sparse point cloud by finding the positions of the cameras when the photos are taken through the input POS data, and the image alignment is performed while reading the internal calibration parameters of the camera to correct for the image distortion present in each image.

(3) Point cloud generation. The program uses the acquired image pixel value to calculate the image depth information based on the predicted orientation of the camera, then generates a dense point cloud.

(4) Create a grid model. The program will quickly reconstruct the 3D model of the target based on the dense point, that is, using the internal lines, surfaces, and other data of the images, to reproduce the real morphological characteristics of the objects.

(5) Given texture. For the completed grid model, each part of the model will be given the texture of the original image. The final texture and the ground surface resolution (GSD) will depend on the quality of the images obtained in this study.

(6) DOM output. Choose orthophoto as the mapping mode, then output the digital orthophoto map of the study area.

6.3.4. Field data collection

This research used Trimble R10 RTK GPS to get centimeter-level accuracy ground sampling points, ensuring accuracy for high spatial resolution remote sensing classification. The experiment setups included drone flights with ground vegetation sampling based on RTK GPS. The team distributed ten targets at the relatively flat areas as ground control points for accurate georeferencing of each field survey samples. The flight was conducted in clear, cloud-free conditions between 11:00 and 14:00, with a flight height of 120 m, 70% overlap, and 8m/s flight speed. The final orthophotos generated from Agisoft had around 8 cm spatial resolution. Then the project team will collect randomly distributed samples and the targets for classification and accuracy assessment with RTK GPS. The project team repeated the drone data collection procedure on March 22, September 24, November 7, 2021, and April 28, 2022, for multi-temporal data collection.

6.3.5. Drone Sampling

Considering the difficulty faced in the field survey, this research adopted two ways to obtain sample data in the field: one way is to take measurements by centimeter-level positioning accuracy RTK GPS; the other way is to use another drone flight at a much lower altitude with much higher resolution images for visual identification of randomly selected samples. While fully utilizing the available battery power from the industrial drones for the maximum extent of habitat mapping, the relatively cheaper DJI phantom drones with a natural color camera and more battery packs allow lower flights for higher resolution images in partial or entire study areas. The higher-resolution images provide enhanced texture information that is useful and critical for separating plant types. For example, in this research, Roseau cane vegetation on the 8 cm images might look very similar to other wetland marshes, and hence is difficult to determine the vegetation types. But its unique tall crown structure in the 1 cm resolution drone sampling images can be identified.

The drone used in the drone sampling is DJI Phantom 4, which is a multi-rotor vehicle equipped with six visual sensors, two sets of infrared sensors, one set of ultrasonic sensors, a GPS/GLONASS dual-mode satellite positioning system, and a compass dual redundant sensor to help the vehicle acquire the stable and high-precision image and positioning data. The drone carries a digital camera with three visible bands, with a camera pixel count of 20 million and a dimension of 5472 × 3678 pixels. The flight height were 40 m, flight speed were 8m/s, 70% overlap, and 70% sidelap. The flight control platform software used is Atlas Flight, which is our MicaSense camera recommended and can generate flight plans based on presetting flight parameters (Jiang *et al*. 2020).

In this section, the results of the field survey and the drone images were both taken into consideration, and 9 categories were identified, including Dead Vegetation, Delta Phragmites, European Phragmites, Man Made, Marsh Grass, Mud, Water, Shrub/Woody Vegetation and Shadow. The number of samples for training (T) and accuracy assessment (A) in each field trip is listed in Table 19.

Table 19. Training and accuracy assessment sample numbers for Roseau cane habitat classification

	03.21.2021		09.24.2021		11.07.2021		04.22.2022	
Class	**T**	**A**	**T**	**A**	**T**	**A**	**T**	**A**
Dead Vegetation	26	10	38	11	28	17	35	10
Delta Phragmites	63	10	73	12	71	11	97	16
European Phragmites	20	10	34	11	39	10	20	10
Man Made	10	5	10	5	13	5	10	5
Marsh Grass	76	23	93	26	82	17	105	31
Mud	12	5	14	5	20	15	20	10
Water	45	10	45	10	23	21	39	10
Shadow	20	10	20	10	22	13	20	10
Shrub/Woody Vegetation	20	10	20	10	20	10	20	10
Overall	292	93	347	100	318	119	366	112

6.3.6. Wetland Landscape Index

Landscape spatial pattern refers to the spatial arrangement of landscape patches of different sizes and shapes. It is an important indicator of landscape heterogeneity (O'Neill *et al*, 1988). Wetland landscape pattern is the result of the combined effect of various ecological and hydrological processes. By calculating the landscape index, a series of data with statistical characteristics can be obtained, so that the distribution pattern of wetland landscapes at different times can be comparatively analyzed.

When analyzing the landscape pattern by landscape index, the landscape is usually divided into three metrics: landscape metrics, class metrics, and patch metrics. In this study, the landscape metrics and class metrics are mainly studied, and the main software for calculation is the landscape pattern index software Fragstas 4.2. This research combined remote sensing technology and knowledge of landscape ecology to preprocess the wetland landscape classification map of the drone site and calculated the landscape indices of each typical wetland vegetation (Delta Phragmites, European Phragmites, and Marsh Grass, etc.) for each period by ArcGIS and Fragstats software. Since there is limited research on the small-scale landscape pattern method as a reference, this research selected several key landscape indices for analysis by combining the characteristics of the internal landscape of the research area.

Some of the selected indicators and calculation formulae are as follows:

(1) Class Area (CA), CA is the area of individual landscapes.

(2) Percentage of Landscape (PLAND)

$$PLAND = \frac{\sum_{j=1}^{n} a_{ij}}{A}(100)$$

Where, and represents the area of the j patch in the i landscape type; A is the total area of all landscapes. The PLAND characterizes the percentage of the area of a patch type to the total area of the landscape and is an important basis for determining the dominant species in the landscape.

(3) Patch Density (PD)

$$PD = \frac{N_i}{A_i}$$

where N_i represents the total number of patches of this landscape type and A_i represents the total area of this landscape type. PD reflects the degree of fragmentation and spatial heterogeneity of the landscape. In general, the higher the PD, the higher the fragmentation level of the landscape type.

(4) Mean Patch Size (MPS)

$$MPS = \frac{CA}{NP}$$

Where CA represents the total area of a patch type, and NP is the number of patches. The MPS is used to characterize the integrity and fragmentation of the landscape type, the larger the MPS, the lower the fragmentation level of the landscape type.

(5) Landscape Shape Index (LSI)

$$LSI = \frac{0.25E}{\sqrt{A}}$$

Where E indicates the total length of all patch boundaries. LSI reflects the complexity of the landscape, the lower value of LSI, the better the roundness of the landscape, which represents the simpler its shape, and conversely, with the larger value of LSI, the more complex its shape.

(6) Largest Patch Index (LPI)

$$LPI = \frac{\max(a_{ij})}{A}(100)$$

where $\max(a_{ij})$ represents the maximum patch area in each type, and A represents the overall path area. The LPI helps to determine the dominant type of landscape.

(7) Shannon's Evenness Index (SHEI)

$$SHEI = \frac{-\sum_{j=1}^{m}(p_i \times ln\, p_i)}{ln\, m}(0 \leq SHEI \leq 1)$$

Where m indicates the number of landscape types in the study area, and P_i indicates the proportion of the area of the i type of landscape to the total area of the whole landscape. The larger the value of SHEI, the closer the ratio of the area occupied by different patch types in the landscape and the higher the degree of homogeneity.

(8) Shannon's Diversity Index (SHDI)

$$SHDI = -\sum_{j=1}^{m}(p_i \times ln\, p_i)$$

The value of SHDI reflects the level of diversity of the landscape. In the whole study area, if the area of different types of landscapes is in equal proportion, it indicates high diversity of the landscape. On the contrary, if the proportion of the area of different types of landscape in the whole study area is very different, the landscape shows low diversity.

6.4 Drone Classification

This study conducted high-resolution drone remote sensing image classification based on field survey points combined with drone sampling points to extract wetland vegetation distribution information and change pattern during the year. To improve the accuracy of change analysis, comparison experiments of four commonly used classification methods were designed and implemented. In addition, this research also tested whether the addition of texture information could improve the overall accuracy.

6.4.1 Classification Method Comparison

This study has selected orthophotos taken from April 22, 2022, for the classification comparison test. Based on the usage of each classifier algorithm in current research on classification problems, this paper selects typical methods of KNN, MLC, SVM, and RF. The accuracy of the classification results was verified by using the validation samples collected in the field and through drone sampling. The overall accuracy (OA), Kappa coefficient, user accuracy (UA), and producer accuracy (PA) of each classification result were calculated separately by establishing confusion matrices for the classification schemes in the drone study areas. The comparison result is listed in Table 20.

Table 20. Classification accuracy of Roseau cane habitat based on the drone image collected on April 22, 2022

	KNN		MLC		SVM		RF	
Class	**UA**	**PA**	**UA**	**PA**	**UA**	**PA**	**UA**	**PA**
Dead Vegetation	76.92	100.00	55.56	100.00	100.00	100.00	90.91	100.00
Delta Phragmites	66.67	75.00	68.18	93.75	76.19	100.00	69.57	100.00
European Phragmites	47.06	80.00	70.00	70.00	100.00	90.00	100.00	40.00
Man Made	100.00	60.00	100.00	40.00	100.00	100.00	100.00	60.00
Marsh Grass	80.00	51.61	80.00	77.42	90.00	87.10	76.47	83.87
Mud	77.78	70.00	100.00	70.00	100.00	80.00	90.00	90.00
Water	90.91	100.00	100.00	100.00	90.91	100.00	100.00	100.00
Shadow	100.00	100.00	100.00	60.00	100.00	100.00	100.00	100.00
Shrub/Woody Vegetation	90.91	100.00	100.00	70.00	100.00	80.00	100.00	70.00
Overall Accuracy	76.79		78.57		91.96		84.82	
Kappa	0.73		0.75		0.91		0.82	

In terms of classification accuracy, the SVM method has the best overall accuray (91%) compared to KNN (77%), MLC (78%), and RF (84%). In terms of each class type, KNN and MLC both have lower accuracy in Dead vegetation, Delta Phragmites, and European Phragmites. For KNN, European Phragmites clearly showed overestimation in the whole study site, and poor classification accuracy at 47%. For MLC, Dead vegetation showed a relative overestimation in the whole study site, while MLC has a significant underestimation of Delta Phragmites distribution shown in Figure 21. RF, on the other hand, performs poorly in the classification of the two variants of Roseau cane, especially the poor performance of European Phragmites with a PA of only 40%, indicating that it is difficult to accurately distinguish between Delta Phragmites and European

Phragmites in this study compared to SVM, besides some shallow water area also been misclassified as mud. In general, SVM produced highest classification accuracy and can distinguish Delta Phragmites and European Phragmites more accurately and can improve the detection of water boundaries to a certain extent, so the subsequent studies of this experiment are based on SVM.

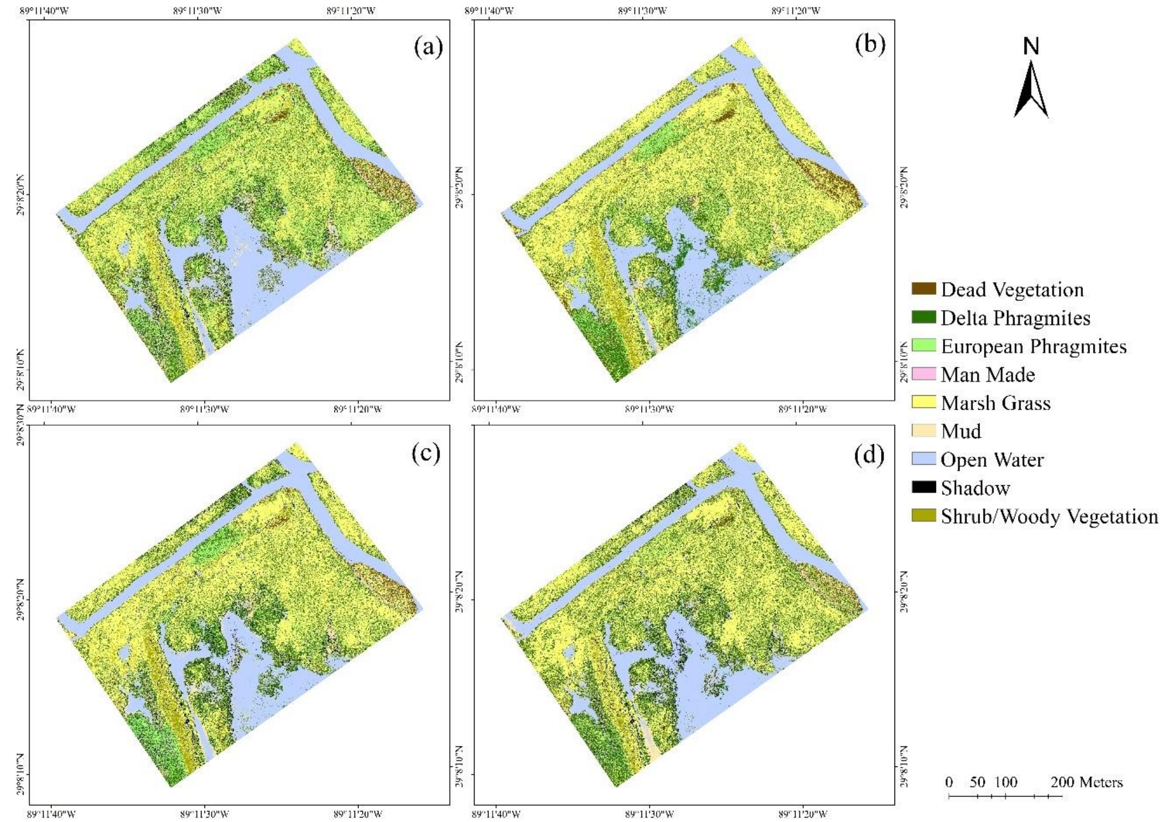

Figure 21. Results of Roseau cane habitat classification based on drone survey on April 22, 2022: (a) KNN; (b) MLC; (c) SVM; (d) RF

6.4.2 Will Texture improve Roseau cane classification accuracy?

When optical data were used for classification, it may be difficult to distinguish some marsh vegetation clusters with similar spectral curves because they had a similar spectral curve. Therefore, in this research, we further extracted texture features from the images and used the texture information for marsh wetland vegetation cluster identification. From the last section, this research found SVM has the best classification accuracy, thus different window sizes of texture information were applied in SVM classification. The texture images were generated using the standard deviation value of the pixel in the window, and the experimented window sizes include 3 × 3, 5 × 5, and 7 × 7. The classification result is listed in Table 21.

Table 21. Classification Accuracy of Texture Image added to the SVM classification (%)

	SVM		**SVM+Texture (3×3)**		**SVM+Texture (5×5)**		**SVM+Texture (7×7)**	
Class	**UA**	**PA**	**UA**	**PA**	**UA**	**PA**	**UA**	**PA**
Dead Vegetation	100.00	100.00	80.00	80.00	77.78	70.00	100.00	90.00
Delta Phragmites	76.19	100.00	77.78	87.50	92.86	81.25	100.00	81.25
European Phragmites	100.00	90.00	100.00	60.00	85.71	60.00	85.71	60.00
Man Made	100.00	100.00	75.00	60.00	60.00	60.00	83.33	100.00
Marsh Grass	90.00	87.10	82.35	90.32	80.00	90.32	76.92	96.77
Mud	100.00	80.00	88.89	80.00	90.91	100.00	100.00	90.00
Water	90.91	100.00	90.91	100.00	100.00	100.00	100.00	100.00
Shadow	100.00	100.00	100.00	100.00	100.00	100.00	100.00	100.00
Shrub/Woody Vegetation	100.00	80.00	90.00	90.00	81.82	90.00	100.00	80.00
Overall Accuracy	**91.96**		**85.71**		**85.71**		**89.29**	
Kappa	**0.91**		**0.83**		**0.83**		**0.87**	

When texture information was added, the classification results showed a reduction in the number of small patches and a slight reduction of the overall accuracy which is similar to the texture result in the WV-2 experiment. The overall accuracy slightly increased with the larger window size may indicate that more background texture input may improve the classification result. In general, the differentiation effect is not obvious for the classification compared with spectral features, and the following research will only use SVM without texture input in the next section about the change analysis.

6.5 Change Analysis

6.5.1 Multitemporal Classification

To investigate the vegetation cover changes reflected by the multi-temporal images, this study used the classification method selected in the previous section to classify the collected multitemporal drone-derived orthophotos for each period, and the changing pattern of the study site was analyzed in terms of landscape indices. The accuracy of the classified results is listed in Table 22.

Table 22. Classification Accuracy of Each period Drone image (%)

	03.21.2021		**09.24.2021**		**11.07.2021**		**04.22.2022**	
Class	**UA**	**PA**	**UA**	**PA**	**UA**	**PA**	**UA**	**PA**
Dead Vegetation	90.91	100.00	83.33	90.91	80.00	94.12	100.00	100.00
Delta Phragmites	71.43	100.00	73.33	91.67	77.78	63.64	76.19	100.00
European Phragmites	88.89	80.00	100.00	36.36	77.78	70.00	100.00	90.00
Man Made	100.00	100.00	100.00	60.00	83.33	100.00	100.00	100.00
Marsh Grass	94.74	78.26	83.33	96.15	93.75	88.24	90.00	87.10
Mud	100.00	80.00	83.33	100.00	100.00	100.00	100.00	80.00
Water	100.00	100.00	90.91	100.00	100.00	100.00	90.91	100.00
Shadow	100.00	100.00	100.00	100.00	100.00	100.00	100.00	100.00
Shrub/Woody Vegetation	90.91	100.00	100.00	90.00	100.00	100.00	100.00	80.00
Overall Accuracy	91.40		87.00		91.60		91.96	
Kappa	0.90		0.85		0.90		0.91	

Among all the 4 periods of orthophoto, the overall classification accuracy of the SVM method is higher than 85%. The accuracy of September data is slightly lower, the OA of September data is 87% and the Kappa coefficient is 0.85, partially because the data was captured under the very strong interference of sunlight change due to cloud. The classification accuracy of other periods both reached OA above 91% and Kappa coefficient above 0.90. The classification accuracy of the Mud, Water, and Man Made classes was relatively stable in all four periods, with UA between 83.3% to 100% and PA between 83.3% to 100%.

The accuracy of the vegetated area varied slightly between the four periods. The best results were obtained in Shrub/Woody vegetation, then the Marsh Grass, and Dead Vegetation. For variants of the Roseau cane, the accuracy of Delta Phragmites or European Phragmites was relatively low among the 9 categories, with UA around 75% and PA of 80% in all the periods.

From the distribution of each period result seen in Figure 22, it is seen that there is a significant change in dead vegetation coverage since March 2021 when the study site experienced a severe cold weather event in February 2021, and the September result showed a significant impact of vegetation death might be caused by the Hurricane Ida. In addition, the low water level in the winter season turned the large area of shallow water to mud in November 2021 data. After that, there is a recovery process of vegetation in the study area, and almost all the previous dead vegetation areas were replaced with newly grown wetland vegetation. The distribution of the variants of Roseau cane, Delta Phragmites and European Phragmites is mostly located in the bank area of the water channel.

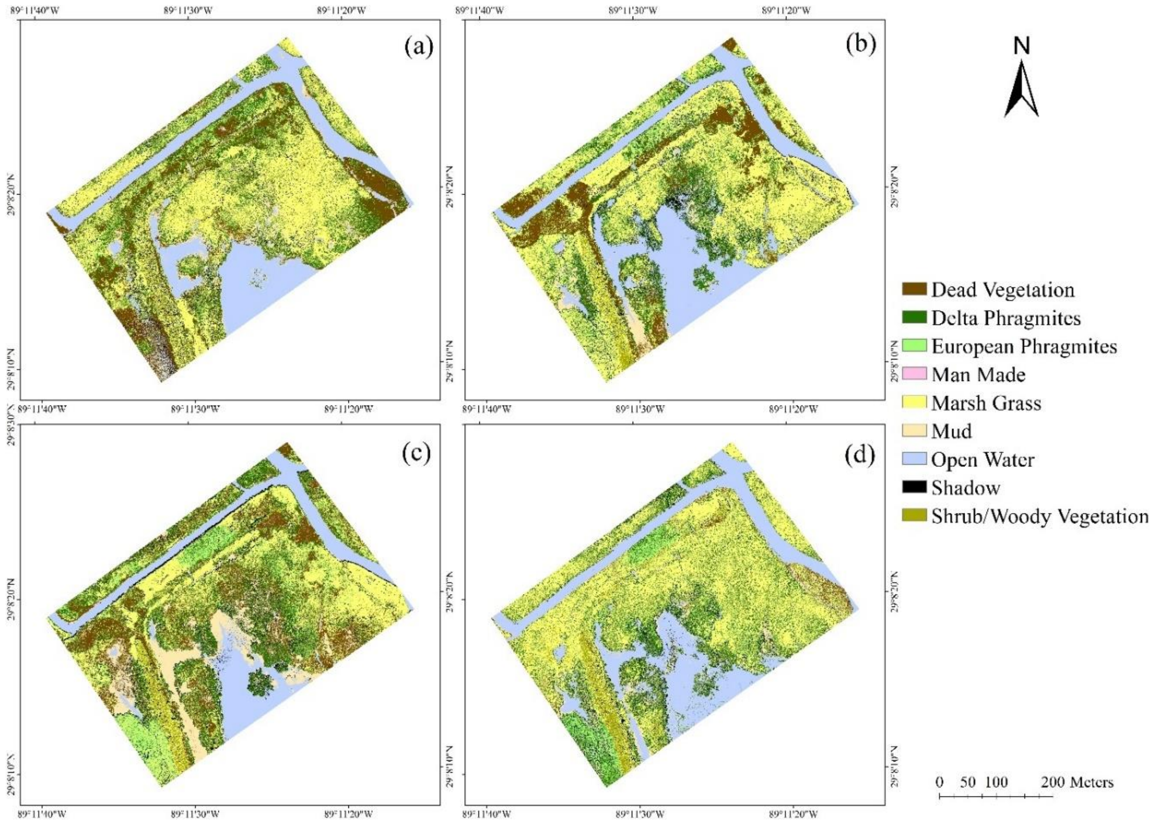

Figure 22. Multitemporal Roseau cane habitat Classification Result: (a) 03.21.2021; (b) 09.24.2021; (c) 11.07.2021; (d) 04.22.2022

6.5.2 Wetland Vegetation Landscape Change

This research collected the selected landscape indices for vegetation change analysis. These indices include Class Area (CA); Percentage of Landscape (PLAND); Patch Density (PD); Mean Patch Size (MPS); Largest Patch Index (LPI); Landscape Shape Index (LSI); Shannon's Diversity Index (SHDI) and Shannon's Evenness Index (SHEI). The 5 vegetation classes have been selected for analysis, including Dead Vegetation, Delta Phragmites, European Phragmites, Marsh Grass, and Shrub/Woody Vegetation.

In our study area, the dominant vegetation coverage is Marsh Grass which occupied around 30%-40% vegetated area, while Delta Phragmites occupied around 20%, European Phragmites occupied less than 10%, and Shrub/Woody vegetation occupied around 3%. From Figure 23, there is a significate drop in CA/PLAND of Marsh Grass can be observed from September 2021 to November 2021, while it also accompanied by an increased CA/PLAND of Dead Vegetation which indicates that Marsh Grass experienced severe damage during this period. This might be caused by Hurricane Ida happened in September 2021. Meanwhile, the Delta Phragmites and European Phragmites slightly increased in the study area and might claim some area after the death of Marsh Grass. The CA/PLAND of Marsh Grass slightly back to normal in April 2022, indicating a fast recovery of wetland marshes within half a year. A significant decrease of CA/PLAND of Dead Vegetation indicates that healthy vegetation expanded in the study area for a fast recovery.

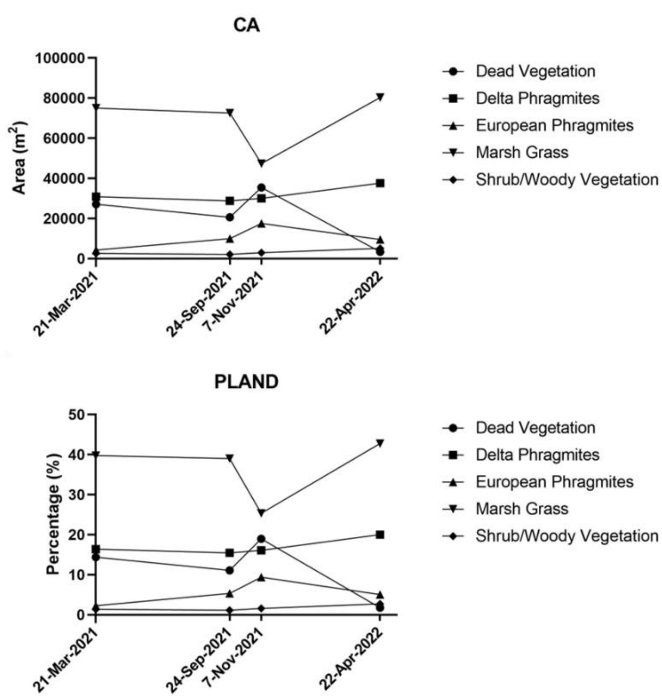

Figure 23. CA and PLAND change for vegetation-related classes.

LPI represents the dominant species in the study area, which prove to be the Marsh Grass in our study area in all four periods, as seen in Figure 24. The LPI of Marsh Grass is significantly higher than other vegetation types, however, it experienced a decreasing trend between September and November, indicating the degree of domination declined due to the massive death of Marsh Grass during this period. LSI represents the fragmentation level of the class. In our study area, Delta Phragmites has the highest LSI than other vegetation types, indicating it is the most fragmented vegetation class. This might be because of the resolution impact on plant appearance in high-resolution drone images. Delta Phragmites often has tall stems and sparse leaves. At the centimeter level, high-resolution drone images, the understory plants, water, and mud between the gaps among stems may cause a fragmented appearance of Phragmites patches.

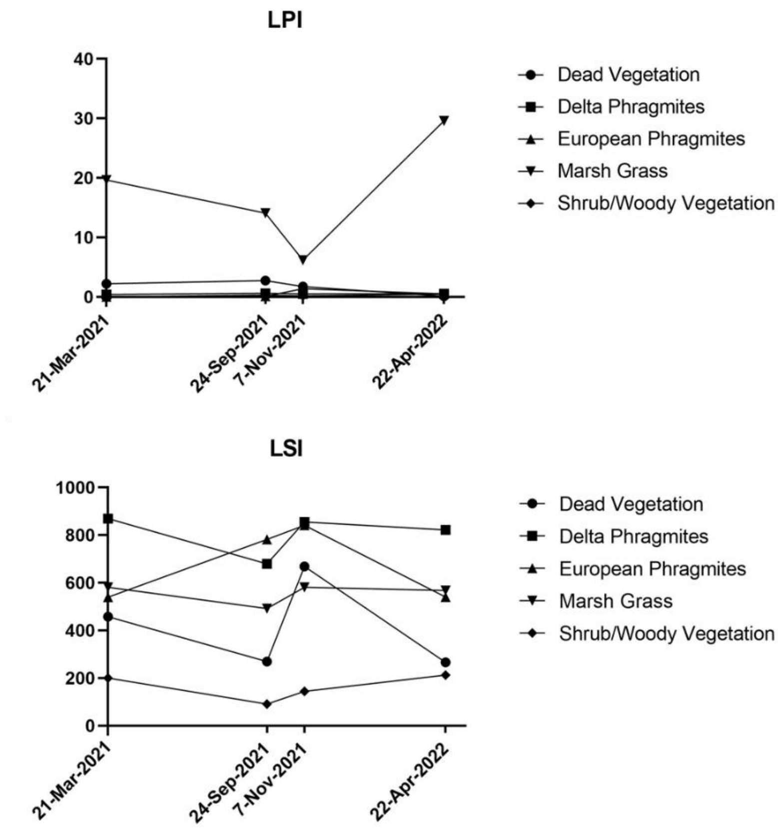

Figure 24. LPI and LSI change for vegetation-related classes.

As can be seen from Figure 25, the Point Density (PD) of Delta and European Phragmites is the highest among all the vegetation types, which means they are more fragmented than other vegetation, like the LSI result, the patches of variants of Roseau cane tend to be dispersed and the overall landscape appears fragmented, it is more likely been influenced by stressors in the study area. Shrub/Woody vegetation, on the other hand, is the least fragmented vegetation type in the study area and very stable in all four periods. For MPS, the Marsh Grass has the highest value which means the patch of Marsh Grass is normally bigger than other vegetation types, it also experienced a significant decline after September, considering the PD increased in the same period, it indicts many big patches been cut into a small one.

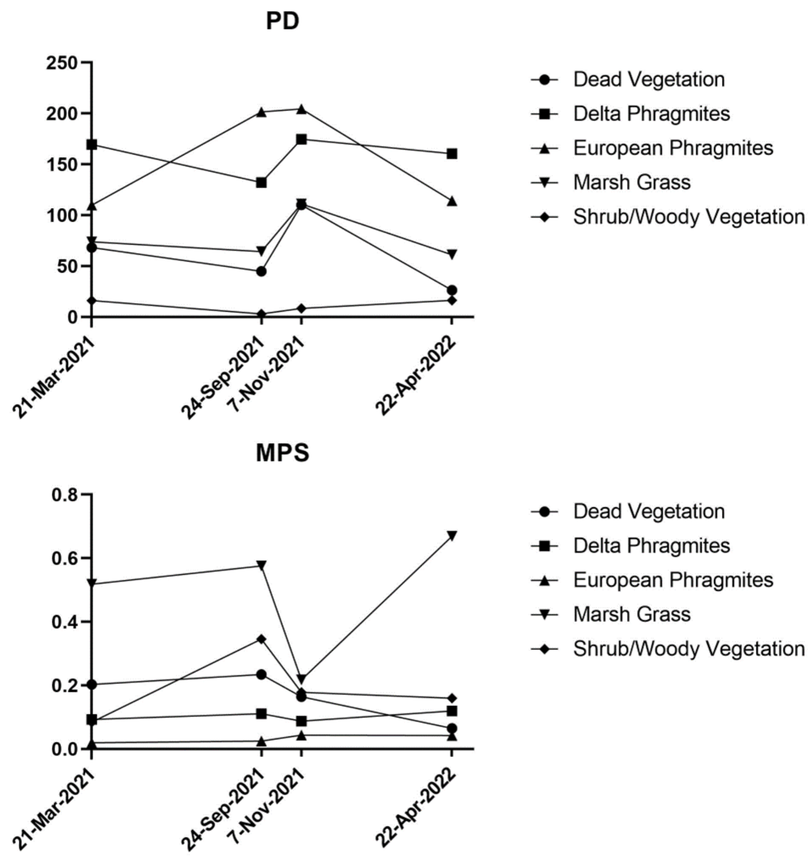

Figure 25. PD and MPS change for vegetation-related classes.

As for Figure 26, the Shannon's Diversity Index (SHDI) and Shannon's Evenness Index (SHEI) in the entire study showed a stable increase trend from March 2021 to November 2021, which indicates an increase in landscape diversity and evenness. The sudden decline after November 2021 indicates some vegetation types expanded more than other vegetation types, which is the rapid growth of Marsh Gross in this study site.

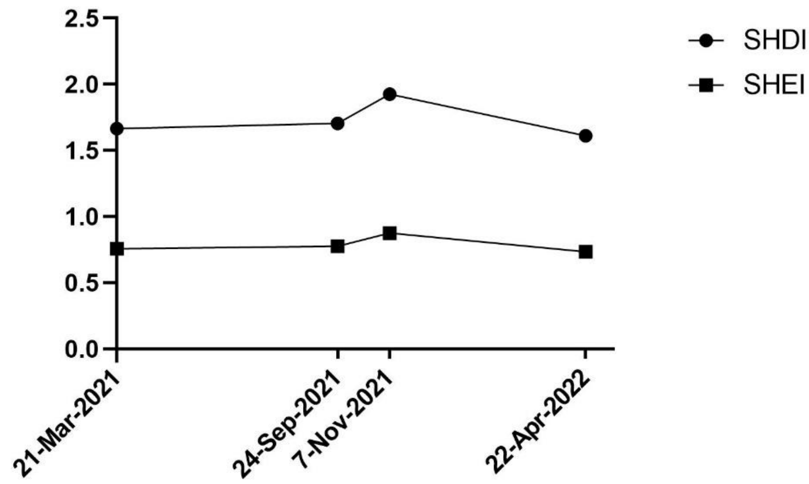

Figure 26. SHDI and SHEI change for vegetation-related classes.

6.5.3 Impact of Hurricane Damage and Recovery Process

The MRD experienced severe damage caused by Hurricane Ida during the first week of September 2021. The September drone image shortly captured the after-event status especially the wiped-out areas due to strong wind. The November field trip observed obvious vegetation recovery in some dead vegetation areas but the impact of the Hurricane on vegetation may continue due to possible saltwater intrusion. To examine whether specific vegetation types are more vulnerable to hurricane damage, this research extracts the dead vegetation area from September 24 orthophotos and overlaps it with the previous March 2021 classified result to analyze the vegetation composition that was wiped out by the hurricane. This study cross-compared this result with the class type to total vegetation coverage in March, the comparison result is listed in Table 23. The results showed that the main Dead Vegetation was from 56.31% of Marsh Grass, 21.39% of Delta Phragmites, and 16.61% of already dead vegetation. These three accounted for 94.31%. European phragmites accounted for 3.38%. One may interpret these vegetation classes with higher numbers as being more vulnerable. However, when cross-checking these percentages with the coverage percentage in the wetland area, these two percentage numbers are comparable, indicating those vegetation classes with higher coverage may suffer more due to their larger coverage. This is different from the assumption that taller Phragmites plants may suffer more damage from the strong hurricane wind. In addition, this research observed massive Marsh Grass death in November data. Since most of the inner wetland areas in the Mississippi River outlets usually receive more fresh water from the Mississippi River, more freshwater vegetation may present in the marsh grass class, and Phragmites are relatively more salt-tolerant in this study site. Therefore, the continued death of large marsh grass areas might indicate the impact of saltwater intrusion that killed freshwater vegetation for a much longer period.

Table 23. The percentage of each vegetation type in March corresponding to the Dead vegetation area in September and their total coverage in March

Class type	**% Of Dead Vegetation in September**	**% Of The Class type to Total Vegetation Coverage in March**
Dead Vegetation	16.61	19.39
Delta Phragmites	21.39	22.07
European Phragmites	3.38	3.05
Marsh Grass	56.31	53.59
Shrub/Woody Vegetation	2.31	1.89

This research further explored the recovery process of our study area based on the April 2021 survey as shown in Table 24. The result showed that from September to November, half of the dead vegetation remain dead, and the first phase of recovery mainly lead by the Delta Phragmites, with around 21% dead vegetation area occupied by the Delta Phragmites. Then from November 2021 to April 2022, Marsh Grass expanded to around 64% of the dead vegetation area, which is significantly larger compared with other vegetation types.

Table 24. The percentage of each changed type of Dead Vegetation in November 2021 and April 2020

Changed type	% From September to November	% From November to April
No change	56.12	2.18
Delta Phragmites	21.24	26.32
European Phragmites	8.60	4.88
Marsh Grass	12.81	64.01
Shrub/Woody Vegetation	1.22	2.62

6.6 Summary

To solve the challenge of limited accessibility in a wetland environment, this research introduced a drone sampling method using a second small drone to fly at lower altitudes through these areas. This method could be made wetland habitat classification possible without sufficient field survey samples. The final classification results showed high accuracy and fit our field observations of the vegetation coverage in the study area.

Then, this study used a drone to conduct habitat change analysis and observations at our study site. To accurately depict the boundary of each vegetation type, KNN, MLC, SVM, and RF classification methods were compared, and SVM proved to be the most accurate one with an overall accuracy above 87% in all 4 periods of time. This research also tested the hypothesis that adding texture info might be helpful for classification, however, our test result on 8 cm orthophotos disproved it. This might be due to the limitation of the pixel-based approach method applied in the study. The overall result showed the distribution of each vegetation type experienced significant change during our study periods. Marsh Grass is the dominant vegetation type in our study area and the Delta Phragmites proved to be the most fragmented. Our results showed an increase in landscape diversity and evenness of our study area until November 2021 before the hurricane event. In general, the overall landscape is still fragmented with a little variation that might cause by seasonal change or hazardous events.

Finally, this research applied drone monitoring for hurricane damage and wetland vulnerability and recovery analysis. The expansion of dead vegetation due to the hurricane damage was observed, and the massive death of vegetation coverage since then indicate that hurricane event has a non-negligible impact on small-scale ecosystems. This research also observed that the following recovery process was led by the expansion of Delta Phragmites at first then Marsh Grass took the major role.

Chapter 7. Discussion and Conclusions

The overall objectives of this research include assessing the Roseau cane dieback condition in lower MRD and analyzing the spatial and species variations based on moderate resolution Landsat imagery; conducting mid-scale Roseau cane habitat mapping based on high-resolution and multispectral satellite imagery of WV; developing an approach for flexible and reliable multitemporal Roseau cane habitat monitoring based on drone technologies. In addition, this research also discussed whether texture could improve Roseau cane habitat classification accuracy under different scale level.

From the large-scale perspective of the lower MRD, the spatial and temporal changes of the vegetation coverage and land boundary vegetation in the past 20 years were revealed by combining the multi-temporal Landsat series remote sensing images and NAIP aerial photos. The dieback area has been detected through NDVI change of vegetation and analysis with the distribution of Roseau cane in the region. Combining these two analyses, this research can separate Roseau cane distribution and compare its dieback with the overall wetland dieback with mixed vegetation.

From the mid-scale perspective of the Main pass and South pass of MRD, the spatial and temporal distributions of wetland vegetation species, especially the two variants of Roseau cane, were accurately extracted using the SVM classification method based on Worldview images. The result was also used to cross-validate Landsat-derived Roseau cane distribution and further discuss the difference between Delta Phragmites with European Phragmites in the dieback area.

From the selected small-scale local ecosystem landscape of MRD, the spatial and temporal variation characteristics and expansion patterns of wetland vegetation communities were extracted through multi-temporal drone surveys and analyzed based on landscape indices. In addition, the impacts of the hurricane and the recovery process were discussed.

7.1 Summary of the Results and Conclusions

From the large-scale analysis, a more accurate adjusted threshold was applied for vegetation/water boundary extraction. Twenty years of vegetation/land change maps for the MRD from 2001-2021 were generated, as well as the distribution map of Roseau Cane in selected years. Thus, a strong increasing trend of vegetation expansion was found in the MRD during the growing season, which may be a result of growing sediment stabilization from the Mississippi river. The dieback area detected through NDVI difference accounted for approximately 51 km^2 of wetlands in the MRD from 2010 to 2019, representing 11% of the overall wetland vegetation coverage in the area. When combining dieback distribution with the classified Roseau cane distribution, this research found that nearly 65% of the overall dieback was from Roseau cane. This percentage was much higher than its proportion of the overall vegetation, which indicated that the Roseau cane suffered more damage than other vegetation species in lower MRD.

From the mid-scale analysis, several classification methods were compared, and found that SVM had the highest accuracy. After generating the classification result, Delta Phragmites can successfully be distinguished from European Phragmites in the study area. This study found Delta Phragmites occupied about 80% of the overall vegetation cover in the study area in contrast with only 2.7% of the European Phragmites in the vegetation area. The results also shared around 79% of agreement with the Landsat-derived classification result, validating the effectiveness of the large-scale Reseau cane extraction result. In addition, the results indicate no significant differences between European Phragmites and Delta Phragmites in the detected areas where dieback occurred between 2019 and 2021 since their dieback percentages were proportional to their coverage percentage.

From the small-scale analysis, this research also compared several classification methods and had a similar result that SVM produced the highest accuracy. This research has successfully used field survey points combined with drone sampling methods to classify the study area. This study found marsh grass type to be the dominant vegetation type and Delta Phragmites proved to be the most fragmented vegetation type in the study area in the centimeter-level drone mapping. In general, the overall landscape remained fragmented with little variation that could be caused by seasonal changes or hazardous events.

The texture of images is an import characteristic in remote sensing. This study conducted experiment of impact of adding texture images in different scale level. The result showed adding texture images helped improving the overall classification accuracy in large scale remote sensing images such as Landsat. For mid-scale high-resolution images such as WV-2 and small-scale drones images, due to highly fragmented appearance of certain wetland vegetations under these scale level, adding texture images have no significant improvement of the overall accuracy.

7.2 Limitation and Future Work

Although this paper combines multi-source remote sensing data and a supervised classification method to extract Roseau cane habitats and analyze wetland landscape features and patterns with application of landscape ecology theory, some work needs further investigation due to the limitation of time and platform.

(1) This research mainly analyzes spectral features, using a pixel-based classification method without considering the object-oriented method. The produced salt and pepper noise in the study area suggests that current pixel-based classification methods cannot

fully take advantage of texture information. Whether the object-oriented method can further improve the classification accuracy needs to be further investigated.

(2) When analyzing the landscape characteristics of wetland vegetation, this study selects some landscape indices for analysis, but due to the limitation of data availability, only 4 periods of change of landscape patterns are analyzed. Further long-term research is needed for the landscape patterns of the seasonal change on small-scale ecosystems and the driven factor behind it.

(3) The research on the relationship between dieback with water level and salinity is not sufficient. In future work, the spatial distribution pattern of vegetation in lower MRD wetlands under water-salinity gradient change might be quantitatively analyzed by combining the wetland vegetation biomass survey data and water depth and salinity data.

References

Alber, M., Swenson, E. M., Adamowicz, S. C., & Mendelssohn, I. A. (2008). Salt marsh dieback: an overview of recent events in the US. Estuarine, Coastal and Shelf Science, 80(1), 1-11.

Amani, M., Salehi, B., Mahdavi, S., Granger, J. E., Brisco, B., & Hanson, A. (2017). Wetland classification using multi-source and multi-temporal optical remote sensing data in Newfoundland and Labrador, Canada. Canadian Journal of Remote Sensing, 43(4), 360-373.

Antonielli, M., Pasqualini, S., Batini, P., Ederli, L., Massacci, A., & Loreto, F. (2002). Physiological and anatomical characterisation of Phragmites australis leaves. Aquatic Botany, 72(1), 55-66.

Bao, X., Xu, T., & Hou, H. (2009, September). Network intrusion detection based on support vector machine. In 2009 International Conference on Management and Service Science (pp. 1-4). IEEE.

Barbier, E. B., Hacker, S. D., Kennedy, C., Koch, E. W., Stier, A. C., & Silliman, B. R. (2011). The value of estuarine and coastal ecosystem services. Ecological monographs, 81(2), 169-193.

Barton, I. J., & Bathols, J. M. (1989). Monitoring floods with AVHRR. Remote sensing of Environment, 30(1), 89-94.

Beaudette, A. M. (2020). Estimating the Onset and Extent of Dieback Of Phragmites australis Using the Normalized Difference Vegetation Index and Remotely Sensed Land Cover Classifications. Louisiana State University and Agricultural & Mechanical College.

Belluco, E., Camuffo, M., Ferrari, S., Modenese, L., Silvestri, S., Marani, A., & Marani, M. (2006). Mapping salt-marsh vegetation by multispectral and hyperspectral remote sensing. Remote sensing of environment, 105(1), 54-67.

Berni, J. A., Zarco-Tejada, P. J., Suárez, L., & Fereres, E. (2009). Thermal and narrowband multispectral remote sensing for vegetation monitoring from an unmanned aerial vehicle. IEEE Transactions on geoscience and Remote Sensing, 47(3), 722-738.

Blum, M. D., & Roberts, H. H. (2012). The Mississippi delta region: past, present, and future. Annual Review of Earth and Planetary Sciences, 40, 655-683.

Breiman, Leo. (2001). "Random forests." Machine learning, 45.1: 5-32.

Brix, H. (1999). The European research project on reed die-back and progression (EUREED). Limnologica, 29(1), 5-10.

Cao, J., Liu, K., Liu, L., Zhu, Y., Li, J., & He, Z. (2018). Identifying mangrove species using field close-range snapshot hyperspectral imaging and machine-learning techniques. Remote Sensing, 10(12), 2047.

Carle, M. V., Wang, L., & Sasser, C. E. (2014). Mapping freshwater marsh species distributions using WorldView-2 high-resolution multispectral satellite imagery. International journal of remote sensing, 35(13), 4698-4716.

Chambers, R. M., Meyerson, L. A., & Saltonstall, K. (1999). Expansion of Phragmites australis into tidal wetlands of North America. Aquatic botany, 64(3-4), 261-273.

Chen*, D., Stow, D. A., & Gong, P. (2004). Examining the effect of spatial resolution and texture window size on classification accuracy: an urban environment case. International Journal of Remote Sensing, 25(11), 2177-2192.

Clevering, O. A. (1997). Effects of litter accumulation and water table on morphology and productivity of Phragmites australis. Wetlands Ecology and Management, 5(4), 275-287.

Coleman, J. M., Roberts, H. H., & Stone, G. W. (1998). Mississippi River delta: an overview. Journal of Coastal Research, 699-716.

Colomina, I., & Molina, P. (2014). Unmanned aerial systems for photogrammetry and remote sensing: A review. ISPRS Journal of photogrammetry and remote sensing, 92, 79-97.

Costanza, R., De Groot, R., Sutton, P., Van der Ploeg, S., Anderson, S. J., Kubiszewski, I., ... & Turner, R. K. (2014). Changes in the global value of ecosystem services. Global environmental change, 26, 152-158.

Costanza, R., Farber, S. C., & Maxwell, J. (1989). Valuation and management of wetland ecosystems. Ecological economics, 1(4), 335-361.

Corbett, D. R., McKee, B., & Allison, M. (2006). Nature of decadal-scale sediment accumulation on the western shelf of the Mississippi River delta. Continental Shelf Research, 26(17-18), 2125-2140.

Couvillion, B. R., & Beck, H. (2013). Marsh collapse thresholds for coastal Louisiana estimated using elevation and vegetation index data. Journal of Coastal Research, (63 (10063)), 58-67.

Cronin, J. T., Johnston, J., & Diaz, R. (2020). Multiple potential stressors and dieback of Phragmites australis in the Mississippi River Delta, USA: Implications for restoration. Wetlands, 40(6), 2247-2261.

DaMatta, F. M., & Ramalho, J. D. C. (2006). Impacts of drought and temperature stress on coffee physiology and production: a review. Brazilian journal of plant physiology, 18, 55-81.

Davranche, A., Lefebvre, G., & Poulin, B. (2010). Wetland monitoring using classification trees and SPOT-5 seasonal time series. Remote sensing of environment, 114(3), 552-562.

Dechka, J. A., Franklin, S. E., Watmough, M. D., Bennett, R. P., & Ingstrup, D. W. (2002). Classification of wetland habitat and vegetation communities using multi-temporal Ikonos imagery in southern Saskatchewan. Canadian Journal of Remote Sensing, 28(5), 679-685.

Du, P., Xia, J., Zhang, W., Tan, K., Liu, Y., & Liu, S. (2012). Multiple classifier system for remote sensing image classification: A review. Sensors, 12(4), 4764-4792.

Duarte, C. M., Losada, I. J., Hendriks, I. E., Mazarrasa, I., & Marbà, N. (2013). The role of coastal plant communities for climate change mitigation and adaptation. Nature climate change, 3(11), 961-968.

Elias, T. S., & Dykeman, P. A. (1990). Edible wild plants: a North American field guide. Sterling Publishing Company, Inc..

Elmer, W. H., Useman, S., Schneider, R. W., Marra, R. E., LaMondia, J. A., Mendelssohn, I. A., ... & Caruso, F. L. (2013). Sudden vegetation dieback in Atlantic and Gulf Coast salt marshes. Plant Disease, 97(4), 436-445.

Elsey-Quirk, T., Graham, S. A., Mendelssohn, I. A., Snedden, G., Day, J. W., Twilley, R. R., ... & Lane, R. R. (2019). Mississippi river sediment diversions and coastal wetland sustainability: Synthesis of responses to freshwater, sediment, and nutrient inputs. Estuarine, Coastal and Shelf Science, 221, 170-183.

Fernandes, M. R., Aguiar, F. C., Silva, J. M., Ferreira, M. T., & Pereira, J. M. (2013). Spectral discrimination of giant reed (Arundo donax L.): A seasonal study in riparian areas. ISPRS journal of photogrammetry and remote sensing, 80, 80-90.

Gao, H., Wang, L., Jing, L., & Xu, J. (2016, April). An effective modified water extraction method for Landsat-8 OLI imagery of mountainous plateau regions. In IOP conference series: earth and environmental science (Vol. 34, No. 1, p. 012010). IOP Publishing.

Gedan, K. B., Kirwan, M. L., Wolanski, E., Barbier, E. B., & Silliman, B. R. (2011). The present and future role of coastal wetland vegetation in protecting shorelines: answering recent challenges to the paradigm. Climatic change, 106(1), 7-29.

Goodbody, T. R., Coops, N. C., Marshall, P. L., Tompalski, P., & Crawford, P. (2017). Unmanned aerial systems for precision forest inventory purposes: A review and case study. The Forestry Chronicle, 93(1), 71-81.

Harris, J. M. (2020). Evaluating Coastal Wetland Restoration in Louisiana Using Drones (Doctoral dissertation, University of Louisiana at Lafayette).

Heenkenda, M. K., Joyce, K. E., Maier, S. W., & Bartolo, R. (2014). Mangrove species identification: Comparing WorldView-2 with aerial photographs. Remote Sensing, 6(7), 6064-6088.

Hladik, C., Schalles, J., & Alber, M. (2013). Salt marsh elevation and habitat mapping using hyperspectral and LIDAR data. Remote Sensing of Environment, 139, 318-330.

Hsu, C. W., & Lin, C. J. (2002). A comparison of methods for multiclass support vector machines. IEEE transactions on Neural Networks, 13(2), 415-425.

Hu, Y. X., Huang, J. L., Du, Y., Han, P. P., Wang, J. L., & Huang, W. (2015). Monitoring wetland vegetation pattern response to water-level change resulting from the Three Gorges Project in the two largest freshwater lakes of China. Ecological Engineering, 74, 274-285.

Hu, K., Meselhe, E., & Nyman, J. A. (2021). The Effect of Phragmites australis Dieback on Channel Sedimentation in the Mississippi River Delta: A Conceptual Modeling Study. Water, 13(10), 1407.

Jaccard, A. M. (2018). Article 450 to the Rescue: How the Louisiana Civil Code Promotes and Prevents Comprehensive Coastal Restoration. Tul. L. Rev., 93, 681.

Ji, L., Zhang, L., & Wylie, B. (2009). Analysis of dynamic thresholds for the normalized difference water index. Photogrammetric Engineering & Remote Sensing, 75(11), 1307-1317.

Jiao, D., Yao, L., & Yang, Y. (2015). Differed Bud Bank Dynamics of Phragmites australis in Heterogeneous Habitats in Zhalong Wetland. Journal of Computational and Theoretical Nanoscience, 12(12), 5796-5801.

Jiang, R., Wang, P., Xu, Y., Zhou, Z., Luo, X., Lan, Y., ... & Laakso, K. (2020). Assessing the operation parameters of a low-altitude UAV for the collection of NDVI values over a paddy rice field. Remote Sensing, 12(11), 1850.

Jing, R., Deng, L., Zhao, W. J., & Gong, Z. N. (2016). Object-oriented aquatic vegetation extracting approach based on visible vegetation indices. The Journal of Applied Ecology, 27(5), 1427-1436.

Kaplan, G., & Avdan, U. (2017). Mapping and monitoring wetlands using Sentinel-2 satellite imagery.

Knight, I. A., Wilson, B. E., Gill, M., Aviles, L., Cronin, J. T., Nyman, J. A., ... & Diaz, R. (2018). Invasion of Nipponaclerda biwakoensis (Hemiptera: Aclerdidae) and Phragmites australis die-back in southern Louisiana, USA. Biological Invasions, 20(10), 2739-2744.

Knight, I. A., Cronin, J. T., Gill, M., Nyman, J. A., Wilson, B. E., & Diaz, R. (2020). Investigating plant phenotype, salinity, and infestation by the roseau cane scale as factors in the die-back of Phragmites australis in the Mississippi River Delta, USA. Wetlands, 40(5), 1327-1337.

Komárek, J., Klouček, T., & Prošek, J. (2018). The potential of unmanned aerial systems: a tool towards precision classification of hard-to-distinguish vegetation types?. International Journal of Applied Earth Observation and Geoinformation, 71, 9-19.

Kumar, L., Sinha, P., Taylor, S., & Alqurashi, A. F. (2015). Review of the use of remote sensing for biomass estimation to support renewable energy generation. Journal of Applied Remote Sensing, 9(1), 097696.

Laba, M., Downs, R., Smith, S., Welsh, S., Neider, C., White, S., ... & Baveye, P. (2008). Mapping invasive wetland plants in the Hudson River National Estuarine Research Reserve using quickbird satellite imagery. Remote sensing of Environment, 112(1), 286-300.

Li, H., Wang, C., Ellis, J. T., Cui, Y., Miller, G., & Morris, J. T. (2020). Identifying marsh dieback events from Landsat image series (1998–2018) with an Autoencoder in the NIWB estuary, South Carolina. International Journal of Digital Earth, 13(12), 1467-1483.

Li, L., Su, H., Du, Q., & Wu, T. (2021). A novel surface water index using local background information for long term and large-scale Landsat images. ISPRS Journal of Photogrammetry and Remote Sensing, 172, 59-78.

Li, Q., Wong, F. K. K., & Fung, T. (2019). Classification of mangrove species using combined WordView-3 and LiDAR data in Mai Po nature reserve, Hong Kong. Remote Sensing, 11(18), 2114.

Li, Z., Li, Z., Fairbairn, D., Li, N., Xu, B., Feng, H., & Yang, G. (2019). Multi-LUTs method for canopy nitrogen density estimation in winter wheat by field and UAV hyperspectral. Computers and Electronics in Agriculture, 162, 174-182.

Lissner, J., & Schierup, H. H. (1997). Effects of salinity on the growth of Phragmites australis. Aquatic botany, 55(4), 247-260.

Liu, D., Li, S., Fu, D., & Shen, C. (2018). Remote sensing analysis of mangrove distribution and dynamics in Zhanjiang from 1991 to 2011. Journal of Oceanology and Limnology, 36(5), 1597-1603.

Liu, Y., Song, P., Peng, J., & Ye, C. (2012). A physical explanation of the variation in threshold for delineating terrestrial water surfaces from multi-temporal images: effects of radiometric correction. International Journal of Remote Sensing, 33(18), 5862-5875.

Liu, X., Yang, X., Zhang, T., Wang, Z., Zhang, J., Liu, Y., & Liu, B. (2022). Remote Sensing Based Conservation Effectiveness Evaluation of Mangrove Reserves in China. Remote Sensing, 14(6), 1386.

Lou, P., Fu, B., He, H., Li, Y., Tang, T., Lin, X., ... & Gao, E. (2020). An optimized object-based random forest algorithm for marsh vegetation mapping using high-spatial-resolution GF-1 and ZY-3 data. Remote Sensing, 12(8), 1270.

Lu, D., & Weng, Q. (2007). A survey of image classification methods and techniques for improving classification performance. International journal of Remote sensing, 28(5), 823-870.

Lu, J. J., & Li, S. H. (1992). Improvement of the techniques for distinguishing water bodies from TM data. Remote Sensing of Environment, 7(1), 17-23.

Lu, S., Wu, B., Yan, N., & Wang, H. (2011). Water body mapping method with HJ-1A/B satellite imagery. International Journal of Applied Earth Observation and Geoinformation, 13(3), 428-434.

Ma, L., Cheng, L., Li, M., Liu, Y., & Ma, X. (2015). Training set size, scale, and features in Geographic Object-Based Image Analysis of very high resolution unmanned aerial vehicle imagery. ISPRS Journal of Photogrammetry and Remote Sensing, 102, 14-27.

Mehlhorn, H. (2019). Important rivers and their worldwide contributions to epidemics on the continents. In Parasite and Disease Spread by Major Rivers on Earth (pp. 1-111). Springer, Cham.

McFeeters, S. K. (1996). The use of the Normalized Difference Water Index (NDWI) in the delineation of open water features. International journal of remote sensing, 17(7), 1425-1432.

Miller, G. J., Morris, J. T., & Wang, C. (2017). Mapping salt marsh dieback and condition in South Carolina’s North Inlet-Winyah Bay National Estuarine Research Reserve using remote sensing. Aims Environ. Sci, 4, 677-689.

Mountrakis, G., Im, J., & Ogole, C. (2011). Support vector machines in remote sensing: A review. ISPRS Journal of Photogrammetry and Remote Sensing, 66(3), 247-259.

Mueller-Dombois, D. (1986). Perspectives for an etiology of stand-level dieback. Annual Review of Ecology and Systematics, 221-243.

Nghi, D. H., & Mai, L. C. (2008). An object-oriented classification techniques for high resolution satellite imagery. GeoInformatics for Spatial-Infrastructure Development in Earth and Allied Sciences (GIS-IDEAS), 42, 230-240.

O’Donnell, J. P., & Schalles, J. F. (2016). Examination of abiotic drivers and their influence on Spartina alterniflora biomass over a twenty-eight year period using Landsat 5 TM satellite imagery of the Central Georgia Coast. Remote Sensing, 8(6), 477.

O'Neil, G. L., Goodall, J. L., & Watson, L. T. (2018). Evaluating the potential for site-specific modification of LiDAR DEM derivatives to improve environmental planning-scale wetland identification using Random Forest classification. Journal of Hydrology, 559, 192-208.

O'Neill, R. V., Krummel, J. R., Gardner, R. E. A., Sugihara, G., Jackson, B., DeAngelis, D. L., ... & Graham, R. L. (1988). Indices of landscape pattern. Landscape ecology, 1(3), 153-162.

Pande-Chhetri, R., Abd-Elrahman, A., Liu, T., Morton, J., & Wilhelm, V. L. (2017). Object-based classification of wetland vegetation using very high-resolution unmanned air system imagery. European Journal of Remote Sensing, 50(1), 564-576.

Peters, G. (2007, July). Aesthetic primitives of images for visualization. In 2007 11th International Conference Information Visualization (IV'07) (pp. 316-325). IEEE.

Piazza, B. P. (2014). The Atchafalaya River Basin: history and ecology of an American wetland (No. 26). Texas A&M University Press.

Rapinel, S., Bouzillé, J. B., Oszwald, J., & Bonis, A. (2015). Use of bi-seasonal Landsat-8 imagery for mapping marshland plant community combinations at the regional scale. Wetlands, 35(6), 1043-1054.

Ren, G. B., Wang, J. J., Wang, A. D., Wang, J. B., Zhu, Y. L., Wu, P. Q., ... & Zhang, J. (2019). Monitoring the invasion of smooth cordgrass Spartina alterniflora within the modern Yellow River Delta using remote sensing. Journal of Coastal Research, 90(SI), 135-145.

Richard Allen, T., Wang, Y., & Gore, B. (2013). Coastal wetland mapping combining multi-date SAR and LiDAR. Geocarto International, 28(7), 616-631.

Sabins, F. F. (2007). Remote sensing: principles and applications. Waveland Press.

Samiappan, S., Turnage, G., Hathcock, L., Casagrande, L., Stinson, P., & Moorhead, R. (2017). Using unmanned aerial vehicles for high-resolution remote sensing to map invasive Phragmites australis in coastal wetlands. International Journal of Remote Sensing, 38(8-10), 2199-2217.

Schneider, S. A. (2019). A key to the flat grass scale genus Nipponaclerda (Hemiptera, Coccomorpha, Aclerdidae). ZooKeys, 862, 81.

Sharitz, R. (1986). Remote sensing inland wetlands: a multispectral approach. Photogrammetric Engineering and Remote Sensing, 52(1), 87-100.

Shih, S.F. (1985). Comparison of ELAS classifications and density slicing Landsat data for water surface area assessment. Hydrol. Appl. Space Technol, 160, 91–97.

Singh, N., Kaur, M., & Katnoria, J. K. (2017). Analysis on bioaccumulation of metals in aquatic environment of Beas River Basin: a case study from Kanjli wetland. GeoHealth, 1(3), 93-105.

Slagter, B., Tsendbazar, N. E., Vollrath, A., & Reiche, J. (2020). Mapping wetland characteristics using temporally dense Sentinel-1 and Sentinel-2 data: A case study in the St. Lucia wetlands, South Africa. International Journal of Applied Earth Observation and Geoinformation, 86, 102009.

Sona, G., Pinto, L., Pagliari, D., Passoni, D., & Gini, R. (2014). Experimental analysis of different software packages for orientation and digital surface modelling from UAV images. Earth Science Informatics, 7(2), 97-107.

Suir, G. M., Saltus, C. L., & Reif, M. K. (2018). Geospatial assessments of Phragmites australis die-off in South Louisiana: preliminary findings.

Sun, C., Fagherazzi, S., & Liu, Y. (2018). Classification mapping of salt marsh vegetation by flexible monthly NDVI time-series using Landsat imagery. Estuarine, Coastal and Shelf Science, 213, 61-80.

Temmerman, S., Meire, P., Bouma, T. J., Herman, P. M., Ysebaert, T., & De Vriend, H. J. (2013). Ecosystem-based coastal defence in the face of global change. Nature, 504(7478), 79-83.

Tweel, A. W., & Turner, R. E. (2012). Watershed land use and river engineering drive wetland formation and loss in the Mississippi River birdfoot delta. Limnology and Oceanography, 57(1), 18-28.

Turner, D., Lucieer, A., & Watson, C. (2012). An automated technique for generating georectified mosaics from ultra-high resolution unmanned aerial vehicle (UAV) imagery, based on structure from motion (SfM) point clouds. Remote sensing, 4(5), 1392-1410.

Upadhyay, P., Ghosh, S. K., Kumar, A., Roy, P. S., & Gilbert, I. (2012). Effect on specific crop mapping using WorldView-2 multispectral add-on bands: soft classification approach. Journal of Applied Remote Sensing, 6(1), 063524.

Vapnik, V. N. (1999). " An Overview of Statistical Learning Theory", IEEE transactions on neural networks, vol. 10,№ 5.

Wang, C., Lu, Z., & Haithcoat, T. L. (2007). Using landsat images to detect oak decline in the Mark Twain national forest, Ozark highlands. Forest ecology and management, 240(1-3), 70-78.

Wang, J., Chen, J., Wen, Y., Fan, W., Liu, Q., & Tarolli, P. (2021). Monitoring the coastal wetlands dynamics in Northeast Italy from 1984 to 2016. Ecological Indicators, 129, 107906.

Wang, L., Dronova, I., Gong, P., Yang, W., Li, Y., & Liu, Q. (2012). A new time series vegetation–water index of phenological–hydrological trait across species and functional types for Poyang Lake wetland ecosystem. Remote Sensing of Environment, 125, 49-63.

Wang, X., Xiao, X., Zou, Z., Hou, L., Qin, Y., Dong, J., ... & Li, B. (2020). Mapping coastal wetlands of China using time series Landsat images in 2018 and Google Earth Engine. ISPRS Journal of Photogrammetry and Remote Sensing, 163, 312-326.

Watts, A. C., Ambrosia, V. G., & Hinkley, E. A. (2012). Unmanned aircraft systems in remote sensing and scientific research: Classification and considerations of use. Remote Sensing, 4(6), 1671-1692.

Wulder, M. A., White, J. C., Loveland, T. R., Woodcock, C. E., Belward, A. S., Cohen, W. B., ... & Roy, D. P. (2016). The global Landsat archive: Status, consolidation, and direction. Remote Sensing of Environment, 185, 271-283.

Xie, D., Gao, F., Sun, L., & Anderson, M. (2018). Improving spatial-temporal data fusion by choosing optimal input image pairs. Remote Sensing, 10(7), 1142.

Xiong, J., S. Wang, and Y. Zhou. (2010). A Sensitivity Analysis and Accuracy Assessment of Different Water Extraction Index Models Based on ALOS AVNIR-2 Data. Remote Sensing for Land & Resources, 22(4), 46-50.

Xu, C., Pu, L., Zhu, M., Li, J., Chen, X., Wang, X., & Xie, X. (2016). Ecological security and ecosystem services in response to land use change in the coastal area of Jiangsu, China. Sustainability, 8(8), 816.

Xu, H. (2005). A study on information extraction of water body with the modified normalized difference water index (MNDWI). Journal of Remote Sensing-Beijing-, 9(5), 595.

Yang, C. C., Prasher, S. O., Enright, P., Madramootoo, C., Burgess, M., Goel, P. K., & Callum, I. (2003). Application of decision tree technology for image classification using remote sensing data. Agricultural Systems, 76(3), 1101-1117.

Zedler, J. B., & Kercher, S. (2005). Wetland resources: status, trends, ecosystem services, and restorability. Annu. Rev. Environ. Resour., 30, 39-74.

Zhang, C., & Xie, Z. (2013). Object-based vegetation mapping in the Kissimmee River watershed using HyMap data and machine learning techniques. Wetlands, 33(2), 233-244.

Zhou, Z. M., Yang, Y. M., & Chen, B. Q. (2016). Fractional vegetation cover of invasive Spartina alterniflora in coastal wetland using unmanned aerial vehicle (UAV) remote sensing. The Journal of Applied Ecology, 27(12), 3920-3926.

Vita

Nan Shang was born in Yuncheng City, Shanxi Province, China. He received his Bachelor of Engineering degree in Remote Sensing Science and Technology from Wuhan University, Wuhan, China, in the fall of 2011. He then continued his graduate study and earned Master of Science degree in Cartography and Geographic information Systems from University of Chinese Academy of Sciences, Beijing, China, in 2014. Since the fall of 2015, he has been a Ph.D. student in the Department of Geography and Anthropology, Louisiana State University, supported by a teaching assistantship and graduate assistantship and supervised by Dr. Xuelian Meng. His research interests include remote sensing, GIS, UAV and coastal wetland study.